University of Nevada, Reno

A Voice-Based Biometric Watermarking Scheme For Digital Rights Management of 3D Mesh Models

A dissertation submitted in partial fulfillment of the requirements for the degree of Doctor of Philosophy in Computer Science and Engineering

by

Rakhi C. Motwani

Dr. Frederick C. Harris, Jr./Dissertation Advisor

May, 2010

University of Nevada, Reno
Statewide • Worldwide

THE GRADUATE SCHOOL

We recommend that the dissertation
prepared under our supervision by

RAKHI C. MOTWANI

entitled

**A Voice-Based Biometric Watermarking Scheme For
Digital Rights Management Of 3D Mesh Models**

be accepted in partial fulfillment of the
requirements for the degree of

DOCTOR OF PHILOSOPHY

Dr. Frederick C. Harris, Jr., Advisor

Dr. Sergiu Dascalu, Committee Member

Dr. Konstantinos Bekris, Committee Member

Dr. William Kuechler, Committee Member

Dr. Daulatram Lund, Graduate School Representative

Marsha H. Read, Ph. D., Associate Dean, Graduate School

May, 2010

Abstract

Widespread use of 3D artwork has necessitated the need for managing digital rights of content owners due to illegal peer-to-peer (P2P) distribution of artwork, which has been one of the major sources of revenue loss for the art industry. Existing Digital Rights Management (DRM) systems attempt to provide an anti-piracy framework that restricts the use of content to its rightful user. However, limitations of technology have consequently led to solution designs that are either very restrictive (i.e. device-limiting or usage restrictions) or only succeed in discouraging unlawful distribution by employing tracing mechanisms.

The objective of this dissertation is to contribute towards DRM implementations to ensure fair rights management such that the needs of both the authors and consumers are balanced. The proposed biometric-based watermarking scheme allows DRM systems to enforce copyright protection by imposing individual-limiting usage rights, thereby eliminating any device dependency or usage restrictions.

The proposed technique embeds the identity of the consumer in the form of a voice print, into the graphic content. This voice print serves as a watermark and is created by using a statistical model (Gaussian Mixture Model) representation of the consumer's voice sample. Mel-frequency cepstral coefficients, representing feature vectors of the speaker from the speech signal, are used to generate the statistical model. Comparison of the embedded watermark with feature vectors extracted from a newly acquired voice sample from the consumer enable the biometric-based DRM system to verify the authenticity of the consumer for legitimate access and usage of the 3D artwork. The scope of this dissertation is limited to 3D mesh models.

Acknowledgments

My sincere thanks go to my advisor, Dr. Frederick C. Harris, Jr. for his endless support and guidance over the past several years. I am also thankful to my committee members: Dr. Sergiu Dascalu, Dr. Kostas Bekris, Dr. William Kuechler, and Dr. Daulatram Lund for their time and feedback on drafts of various publications.

My gratitude goes to my elder brother, Mukesh, who dedicated countless number of hours in discussion and reading of my work to provide invaluable feedback and suggestions. I owe special thanks to my parents and friends for their unconditional love, encouragement and support. I also thank my cat for being patient with not getting my regular attention and time.

Last but not the least, I am thankful to God for giving me the potential to complete this work.

Contents

List of Tables

List of Figures

Chapter 1

Introduction

1.1 Motivation

The past decade has witnessed an explosion of 3D graphics content. Numerous 3D model catalogs are available online for various industries such as architecture, computer aided design, entertainment, science, medical imaging, archaeological artifacts, and much more. Such widespread use of 3D artwork has necessitated the need for managing digital rights of content owners due to illegal peer-to-peer (P2P) distribution of artwork, which has been one of the major sources of revenue loss for the art industry. Existing Digital Rights Management (DRM) solutions for 3D multimedia are either very restrictive (i.e. device-limiting or usage restrictions) or only succeed in discouraging unlawful distribution by employing tracing mechanisms. While the objective of DRM is to restrict the use of content to its rightful user, limitations of technology have consequently led to solution designs that can be broadly classified into two categories - a) implementations that violate consumer's rights to fair use(i.e. using the content without any restrictions) thereby tilting the balance in favor of the owners, or b) implementations that are ineffective in avoiding unauthorized users from accessing the content thereby tilting the balance in favor of the consumer. As a result, DRM systems face the challenge of ensuring fair rights management along with controlling content access to legal users.

The objective of this dissertation is to contribute towards DRM implementations such that the needs of both the authors and users are balanced. This research work focuses on addressing the shortcomings and challenges of current DRM schemes, by proposing to employ a biometric based watermarking solution. Watermarking or information hiding is an identification technology. Thus far, the most any DRM system has achieved from utilizing watermarking schemes is a piracy tracing mechanism - by embedding consumer specific identifiers into the digital content and retrieving these identifiers from pirated content to determine the consumer responsible for piracy. The proposed watermarking scheme when used in conjunction with DRM solutions serves as an access control technology.

1.2 Methodology

The proposed watermarking method embeds a representation of a biometric trait, which corresponds to the identity of consumer, in the graphic content. Various biometrics such as fingerprint, palm print, iris, retina, hand geometry, face, voice, and signature are evaluated to select the most feasible biometric trait for the DRM application. Upon electing an appropriate biometric characteristic, the next step is to research feature extraction techniques that measure features, from the biometric trait sample, which uniquely characterize an individual. Factors such as improper user interaction with the sensor, temporary alterations of the biometric trait itself caused by aging and illness, and environmental factors affect the quality and consistency of captured biometric data. To incorporate these intra-user variations, feature representation techniques have to be incorporated in order to generate a statistical model of the biometric features. This generated model is then used as a watermark. Comparison of the embedded watermark with the real-time generated features from the live capture of the biometric trait from the user allows a DRM system to perform biometric based authentication for graphic content access and usage.

Use of biometric watermarks enables the DRM system to a) enforce graphic content access to a legitimate user, b) eliminate the usage-restrictions and device-limiting drawbacks by imposing human-limiting usage rights, c) track down the traitor in the distribution chain via the biometric tracer embedded as watermark in the graphic content, and d) prevent large scale online distribution thereby making piracy substantially harder. However, the underlying assumption for the proposed scheme is that users are willing to share their biometrics with the graphics distribution agency(considered as a reliable authority) and are unwilling to share their biometrics on peer-to-peer networks (fearing misuse of personal biometric data by strangers) to allow illegitimate users to access the copyright protected graphics.

1.3 Contributions

This dissertation contributes to the research community in three directions - i) a novel biometric watermarking algorithm for 3D mesh models, ii) design of a novel biometric-watermarking based DRM system, and iii) assessment of the feasibility of integrating a biometric system with a watermarking system by evaluating the performance of the overall system and providing directions for future work to develop a commercially viable system.

1.4 Dissertation Organization

The remainder of this dissertation is structured as follows: Chapter 2 gives relevant background information on digital rights management systems, biometrics, digital watermarking, and voice signal processing along with presenting reviewed literature on 3D multimedia DRM systems, biometric watermarking, and 3D mesh model watermarking techniques. Chapter 3 presents details on the proposed scheme and outlines the framework for the proposed biometric watermarking based DRM system. Chapter 5 presents experiments to evaluate the performance of the proposed method. Limitations, conclusions, and future research directions are provided in Chapter 6.

Chapter 2

Background and Literature Review

2.1 Introduction

This chapter covers the background information for four domains - DRM, biometrics, 3D watermarking, and voice signal processing, and is therefore split into four sections. Section 2.2 presents the basic architecture of DRM systems along with limitations of existing DRM solutions for 3D multimedia. Section 2.3 gives relevant background information on biometrics and outlines characteristics of various biometric traits. Section 2.4 provides definitions and background information on watermarking including a survey of the related literature on - i) biometric watermarking of digital media, and ii) 3D mesh model watermarking. Section 2.5 discusses fundamentals of voice signal processing with emphasis on speaker verification techniques and outlines factors that govern the performance of voice biometric systems.

2.2 Digital Rights Management Systems

2.2.1 Technology Overview

Digital Rights Management (DRM) is a scheme by which content owners use technological mechanisms to enforce and protect copyrights over the authored digital work. The objective of a DRM system is to restrict the use of content to its rightful user in order to facilitate rightful compensation to artists for their work. Depending on usage scenarios and operating environments, DRM systems architecture [37] and implementation vary from vendor to vendor but the basic functionality provided by each system is equivalent, to facilitate publishing of digital content in a manner such that the usage of this content can be controlled. Figure 2.1 illustrates the various DRM systems types along with the respective functionality achieved by the type of implementation.

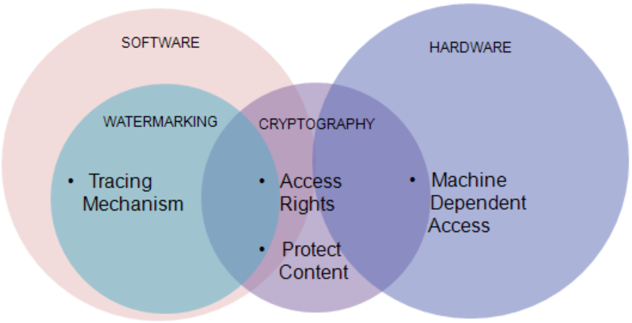

Figure 2.1: DRM System Types

A typical DRM solution [88] is implemented through software and involves proprietary formats (file formats and viewers) and generally operates in a client-server context. The technologies used for digital management of rights include cryptography and watermarking. Cryptography is used for license management. User rights are expressed in the licenses which are typically implemented as digital certificates. User rights specify the number of usages, temporary or partial use, duration of access, lending rights, and number of devices on which the content can be used. Licenses generally contain an identifier of a user who has purchased the content, or an identifier of a device on which the license may be used. Watermarking is a data embedding technology used primarily for tracing purposes. It is used to identify the source of illegal distribution by analyzing the user-specific identifier embedded in the digital content prior to its distribution. DRM systems can also be realized in hardware through integrated circuits [132] and biometric devices [82].

DRM System Architecture

Figure 2.2 portrays the framework of a typical client-server based DRM scheme. The

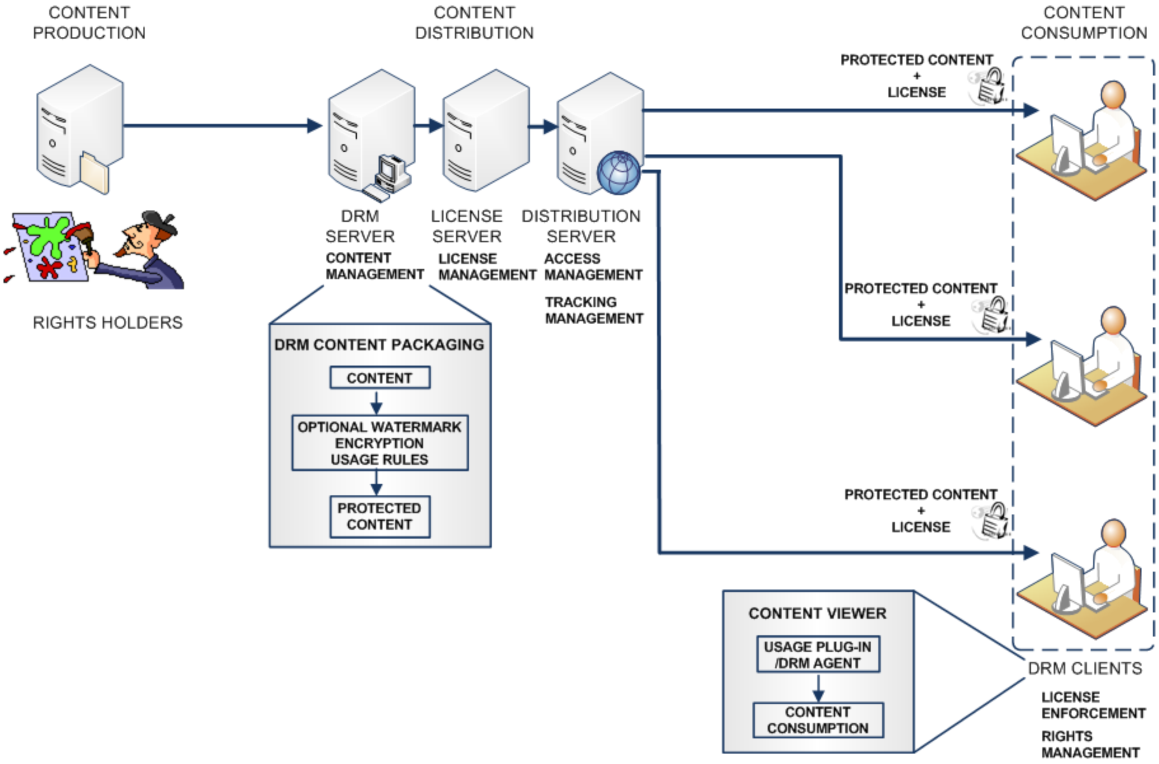

Figure 2.2: Software-Based DRM System

functional components of this system include - i) server-side content management: responsible for packaging of the digital content by translating the contents into a proprietary format, ii) server-side license management: expression of usage rights pertaining to each customer in terms of licenses, iii) server-side content distribution: responsible for access and tracking management modules that handle the registration of users, payments, authentication, and obtain statistical information about the use of the DRM system, and iv) client-side license enforcement and rights management: a proprietary content consumption application that enforces user-specific access rights specified in the license.

Security Aspects of a DRM System

The goal of an adversary is to try to break the security of the system in order to obtain the digital content in an unprotected form. Therefore, it is necessary to build a security model [64] that states the security goals of the system along with the threat and trust models. The threat model identifies all possible means by which an adversary can attempt to attack the system. The trust model describes entities that are trusted not to have vulnerabilities that give rise to a threat. Readers are advised to refer to [62] or [63] for further details and specifics on how to analyze the security of a DRM system. Section 3.3 analyzes the security aspects of the proposed DRM framework.

2.2.2 Limitations of Existing 3D Multimedia DRM Systems

Published literature on 3D graphics DRM is very limited. The issues with existing DRM systems that are highlighted in the literature can be summarized as:

- Device-limiting access
- Usage restrictions
- Unauthorized access

Related work on digital rights management of 3D graphics is analyzed based on the type of implementation:

Client-Server Based Implementation

Stanford University has signed a contract with the Italian authorities to protect the laser scanned high resolution 3D digital sculptures of Michelangelo by making the artwork available only to established scholars for noncommercial use. The goal of the team [68] that has undertaken the project is to prevent piracy of the 3D models such that simulated marble replicas are not manufactured by unauthorized entities. To achieve this objective, they have implemented a remote-rendering system with client-server architecture that allows interactive display and manipulation of the artwork but provides only low resolution 2D renderings to academic users. To address the analog attack, the authors discourage 3D reconstruction from 2D images by having the server impose constraints on rendering requests, disallowing extremely close-up views of models and requiring a fixed field of view. This DRM model is geared towards shared content security and counters piracy by restricting what users can do with the graphics. The user, however, can share his login credentials but this kind of dishonesty does not impact the content owner's primary objective of preventing piracy. While this system is not device binding and can be accessed from any machine, it does limit the users' flexibility to use the graphics as the user does not own the content. This system is not designed as a business model to trade, manage, and monitor redistribution of sold content.

PTC [17] deployed a product called *Pro/Engineer* which customizes Adobes LiveCycle Rights Management ES [50] software for copyright protection of 3D CAD files. The purpose of the product is to restrict access of 3D CAD files (i.e. open, copy, change access restrictions,) to approved personnel. Implementation of this product is based on use of web services, authentication systems, and enterprise content management systems for centralized document protection, control, and administration. Lightweight Directory Access Protocol (LDAP) and Microsoft Active Directory implementations are used to authenticate recipients' credentials and provide protection based on existing identity and group structures. This DRM solution protects the graphic owner's right by offering content to consumers in a restrictive usage environment.

Cryptography-Based Implementation

There is no published work for this category. However, a product *OwnerGuard* [5] is available in the market and provides DRM functionalities for 3D AutoCAD drawings by use of licenses. Licenses define the rules for how the files can be used. License can be generated by specifying the i) time limitations - license duration or expire date, ii) input output limitations - allow copy to clipboard, screen capture, OLE drag and drop, save to new files, write protect the file, and iii) dependencies - hardware identifier of machine or operating system version.

In addition, *Visual Rights* is another commercial product rolled out by Informative Graphics [36] for enterprise document management by providing security controls that can be applied to a given file when published for viewing by one of company's products. This product provides copyright protection for documents, images, 2D and 3D CAD files. It is a client-server based implementation that utilizes proprietary file formats and viewers. The system utilizes standard AES 256 bit encryption. Users can publish a protected file and add controls such as password protection, hard or relative viewing expiration dates, allow/disallow printing and copying. For 3D CAD models, the product disables measurement and viewing with CAD layer controls and also supports blocking out specific content within a drawing file or hide the interior details of a model completely.

Cryptography-based digital rights management solutions use keys to protect contents and licenses to define access rights [89]. Content is bound to a license, and the content is only accessible as per the rules specified in the license. Implementations vary from vendor to vendor but a typical cryptographic solution locks the graphics file with a public key and packages the locked content with a header. The header contains an identifier to the public key and a location to the license associated with that file. The public key used to lock the file is unique to every user. This packaged content is encrypted and distributed to the consumer. The license consists of a user specific identifier that binds the license to the corresponding content, the public key that unlocks the content, seller's certificate to decrypt the packaged content and rules governing the use of the graphic content such as time limitations, counted number of usages, disabling copying of content, machine dependency, and restricting content editing. The associated license is encrypted and stored on a license management server at the seller's end. To access the purchased protected content, the buyer needs to get the license from the seller. The content consumption application on the buyer's side sends the user specific identifier to query the license server for retrieving the associated license. The user side application then checks the validity of the license, interprets and enforces the rules in the license to provide appropriate content access to the user.

Based on the usage policies defined in the licenses, these systems provide contents in limited usage conditions and usage environments. If the license is machine dependent, containing the hardware ID of the buyer's computer, it forces the content to be accessed on one computer. If the license is machine independent, the license can be illegally shared along with the content on P2P sites. Generally in such cases, the license server monitors the usage of the file from the license requests and multiple simultaneous illegitimate access attempts can be detected and denied by the server. But stand-alone offline systems cannot perform this check and fail to prevent unauthorized usage, thereby falling short of protecting the rights of content owners.

Cryptography and Watermarking-Based Implementation

Sohn *et al.* [134] propose a watermarking based 3D data files security component for an Intelligent Manufacturing System which is used to develop digital prototypes in the manufacturing industry. The objective of this system is to prevent 3D data files from leaking out of the organization. This server-based 3D watermarking system, named 3DGuard, works according to security policies that define the user's access rights and permissions. A watermarking plug-in intercepts a users upload or download action in order to embed, retrieve, or remove watermarks on 3D files as per security policies stored on server. Every 3D data file has a watermark that is specific to the user who last accessed the file from the system. In case a 3D data file is leaked out of the organization, the source of the leak can be determined by analyzing the user-specific watermark embedded into the file.

Kwon *et al.* [71] present a DRM scheme for 3D animation games serviced in mobile devices. Due to the limited bandwidth and high cost associated with directly downloading game content to a mobile device, game sellers allow consumers to download the game on a PC and then transfer the content to a mobile device. The scheme is designed to prevent illegal redistribution of purchased 3D game content by addressing scenarios where consumers illegally transfer the PC downloaded game content to multiple mobile devices. Authors present a solution that employs the Buyer-Seller watermarking protocol [85] for consumers protection and tracing illegal redistribution. The consumer generates a pair of public and private keys. The public key is circulated to a third-party referred to as the Watermarking Certification Authority, who is responsible for generating an encrypted watermark for the buyer. The watermark is then sent to the seller to embed into the game content. The seller inserts a second watermark in the game as well in case the consumer is able to remove the first watermark from the game content. The seller encrypts the game content with the buyer's public key such that the game can only be unlocked by the buyer using his private key. This encryption safeguards the consumer from dishonest sellers who may illegally redistribute a buyer's game to other consumers and hold the buyer responsible for piracy. Since the buyer is the only one with access to the private key that decrypts the game content, that game content cannot be unlocked by anyone else. Should the buyer share his private key and a pirated copy of the game is found, the seller verifies the unique tracer watermark of each buyer and determines the specified buyer suspected of unauthorized distribution.

These DRM solutions offer consumers full access to content, but the nature of the implementations facilitate users to make illegal copies as well. Therefore, these systems fails to prevent unauthorized distribution and usage. However, these systems do succeed in deterring illegal circulation since consumers are aware of the possibility of being tracked down and held responsible for piracy if the pirated content is found by the owners. The underlying assumption is that the watermark has not been damaged by the consumer to remove traces of his identity from the pirated graphic content. However, in order to make sure the tracer watermark identifies a customer without any disputes, the kind of watermark used should be unique to every customer.

Hardware-Based Implementation

Shi *et al.* [132] present a hardware-based digital rights management solution that integrates digital rights functionalities within the Graphics Processing Unit (GPU). Their goal is to counter piracy of real time graphics entertainment software. Authors propose the hardware design and API extensions to integrate cryptography within the GPU. The GPU has two additional components - a cryptographic unit to decrypt graphics data during rendering in real-time, and a license verification unit to process texture and shader binding constraints designated in the licenses of graphics data to circumvent security threats posed by loose coupling of textures and shader programs with geometry data.

Hardware DRM solutions provide a higher level of protection as opposed to software DRM solutions as it is difficult to break the system by software based attacks or by hardware tampering to dump signal traces at chip interconnects. However, hardware systems are not feasible for the consumer market due to cost concerns [26] since appropriate hardware components need to be installed on the consumers computer. Besides, this system is realized on a GPU architecture simulator. Hardware realization of the concept is far from reality yet, as the nature of the presented research requires a cross-disciplinary collaboration in digital rights management (DRM) community, graphics researchers, and GPU architects.

Comparison of DRM Solutions for 3D Multimedia

An assessment of the existing solutions based on - i) owner requirements or rights, ii) user requirements or rights, and iii) system features, and the comparison of various solutions is presented in Figure 2.3.

As far as the owner requirements are concerned, the digital content owner strives to prevent unauthorized usage to compensate for revenue losses incurred due to piracy. Should the content be leaked out of the DRM system, the owner prefers to have a mechanism that facilitates tracing the origin of piracy. Users require a system that provides content in a restriction free environment with no binding to any one machine. A DRM system is mainly characterized by three features - the ease with which it can be circumvented, the technology used for its implementation, and whether the system is interoperable with other systems or adopts a proprietary solution.

The objective of this dissertation is to integrate biometry, watermarking, and cryptography with client-server based DRM systems to support attributes of deter-

Figure 2.3: Comparison of DRM Systems. Notations used in the table Y: Yes, N: No, Crypto: Cryptography, WM: Watermarking, -: Unable to Comment

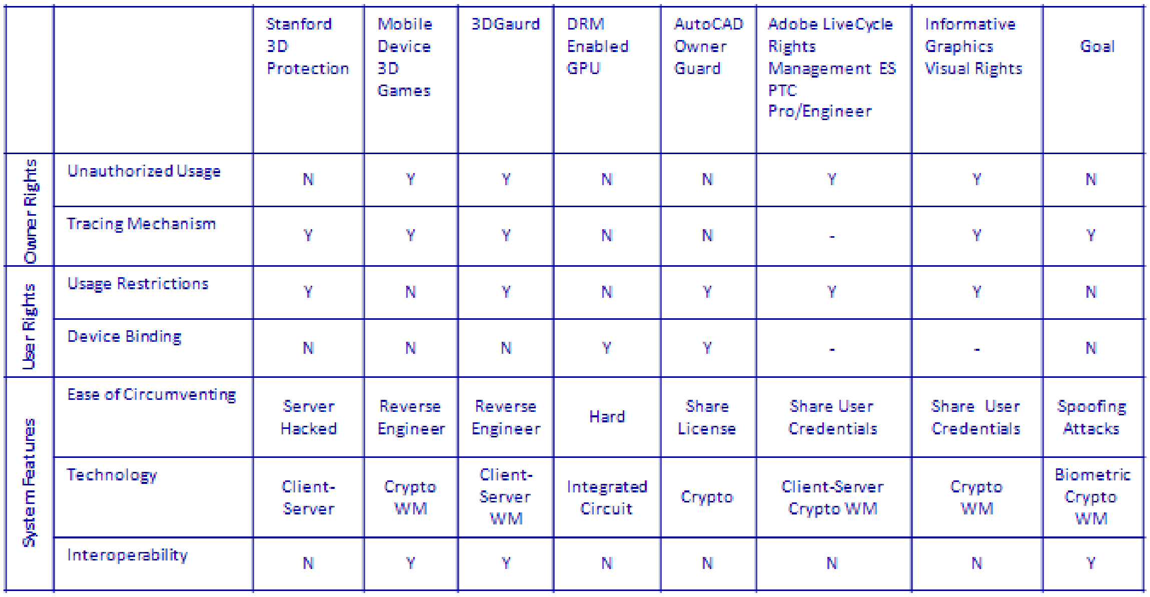

		Stanford 3D Protection	Mobile Device 3D Games	3DGaurd	DRM Enabled GPU	AutoCAD Owner Guard	Adobe LiveCycle Rights Management ES PTC Pro/Engineer	Informative Graphics Visual Rights	Goal
Owner Rights	Unauthorized Usage	N	Y	Y	N	N	Y	Y	N
	Tracing Mechanism	Y	Y	Y	N	N	-	Y	Y
User Rights	Usage Restrictions	Y	N	Y	N	Y	Y	Y	N
	Device Binding	N	N	N	Y	Y	-	-	N
System Features	Ease of Circumventing	Server Hacked	Reverse Engineer	Reverse Engineer	Hard	Share License	Share User Credentials	Share User Credentials	Spoofing Attacks
	Technology	Client-Server	Crypto WM	Client-Server WM	Integrated Circuit	Crypto	Client-Server Crypto WM	Crypto WM	Biometric Crypto WM
	Interoperability	N	Y	Y	N	N	N	N	Y

ring unauthorized usage, tracing origin of piracy, eliminate system imposed usage constraints on consumer, device independent use, and interoperability, as outlined in the last column of the comparison matrix.

2.3 Biometrics

2.3.1 Technology Overview

Definition

Biometrics is defined as the science and technology of measuring and statistically analyzing biological data of humans for the purpose of identification. The biological feature may be based on either a physiological characteristic - such as fingerprints, palm prints, facial features, iris, retina, vein patterns, or a behavioral characteristic - such as voice, handwritten signature, gait, and keystrokes.

Biometric System Functionality

A biometric system involves two phases - enrollment and authentication. During enrollment, the system acquires biometric data samples from an individual, extracts relevant features from the data, creates a mathematical representation of the data and stores it as a template. During authentication, this template is used to compare features extracted from the newly acquired biometric samples of the user to accept or reject the user from the system. Figure 2.4 outlines the components of a generic biometric system.

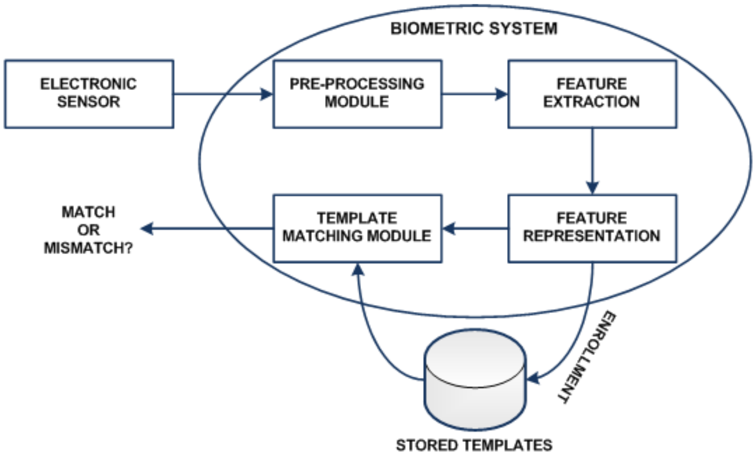

Figure 2.4: Biometric System Components

- Electronic sensor - for acquisition of the biometric trait in digitized form.

- Pre-processor - to simplify the acquired digital signal for subsequent operations without losing relevant information (such as eliminate noise or redundant information, or enhance the signal).

- Feature Extraction - to reduce the size of data by measuring certain features that correspond to the identity of an individual. A comprehensive literature review has been presented in [106] for different approaches employed for biometric feature extraction and template generation.

- Feature Representation - to construct a complex mathematical representation for features extracted for a particular individual. Multiple samples of a users biometric trait very rarely yield the same feature set that was derived from the enrollment sample. This is mainly due to imperfect sensing conditions arising out of faulty sensors, temporary variations in the users biometric characteristic due to injury/illness, changes in environmental conditions that introduce background interference in the signal, and improper interaction of the user with the sensor resulting in incomplete or unusable biometric samples. This variability in the biometric feature set of an individual is referred to as intra-class variation, which the constructed statistical model (also known as the biometric template) attempts to incorporate. For implementation details on various techniques to generate a biometric template for fingerprint, signature, face, and voice, readers should refer to [4].

- Template Matcher - used during authentication and constitutes a matching algorithm to compare the biometric features with the stored templates to determine user legitimacy.

Biometric Characteristics

It must be noted that no biometric measure can identify a person in a large population. Biometrics can only link an individual to a biometric pattern. The quantitative measures derived from a biometric trait can be extensively dissimilar or much alike across a population of individuals. Therefore, the performance of any biometric system is characterized by the following measures:

1. *False Rejection Rate (FRR)* - the probability that a true user identity claim will be falsely rejected, thus causing inconvenience to the user.

2. *False Acceptance Rate (FAR)* - the probability that a false identity claim will be accepted thus allowing fraud.

3. *Equal Error Rate (EER)* - the performance of a biometric system can also be evaluated in terms of this single-valued measure. The plot of FRR against FAR at various thresholds results in the Detection Error Tradeoff (DET) curve, a plot of which is shown in Chapter 5. EER is computed from the DET curve where the FAR equals the FRR.

Additional quantitative measures are:

- *False Non-Match Rate(FNMR)* - the probability that the acquired sample will not match the enrollment model.

- *False Match Rate(FMR)* - the probability that the acquired sample will match the enrollment model of another user.

- *Failure To Enroll Rate (FMR)* - the probability that a user will not be able to supply a readable measure to the system upon enrollment.

In our work we treat FAR/FMR and FRR/FNMR synonymously although these terms are not always equivalent [83]. In order to circumvent a biometric system, a user needs to create a false match by biometric mimicry or forgery of an enrolled user's biometric features. False non-matches arise out of low threshold values. Based on the nature of the application and the desired level of security to be achieved by the biometric system, the threshold can be lowered to reduce false accepts or increased to reduce false rejects.

It must also be noted that biometric measures cannot be revoked if compromised i.e. stolen or mimicked. Furthermore, privacy and security of biometrics is another factor of concern while devising a system that incorporates biometric data [1, 57].

2.3.2 Comparison of Various Biometrics

The choice of a biometric trait for a particular application is based on the error rates and failure rates discussed above, and various other factors discussed below. While each biometric trait has its pros and cons, this section only provides a brief overview of these characteristics for the most commonly used biometric traits. Readers are strongly advised to refer to [52] for an in-depth analysis of each biometric trait.

The most commonly used biometrics [20] for user authentication or personal identification are fingerprints, iris, hand geometry, face, voice, and signature. These traits are evaluated on the following factors [8, 54]: i) ease of use - how easy is it for the user to interact with biometric sensor, ii) user acceptance - a person's willingness to offer this trait for authentication and determining if the system is easier, faster, friendlier, and more convenient than the alternatives, iii) distinctiveness - extent to which the trait shows great variation over the population, iv) circumvention - ease with which the authentication system can be deceived by use of a substitute, v) long-term stability - variance of the trait with age, vi) sensor cost - price for the biometric trait scanning device, vii) template size - memory storage space required by the digitally compact and unique representation of the biometric trait, and viii) variability - factors owing to which the trait is inconsistent and varies among samples taken from the same individual at different instances of time. Figure 2.5 compares the most commonly used biometrics based on these factors.

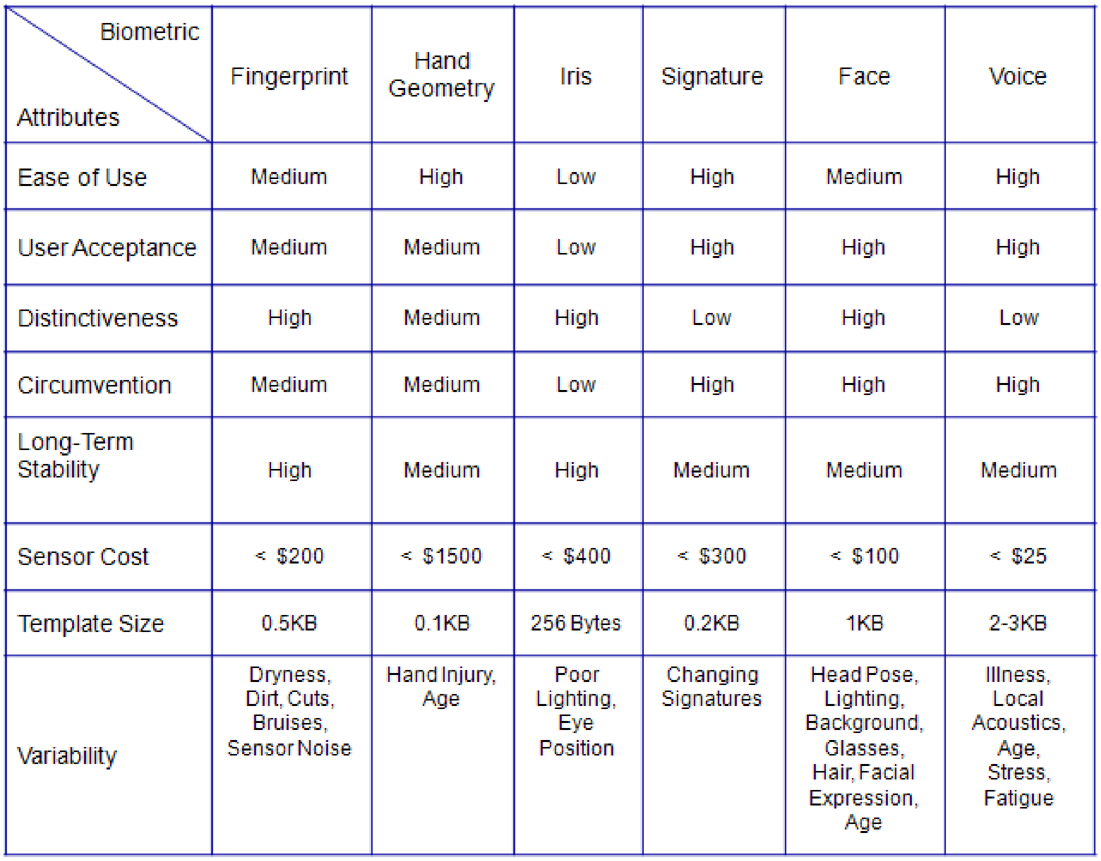

Biometric Attributes	Fingerprint	Hand Geometry	Iris	Signature	Face	Voice
Ease of Use	Medium	High	Low	High	Medium	High
User Acceptance	Medium	Medium	Low	High	High	High
Distinctiveness	High	Medium	High	Low	High	Low
Circumvention	Medium	Medium	Low	High	High	High
Long-Term Stability	High	Medium	High	Medium	Medium	Medium
Sensor Cost	< $200	< $1500	< $400	< $300	< $100	< $25
Template Size	0.5KB	0.1KB	256 Bytes	0.2KB	1KB	2-3KB
Variability	Dryness, Dirt, Cuts, Bruises, Sensor Noise	Hand Injury, Age	Poor Lighting, Eye Position	Changing Signatures	Head Pose, Lighting, Background, Glasses, Hair, Facial Expression, Age	Illness, Local Acoustics, Age, Stress, Fatigue

Figure 2.5: Comparisons of Various Biometrics [8, 54]

The false match and non-match error rates for the most commonly used biometrics are listed in Table 2.1. These numbers are collected from [53].

Table 2.1: Performance Evaluation of Commonly Used Biometrics

Biometric	FTE	FNMR	FMR
Face	N/A	4%	10%
Finger	4%	2%	2%
Hand	2%	1.5%	1.5%
Iris	7%	6%	≤0.001%
Voice	1%	15%	3%

Why did we chose Voice Biometric for our Application?

Studies ([57, 101]) on comparison of various physiological biometrics (fingerprint, face, iris, retina, palm print) and behavioral biometrics (handwritten signature, voice, gait, keystroke dynamics) indicate iris and fingerprints as the most desirable biometric traits due to their persistence over time (least variability of biometric trait with age), performance (lower false accept and false reject rates) and distinctiveness (uniqueness of the trait in the population) properties. However, these traits are not appropriate for use in DRM systems owing to user's unwillingness to offer these traits to non-government organizations due to privacy concerns. Besides, special and expensive hardware device such as fingerprint scanners or high resolution iris image capture cameras would be required to install at the client-side.

Since user acceptance drives the success of any application, we consider signature, face, and voice biometric traits as the most eligible candidates for selection. Hand geometry is not appropriate for DRM applications since is not unique for every individual and requires bulky scanners. In addition to sensor costs for handwritten signature scanning being relatively higher than face and voice biometric sensors, signatures can also be easily forged; therefore, this trait is not considered to be favorable. Face and voice are more practical choices in this context assuming that desktop PCs and laptops are equipped with in-built cameras and microphones. However, face image acquisition requires fixed head pose, fixed background and appropriate illumination conditions. These conditions are not feasible to control at the user's end. On the other hand, local acoustics such as no background noise for voice capture, is relatively easier to impose as a requirement on the user. With face biometrics, the camera can be easily spoofed by a face photograph in place of a live face, while a voice biometric system can be spoofed by a pre-recorded voice sample of an individual. But voice has an added benefit which static biometric traits such as face, fingerprint and iris lack - owing to its behavioral and dynamic nature this biometric serves as a dual channel with the capacity of delivering information (spoken words) along with personal identity (speaker's voice). This unique feature of voice can be exploited to deal with spoofing (using user's pre-recorded speech) and data simulation attacks [151] on the biometrics authentication process. Prompting the user to speak random phrases [41] during authentication introduces an additional layer of verification (since the user's pre-recorded speech can no longer bypass the authentication process) and increases the overall security of the system.

Therefore, factors such as higher security, cost-effectiveness of biometric sensor device (affordable low cost PC microphone device), ease of voice acquisition with less restrictions on the user for capturing the biometric trait, pervasiveness (automated speech recognition telephone systems), and less complexity in signal processing due to voice's one-dimensional nature, make voice a good candidate for selection as a biometric trait for watermarking.

2.4 Digital Watermarking

2.4.1 Technology Overview

Terminology

Digital watermarking is defined as perceptible or imperceptible insertion of information into digital content for the purpose of copyright protection, owner identification, content authentication, tamper detection, data labeling, access control, or various other applications [18].

The digital host medium in which the copyright information is embedded is referred to as the *cover* or *host signal*. The different watermarking host media are - digital documents, digital images, audio, video, 3D models, graphic animations, executable code, and integrated circuits.

The embedded information that is inserted in the cover-signal, is referred to as the *payload* or *watermark*. The digital watermark encoded into digital data is an identifying code and may consist of a bit sequence, random numbers, text representing user's unique ID or copyright ownership message or cryptographic keys or access conditions of the content, logos, image, biometrics or content-based information.

The *watermarking scheme* is defined as the set of algorithms required for insertion and extraction of the watermark. Figure 2.6 shows the two components of a watermarking system - embedder and detector. The embedder is responsible for inserting the watermark into the digital content, while the detector is responsible for retrieving this embedded watermark from the host medium.

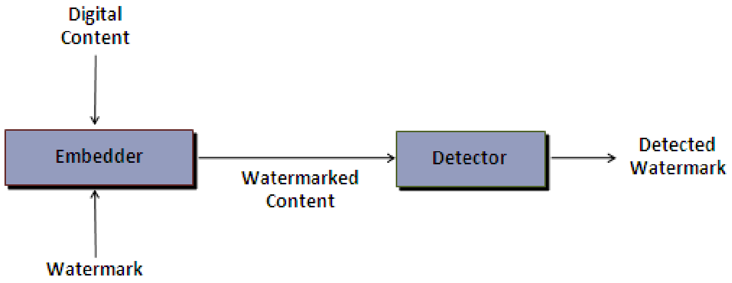

Figure 2.6: Generic Watermarking System

Desired Properties of a Watermark

Watermarking schemes are evaluated on the basis of these two measures:

- Unobtrusiveness - The embedded watermark should not interfere with intended use or function of the host data. Perceptible watermarks are therefore faded to appear in the background as transparent marks or are placed in the bottom or top corner of the visual media to serve as proof of ownership and to imply authenticity of the content. On the other hand, imperceptible watermarks should be embedded in a way that does not distort the original media by creating any visual artifacts.

- Robustness - Robustness requirement is necessary to assure that common signal processing and malicious modifications do not impact the detection or retrieval of the watermark. Any attempts to delete the watermark should destroy the watermark itself or damage the host data or else the watermark should resist all attacks. The embedded watermark should persist despite geometric transformations and noisy transmission channels. The objective of this requirement is to facilitate content owners to prove their ownership over illegitimate copies of their media by retrieving the watermark from a pirated medium and then litigate against the offender.

Watermarking Research Areas

The four principal components of digital watermarking schemes which distinguish one watermarking algorithm from another are - i) what information is inserted as a watermark, ii) where is the watermark inserted into the host media, ii) how is the watermark inserted into the data of the host medium (i.e. addition, subtraction, bitwise operation), and iv) what is the payload size i.e. how many information bits can be embedded as watermark. Components ii)-iv) also constitute as the major areas of research in the watermarking field, with the focus on achieving high payload capacity while maintaining imperceptibility of the embedded watermark.

Classification of Watermarking Schemes

The category of a watermarking scheme is determined by one of the following properties:

1. Perceptibility

   The application scenario of a particular digital content determines whether a watermark should be perceptible or imperceptible. A perceptible watermark is most commonly used for ownership identification and informing users that the content is authentic. However, such watermarks are easy to remove by adversaries since the location of the watermark is known (eg. CNN's logo displayed at the corner of the broadcasted video content), can be aesthetically ugly at times, may cover a portion of the content, and their obtrusiveness increases susceptibility to being cropped. On the other hand imperceptible watermarks are used for proof of ownership, content labeling, and in validation of intended recipient. These watermarks are difficult to remove as their location in the host medium is not known and can only be guessed by an adversary. This distinction gives rise to two types of watermarking schemes:

i) *Visible watermarking*, which refers to the process by which the watermark embedded into the digital content is visible. This watermark is some text or a logo which identifies the owner of the host media.

ii) *Invisible watermarking*, which refers to the process by which the watermark information is added to the multimedia content, such that it cannot be perceived. A watermark can be imperceptibly inserted into a digital host medium by slightly modifying the host signal.

2. Robustness

This property defines the strength and persistence of the watermark to adversary attacks. The three categories of robustness are listed below:

i) *Robust* - The watermark can resist modify and/or delete attacks. It can survive common signal processing operations (such as filtering, compression, noise), printing and scanning, and geometric distortions (such as rotation, translation, scaling).

ii) *Fragile* - The watermark is invalidated by slightest modification of host medium. It does not survive high noise level, compression, or signal processing attacks.

iii) *Semi-Fragile* - The watermark is only destroyed by major changes to the host medium but survives mild signal processing operations.

3. Embedding Method

   Figure 2.7 outlines the embedding component of the watermarking system. Every host medium has different categories into which the embedding processes can be classified. For example: image, audio, and video watermarking techniques modify the host medium in the spatial/temporal domain or the frequency domain or in both domains. For 3D graphics the watermark embedding process can be categorized as geometrical, topological, or vertex re-ordering approaches. Therefore, the type of method used for inserting the watermark serves as an important property for classification of watermarking schemes.

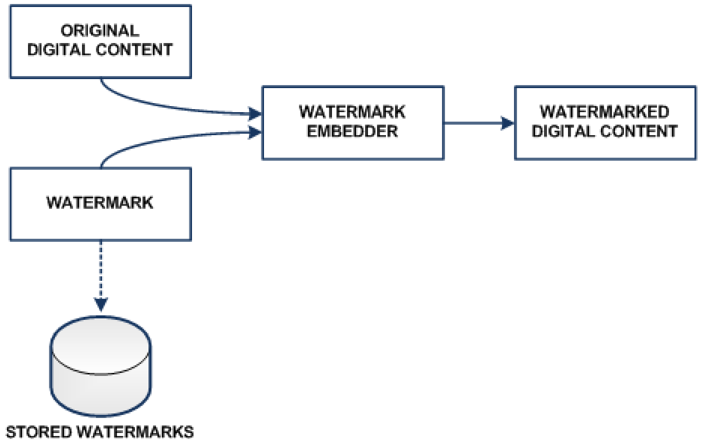

Figure 2.7: Watermark Embedder

4. Retrieval Method

   Figure 2.8 outlines the three types of extraction or detection process of the watermark. The watermark detection/extraction process can be informed/non-blind (retrieval process requires access to the original content (i.e host signal) along with the embedded piece of data), semi-blind (detector requires access to some side information and/or the watermark but not the original content), or blind (detection is performed without access to the original content). In semi-blind watermarking, the embedding and retrieval process is assisted by a secret key, in which lies information on where and to what extent has the original content been modified in order to accommodate the watermark.

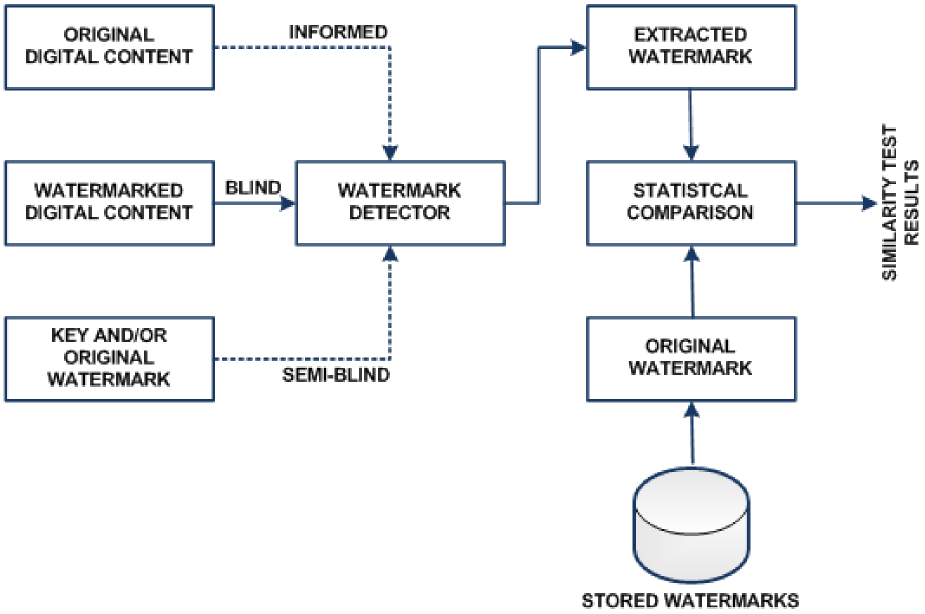

Figure 2.8: Watermark Detector

Attacks

This section lists the most common category of attacks on a watermarking system. Further reading [18, 69] is required for those interested in gaining more insight into different categories of attacks.

- Signal Processing Operations - The adversary subjects the watermarked content to various operations such as filtering, dithering, cropping, scaling, and compression with the intent to destroy the watermark.

- Geometric Operations- If the watermarked digital content survives affine transformations, the watermarking scheme is resistant to geometric attacks.

- Removal Attack - In this attack, the adversary attempts to remove or destroy the watermark, without affecting the host medium.

- Forgery Attack- If the attacker is successful in embedding a valid watermark, then he can claim ownership over the digital content in addition to the true owner, for there is no legal framework or centralized repository for watermarked content that can assist in disputing such false claims.

- Collusion Attack- In this attack, the attacker uses several copies of the watermarked content to construct a copy with no watermark.
- Cryptographic Attacks - The adversary attempts to crack security methods in the watermarking scheme, implements a brute force search for embedded information, and embeds misleading watermarks.
- Protocol Attacks - The adversary subtracts his watermark from the data to claim ownership, thereby falsely accusing the true owner of forgery.

To date, no benchmarking tools exist to evaluate the performance of 3D watermarking algorithms. This dissertation attempts to devise a scheme that can cover only a subset of the above mentioned attacks, such that the effect of most common operations on 3D models i.e. noise, cropping, smoothing, and quantization are analyzed.

Limitations of Watermarking Technology

It is evident from the attacks, that watermarking technology only serves as a deterrent against wrong-doing. It requires a central repository of the original or watermarked work and a proper legal framework to be effective. In addition, the lack of any algorithm being robust to all types of attacks and the lack of a general benchmarking tool for all types of host media (since each host medium has its own set of properties that cannot be generalized to be applicable for another medium), has prevented this technology from penetrating into the industry at a full-fledged scale.

Applications of Watermarking

Watermarks have been used for a wide a variety of applications:

- Authentication - The watermark consists of information that assists in determining that the content is authentic. If the watermark can be extracted and matched to the information representing authenticity of the content then it serves the purpose of content authentication assuring the user that the content has not been altered during its passage through a noisy or non-secure communication channel.

- Copyrights - The watermark contains information about the rules of usage and copying which the content owner wishes to enforce. The content consumption applications or devices that can play the content might look for the watermark and compare it with information, such as whether the content is on a recordable storage device, to identify illegal copies and deny to play the content.

- Signatures - The watermark identifies the owner of the content, and is basically used to help settle ownership disputes.

- Broadcast or Transaction Monitoring - The content consumption applications embed transaction identifiers as watermarks into the content, which serve as transaction logs that are detected by automated systems to monitor television and radio broadcasts, computer networks, and any other distribution channels to keep track of when, how and where the content appears or is being used.

- Fingerprinting - For security applications, where the same content is distributed to multiple users, the content is embedded with different watermarks where each watermark is specific to a user. In case the watermarked content is leaked out to unauthorized personnel, the content is examined for the unique watermark to determine the source of leak.

- Data Labeling - The content is labeled by different data using watermarks to inform the content consumption application of the different purpose or modes of usage for the same content.

Watermarking in the Industry

Despite its limitations, watermarking technology has been adopted by the industry for a wide variety of copyright protection applications. What follows is a list of key industry players in multimedia watermarking: Cinea (Video watermarking) [48], Digimarc (Document watermarking) [47], GCS Research (Satellite Images watermarking) [139], MSInternational (Audio watermarking) [16], Philips Electronics (watermarking of Movies) [33], Signum (Documents and Images watermarking) [140], Civolution (Audion and Video watermarking) [13], Teletrax (Broadcast Monitoring) [141], Thomson (watermarking of Motion Pictures) [136], Verance (Audio watermarking) [146], Verimatrix (Video watermarking) [147], Alpha Tec and Houdini (3D Graphics watermarking) [49, 81].

Since this dissertation deals with biometric watermarking of 3D models, the next two sections provide an extensive review of biometric watermarking and 3D watermarking approaches.

2.4.2 Literature Review of Biometric Watermarking of Digital Content

Biometric watermarking embeds a biometric template into the host medium. While watermarking of multimedia such as image, audio and video is reaching maturity, watermarking of 3D multimedia is still a technology in its infancy phase. Moreover, biometric watermarks have not been explored yet for protecting 3D models. Fingerprint, iris, face, voice features, and signature images have been employed by several biometric watermarking techniques for still images, audio and video. Figure 2.9 shows the various biometric traits that have been explored for use in digital media.

Due to the lack of any published work on biometric watermarking of 3D multimedia, this section is a comprehensive review of biometric watermarking literature for digital documents, images, audio, and video host mediums from the perspective of what benefits does utilizing biometrics as watermarks offer.

Jain *et al.* [55] present a fingerprint image watermarking method that embeds facial information into host fingerprint images. This scheme has the advantage that in addition to fingerprint matching, the recovered face during the decoding can be used to establish the authenticity of the fingerprint and the user. Satonaka ([128]

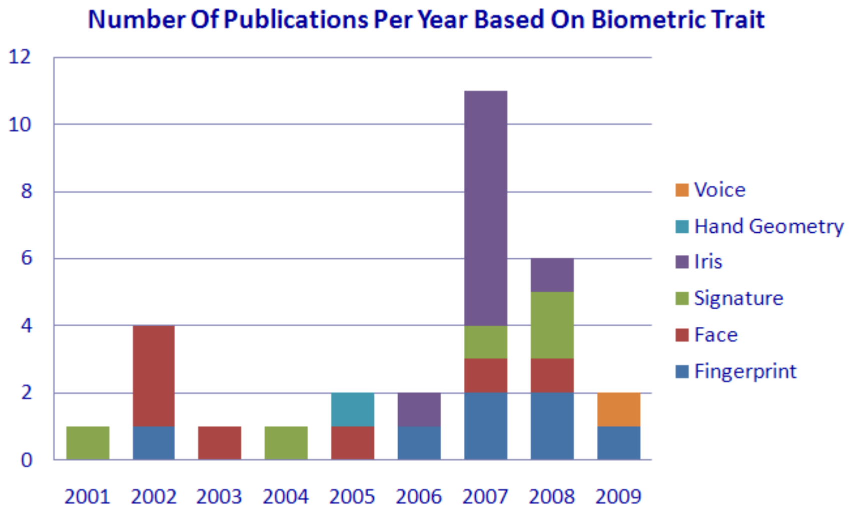

Figure 2.9: Research Trend - Biometric Watermarking

and [129]) embeds a face print as a biometric template into face images for biometric authentication through a distributed network. Biometric watermarking is used for accurate facial signature authentication. Uludag *et al.* [56] hide fingerprint minutiae data in a host image to enable secure exchange of fingerprints. If the host is a face image, the proposed method provides an additional cue in authenticating the user. The host image serves as a carrier of the biometric data used for user authentication.

In [54], the authors use eigen-face coefficients to watermark fingerprint images for security and integrity of fingerprint biometric data. Namboodiri and Jain [103] propose to secure document images by an image watermark generated from the author's digitized handwritten signature. Vatsa *et al.* [145] propose a biometric image watermarking algorithm to improve recognition accuracy of face and fingerprint biometric images in addition to protecting these images from tampering. Sun *et al.* [137] present a multimodal biometric scheme using watermarking technique to provide more secure and reliable personal recognition. Knuckleprint biometric feature is used as watermark to be hidden in the palmprint host image. The knuckleprint watermark not only protects palmprint biometric data, but is also used as a covert recognition. In addition, the bimodal biometrics recognition provides an improvement in the accuracy performance of the biometric identification system.

Hsieh *et al.* [45] discuss a copyright protection scheme for images using fingerprint images. The scheme does not alter the host image but encodes a share image by using features from the host image and scrambled version of the binary fingerprint image. During the fingerprint retrieval phase this share image is used along with features extracted from the suspected image to decode the scrambled fingerprint image. Unscrambling rearranges the fingerprint image, which is used to verify copyright. Hassanien [40] propose to protect the ownership by hiding an iris data into digital image for an authentication purpose. The idea is to secretly embed iris print in the content of the image for the purpose of identifying the owner.

In [46], the authors employ multimodal biometric to improve security and privacy in fingerprint authentication system. The proposed scheme embeds and extracts an iris template in a fingerprint image. Noore *et al.* [104] discuss a digital watermarking technique that uses face image and demographic text data image as multiple watermarks for protecting the evidentiary integrity of fingerprint images. Jung *et al.* [65] present a method that identifies users in compressed video streaming with their biometric watermark. The proposed algorithm generates watermark using the preprocessed fingerprint image, and then inserts the image in H.264-based video coding streams.

Park *et al.* [108] proposed an iris feature watermarking method on face image data for the following objectives - multimodal biometric authentication to increase the authentication accuracy, ownership verification by extracting the embedded iris print, and transmission of biometric data over non-secure and noisy communication channel by embedding it as a watermark into host data. Feng and Lin [27] adopt iris biometric to be inserted as watermark into host document images in order to protect the document and assist in owner identification. Varbanov and Blagoev [143] use an MD5 hash of iris templates to watermark digital images. Low *et al.* [80] use an offline handwritten signature as watermark for host images to authenticate the claimed source of the digital image. Claus *et al.* [148] embed a handwriting biometric trait as a watermark in the form of signatures, passphrases, and sketches for the purpose of user authentication, ownership identification and verification of digital content.

Wang *et al.* [149] describe an authentication scheme of a DRM system which integrates a watermarking technique and a multimodal biometric system to provide more secure and reliable personal recognition. In the watermarking algorithm, a face image is chosen to be the host image and the iris feature is selected to use as a watermark hidden in the host image. Hoang *et al.* [42] adopt biometric watermarking for security of the biometric templates in user authentication systems. Encryption does not provide security once the biometric templates are decrypted; therefore, biometric watermarks are embedded into the decrypted host biometric templates to provide security after decryption. Teoh *et al.* [79] insert a handwritten signature in the host image to establish legitimate ownership.

Paik *et al.* [66] present a user identification method for H.264 video streams using a fingerprint watermark. The biometric watermark is used to reduce the potential danger of forgery or alteration of the host data and to improve reliability of verification using automated fingerprint identification systems. Sharma *et al.* [43] propose a remote multimodal biometric authentication framework based on fragile watermarking for transferring multi-biometrics over networks to server for authentication. A facial image is used as a container to embed other numeric biometrics features. The purpose of the framework is to enhance security and reduce bandwidth. Tee *et al.* [78] embed a handwritten signature in the host image as a notice of legitimate ownership.

Rao *et al.* [117] embed fingerprint biometric features of the owner as a watermark to prove ownership of digital images. Musgrave's [100] patent on a generic biometric watermark system generates a biometrically encoded bitstream from biometric data of a user and from electronic data to be transmitted to the user. The encoded bitstream has the biometric data acting as a biometric watermark. The encoded bitstream is then sent to a decoder of the user, with the biometric watermark providing security in the transmission.

Lastly, Vatsa *et al.* [144] discuss a watermarking algorithm that fuses voice features into a face biometric image. The technique embeds mel-frequency cepstrum coefficients (MFCC) of an individual's voice into the face image of the same individual. However, the watermark formulation ignores the intra-individual variability of the voice data and assumes that the MFCC extracted features are invariant for an individual. A statistical modeling component is required to incorporate variability in an individual's voice features due to factors such as improper interaction with the biometric sensor, background noise during voice capture, and variations in an individual's voice captured at different instances of time. The proposed approach in this dissertation overcomes these shortcomings in the voice print based watermark formulation by statistically modeling the voice feature data.

2.4.3 Literature Review of 3D Mesh Model Watermarking

This section presents related work on 3D watermarking with emphasis on mesh models. Mesh models approximate a 3D object by a set of planar triangles. Due to their simplicity in representation and speedier rendering mesh models are widely used in the industry.

Figure 2.10 shows the mesh representation (right) of a 3D model (left). The dots in the mesh representation represent vertices that define the (x, y, z) co-ordinates of the mesh model. Other 3D model representations use surfaces that interpolate parametric curves such as NURBS, B-Splines, and Beizer curves. However, the focus of this dissertation is to watermark 3D models that are represented by triangular meshes.

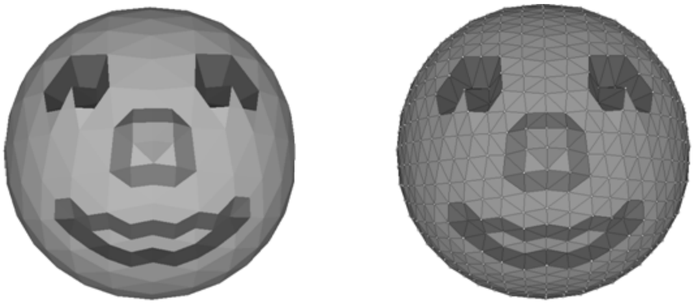

Figure 2.10: Mesh Representataion of 3D Model

Mesh models consist of the 3D model's geometry (a set of (x, y, z) vertices), and connectivity (triangular faces formed by connecting line segments joining three vertices). The watermark can be inserted in the spatial domain by modifying the geometry or connectivity of the mesh model or in the spectral domain by modifying the spectral coefficients of the mesh model [150]. Extraction of the watermark can be blind, semi-blind, or informed(non-blind). A non-blind retrieval process requires access to the original model while semi-blind process requires access to some side information and/or the watermark but not the original model, and blind retrieval is performed without access to the original model or the watermark.

There are 3 main approaches to 3D watermarking: 1) geometry-based techniques, which involve altering the positions of vertices, 2) topology-based techniques, which modify vertex connectivity, and 3) vertex re-ordering techniques, which change the order of vertices in the 3D model's file format representation. An extensive survey of 3D watermarking algorithms based on these three approaches can be found in [60]. In addition, readers are also advised to refer to [2] for a thorough survey with classification and critical analysis of watermarking algorithms for 3D models.

The watermarking approach in this dissertation adopts a geometry based technique and exploits the curvature variation in meshes using surface normals to embed the watermark. Curvature estimation is an important task in 3D object description and recognition because surface curvature provides a description of local surface shape. A variety of curvature computing methods are discussed in [30]. Normal vectors are most widely used for curvature estimation. The presented related work focuses on algorithms that embed an imperceptible watermark into a 3D mesh model by exploiting the normal vector distribution. The related literature is presented by summarizing the watermarking approach and the robustness of the watermark to attacks such as mesh simplification, remeshing, rotation, scaling, translation, cropping, noise, and smoothing operations.

Han *et al.* [38] propose a geometry-based watermarking approach that embeds a content-based watermark and uses a non-blind detection technique. The authors analyze the mean curvature and fluctuation of curvature of the regions of the 3D mesh model to choose the appropriate regions to embed the watermark. The Voronoi method [87] is employed to compute the curvature of the mesh. Fluctuation of curvature is computed from the Gaussian-weighted average of the mean curvature. Regions with large curvature and low curvature fluctuation are selected to accommodate the watermark as these causing least visual distortion to the model. A threshold value for the curvature fluctuation eliminates regions not suitable for watermark insertion. The watermark is embedded by altering the vertex co-ordinate using a visual distortion measure and a normalized vertex normal. The technique is robust against rotation, scaling, cropping, noise, and smoothing.

Kwon *et al.* [70] propose watermarking for 3D polygonal meshes using normal vector distribution and extended Gaussian image (EGI) [44]. The 3D model is divided into patches and the normal vectors of each mesh in the patch are mapped to one of the several bins that subdivide the unit sphere of the EGI. The length of each bin is the sum of area for all the meshes that are mapped into it. These bins are arranged in descending order of their length. Bins with large length are selected as locations for watermark embedding. The watermark is a 1 bit (0 or 1) random sequence of length N and the i^{th} bit is embedded in the i^{th} bin corresponding to each patch. The watermark is embedded by changing the average value of the angle between the normal vectors of mesh surface and the normal vector of the bin center. The normal vectors in the selected bin are changed according to the bit of the watermark, thereby changing the position of vertices in the 3D model. The watermark extraction process does not require the original model. The algorithm is robust against mesh connectivity altering, additive noise, and cropping attacks.

Jabra and Zagrouba [51] present a robust watermarking algorithm that exploits the benefits of geometric, topologic, and spectral schemes to achieve robustness against a wide variety of attacks. The authors segment the original model into multiple sub-connected meshes that are classified into convex, concave, and plane regions. The watermarking scheme for each segment is determined by the Gaussian and mean curvature value of these regions. The Gaussian and mean curvatures of convex regions are positive. Concave regions have a negative mean curvature and a positive Gaussian curvature while plane regions have Gaussian curvature approximately equal to zero. A geometric watermarking approach is utilized for concave regions and convex regions are watermarked using topologic techniques. Spectral watermarking is adopted for the plane regions where insertion is done in low frequencies. The algorithm employs a blind detection approach. The algorithm is robust against affine transformations, mesh simplification, smoothing, remeshing, additive noise, and cropping attacks.

Lee and Kwon [73] propose 3D mesh watermarking using the complex extended Gaussian image (CEGI) distribution. The meshes in a 3D mesh model are clustered into various patches using a distance measure. The surface normal vector of each mesh in a patch is mapped into a unit Gaussian sphere. The weight of each point in the Gaussian sphere is equal to the area of the mesh surfaces for a given normal. The weight mapping represents a histogram that records the variation of the surface area according to the surface orientation. The CEGI concept extends the EGI representation by adding the normal distance of a mesh to the origin of the model as a phase component of the complex weight. Unlike EGI representation, CEGI allows the pose of the 3D mesh to be extracted and also distinguishes a convex model from a non-convex model. The watermark bits (0 or 1) are embedded into the normal vector direction of the meshes that are mapped into cells with large complex weights in the patch CEGIs. The semi-blind watermark extraction is based on two watermark keys, the known center point of each patch and a weight rank table of the cells in each patch. The algorithm is robust against mesh simplification, cropping, and rotation and does not require the original model for extracting the watermark.

Liu and Yang [76] propose a 3D watermarking scheme based on feature points that carry the principal shape information of the model. The selected feature points represent the high variation areas of the model and are used as centroids for a Voronoi diagram to cluster all the vertices of the model into several segments. For each segment, the vertices are projected onto a reference plane. The normalized distance between a reference point on the plane and the intersection point of a ray from this reference point to the surface of the model is used to obtain a range image. A DCT transform is applied to the range image to embed the watermark (bit -1 or 1). The watermarked 3D mesh is reconstructed from the modified range data. The detection of the watermark information requires the original range image. The algorithm is resistant against mesh simplification, additive noise, and cropping. The feature points in this algorithm are used by mesh simplification and surface subdivision techniques and maintain the main shape of the mess. If the 3D mesh is attacked by simplification, its feature points are survivors. Therefore, this algorithm is resistant to mesh simplification.

Alface and Macq [3] discuss a 3D mesh watermarking technique based on feature points. The points for which the minimum and maximum curvatures are equal at a vertex are referred to as umbilical points. These points share the same curvature in all directions of the tangent plane. Since umbilical points may be due to noise in the geometry or due to the coarseness of the sampling of the input mesh, a multi-scale analysis is adopted to discriminate intrinsic umbilical points from those due to noise. The scale is the size of the vertex neighborhood used to estimate the curvature at a vertex. Umbilics representing the larger mean curvature are selected as feature points. The mesh shape is then partitioned using a geodesic Delaunay triangulation of the detected feature points. To tackle remeshing manipulations, each of these geodesic triangle patches is then parameterized and remeshed by a subdivision strategy. These steps provide a mesh which only depends on the mesh shape and resists to connectivity or sampling changes. These remeshed patches are then watermarked in the spectral domain. The algorithm resists affine transforms, white noise addition, smoothing, cropping, and sampling changes such as decimation, subdivision, or remeshing. The watermark is retrieved by blind detection.

Motwani *et. al* [90] propose a wavelet-based watermarking technique that uses fuzzy logic to determine an optimal value for the watermark amplitude to be inserted in a 3D model. The system is adaptive to the local geometry of the mesh and inserts an 8-bit grey scale image as a watermark. Initially, all mesh vertices are normalized and then a wavelet transform is applied by using even vertices to compute scalar coefficients and odd vertices to compute wavelet coefficients. Fuzzy input variables are computed considering the geometry of the model such as area, curvature, and bumpiness of the surface corresponding for each vertex. Curvature and area for the mesh vertices are computed in the spatial domain whereas bumpiness for the corresponding vertex is computed in the wavelet domain. Curvature is the amount by which a geometric object deviates from being flat. Curved surface consist of more number of smaller triangles as compared to a flat surface. Curvature is computed by taking average of the angles between surface normals of 6 neighboring vertices and the average surface normal. Area of the triangular face formed by 3 vertices is computed by the magnitude of the normal to the triangular patch. A bumpy surface is a surface which is not smooth but is irregular and uneven. A bumpy surface has more details associated with it and thus has more watermark holding capacity. Bumpiness is calculated by dividing the wavelet coefficient magnitude by the length of vector joining two even neighbors. The output of the fuzzy system is a single value which corresponds to a perceptual threshold for each corresponding wavelet coefficient. The watermark is inserted by modifying the magnitude of the wavelet coefficient vector based on its fuzzy inference value. An inverse 3D wavelet transform is then computed to get the watermarked model. The algorithm is non-blind and requires the original model and original watermark to extract the watermark. The algorithm is robust against smoothing, cropping, affine operations, and noise attacks.

Benedens [7] proposes a geometry-based 3D mesh watermarking scheme that is resistant to mesh simplification attacks. The system uses a collection of surfaces from the 3D mesh model as an embedding primitive. These collections are generated by grouping mesh normals to distinct sets called bins. Each bin is defined by a bin center, a normal in three dimensional space and a radius, and an angular difference to the center normal. A bin is assigned all model face normals whose angular difference is less or equal than the bins radius. Bin centers and radii are chosen in a way so bins do not overlap. The embedding process takes the original model, a key, and a watermark bit string. From the key, non-overlapping bins, bin centers, and radii, are derived. For encoding one bit of watermark information, the normals in one bin are changed with respect to certain measures called feature types, such as the mean normal of the bin, the mean angle difference of the bin normals to the bin center, and the amount of normals contained in the kernel of the bin relative to the total amount of normals in bin. The embedding algorithm tries to move normals towards or away from the kernel (depending on the bit to be coded) and optimizes the embedding process with the assistance of a cost measure. The outputs of the embedding process are the watermarked model and the original feature values which are needed as reference values in the retrieval process. The semi-blind retrieval process takes the watermarked model, the key, and the feature values.

Lavoué [72] introduces the notion of roughness for a 3D mesh object. The author talks about three principal relevant categories of regions in a 3D object, such as edge, rough, and smooth regions. These categories are associated with different watermark embedding strengths. A rough region exhibits a high degree of watermark insertion capacity, whereas a geometric change on edge or smooth regions is much more visible. For each vertex, the corresponding roughness is processed by computing an asymmetric difference between local average curvatures [14] computed on the original mesh and on a smoothed version. The average curvatures computed over local windows aim at detecting regions associated with high geometric variations. These variations can be due to rough textured regions or edges. On the smoothed version of the object, the geometric variations disappear while edges are preserved. By computing curvature difference between original and smoothed versions, the real geometric variations (i.e. the roughness) are accurately differentiated from the edges. This curvature difference represents the robust roughness measure for the polygonal meshes and can be used for selecting appropriate regions for watermarking.

Table 2.2 provides a comparison of the reviewed literature. The majority of the algorithms reviewed thus far can embed bit sequences only and cannot be adopted for

Table 2.2: Comparison of Various Watermarking Schemes

Algorithm	Watermark	Approach	Retrieval	Robustness
Han *et. al* [38]	Content -Based	Geometry	Informed	Rotation, Scaling, Translation, Cropping, Noise, Smoothing
Kwon *et. al* [70]	1-Bit Sequence	Geometry	Blind	Mesh Simplification, Cropping, Noise
Jabra and Zagrouba [51]	1-Bit Sequence	Geometry, Topology, Spectral	Blind	Mesh Simplification, Remeshing, Rotation, Scaling, Translation, Cropping, Noise, Smoothing
Lee and Kwon [73]	1-Bit Sequence	Geometry	Semi-Blind	Mesh Simplification, Remeshing, Rotation, Translation, Cropping, Noise
Liu and Yang [76]	Bit Sequence	Geometry	Semi-Blind	Mesh Simplification, Cropping, Noise
Alface and Macq [3]	64-Bit Signature	Spectral	Blind	Subdivision, Decimation, Cropping, Noise, Smoothing
Motwani *et. al* [90]	8-Bit Grey Scale Image	Spectral	Non-Blind	Rotation, Scaling, Translation, Cropping, Noise, Smoothing
Benedens *et. al* [7]	Bit Sequence	Geometry	Semi-Blind	Mesh Simplification

our approach as we need to embed a biometric template of size over 2 KB for a voice signal. The proposed watermarking algorithm computes a local smoothness measure to select regions for watermark insertion and it takes motivation from a variety of algorithms reviewed thus far to achieve reasonable embedding capacity that can afford payload ranging from 2-20 KB. Chapter 3 presents the proposed curvature-based watermarking approach that exploits voice biometric as the watermark.

2.5 Voice Signal Processing

The speech signal is a complex wave that not only carries linguistic information but also information representing the identity of the speaker. While speech recognition techniques focus on the linguistic component of the speech wave, voice biometric systems such as speaker verification systems, focus on the speaker specific information conveyed by the speech signal. The focus of this chapter is to briefly introduce the fundamentals of voice signal processing and the elements of a speaker verification system that are utilized in Chapter 3. References [29, 32, 39, 109, 110, 114, 115] are excellent resources for those who desire an in-depth study of the subject.

2.5.1 Speech Production Mechanism

Speech is produced by the movement of vocal organs that disturb the air particles originating from the lungs, causing changes in the air pressure which propagate outwards through the lips and are eventually perceived as sound by the ear. Different patterns of air pressure variations create different sounds [39]. The physiology of speech production involves two main components: the vocal chords and the vocal tract. Figure 2.11, taken from [105], illustrates the various organs that participate in the speech production mechanism. The vocal chords are the folds of skin located at the top of the trachea. The vocal tract mainly consists of the pharynx, mouth cavity (tongue, teeth, lips), and nasal cavity. Air flowing under pressure from the lungs passes through the trachea into the larynx. Based on the interaction of the airflow with the vocal chords, the glottis (gap between left and right vocal chords) opens and closes in accordance with the vibrations of the vocal chords causing puffs of air to be released into the larynx. These air puffs then propagate through the vocal tract and eventually exit through the lips as a pressure wave, causing rapid variations in air pressure outside the lips. The vibrations caused by this pressure wave travel though air and get picked by the ear and are interpreted as sound. This is a very brief explanation of the complex physiological process of speech production and readers are advised to refer to [110] and [135] for further details.

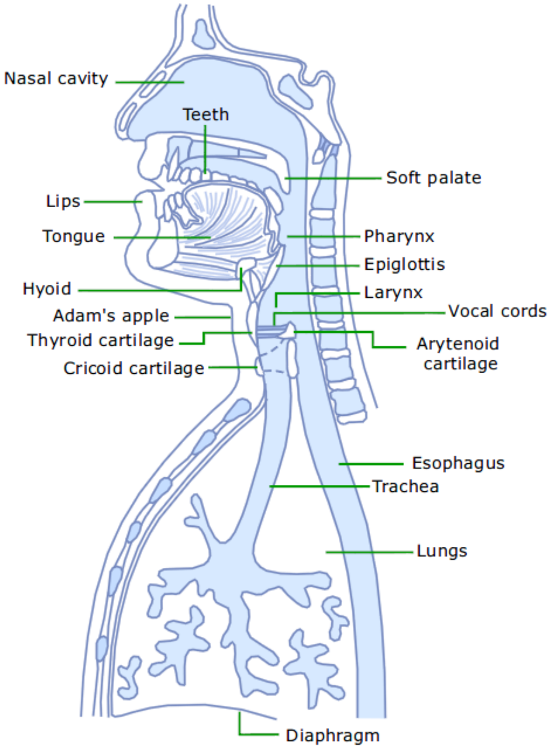

Figure 2.11: The Human Vocal System [105]

Terminology

The volume of air that is forced out of the lungs into the trachea determines the degree of *loudness* of the sound. This is because when more air particles vibrate, the amplitude of the sound wave is increased. The natural frequency at which the vocal chords tend to vibrate is known as the *fundamental frequency* and it correlates to the speaker's *pitch* [123]. During the passage of the sound waves through the vocal tract, some of the wave energy is absorbed by the walls of the tract [61], some waves get reflected while some waves resonate depending on their frequency and the size and shape of the vocal tract. The resonant frequencies are known as *formats* [123]. The shape of the vocal tract determines the frequencies and amplitude of the frequencies at which the waves vibrate as they pass through the vocal tract. Different shapes of the vocal tract produce different linguistic sounds. The vocal tract shape can be changed by the articulators such as moving the tongue, teeth and lips. *Voiced* sounds are produced when the vocal chords vibrate and *unvoiced* sounds are produced out of the attenuation/amplification effects of the vocal tract on the air stream passing through the glottis when the vocal chords do not vibrate.

The Source-Filter Model

G. Fant [24] introduced the source-filter theory to mathematically model the method of speech production. According to this theory, the speech wave is the result of a vocal tract filter system on a sound wave produced by a source. The production of speech represented by a source-filter decomposition is shown in Figure 2.12. The source-filter model is represented by two-phases [52] - the voice wave initiation phase (glottal airflow) and the wave-filtering phase (impact of vocal tract on glottal airflow). The source is the origin of a periodic (vibrating vocal chords) or aperiodic (bursts of air passing through the vocal tract when vocal chords are not vibrating) waveform. The vocal tract filter system comprises of the pharynx cavity, nasal cavity and the mouth cavity. The vocal tract acts as an acoustic filter that suppresses energies of the waveform at certain frequencies and amplifies it at others.

The model assumes that glottal source and the vocal tract filter are independent of each other. It also assumes that the source-filter system is linear. From the signal processing perspective, the filtering effect on the source waveform can be achieved either by convolution in the time domain or by multiplication in the frequency domain. The filtering operation of the vocal tract is represented by a transfer function $H(t)$. The waveform produced by the source is represented by $S(t)$. The resulting waveform

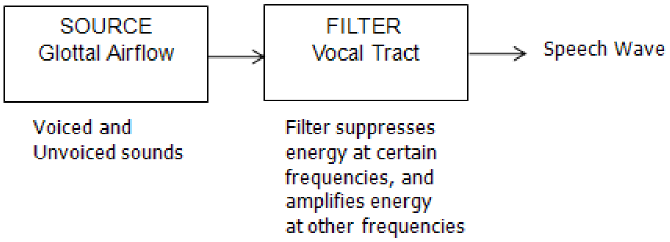

Figure 2.12: Source-Filter Model for Speech Production

generated by the action of the filter on the source is represented by $W(t) = S(t) * H(t)$, (where t denotes time-domain representation, * denotes convolution operation). In the frequency domain, the product of the source $S(f)$ and the transfer function $H(f)$ represents the speech wave $W(f) = S(f)\text{x}H(f)$, (where f denotes frequency-domain representation..

The filtering characteristics of a vocal tract shape and the *fundamental frequency* of vocal chord vibrations, can be estimated from the frequency analysis [115] of the speech waveform, which is discussed in the next section.

Voice Signal Representation

There are three representations [58] of a voice signal:

i) Time-domain - the speech wave propagates as a pressure wave through air. The plot of the magnitude of air pressure variations with respect to time represents the voice signal in the time-domain (see Figure 2.13). This representation allows determination of the speaker's pitch [39].

ii) Frequency domain - applying a Discrete Fourier Transform (DFT) to the waveform in the time domain results in an amplitude spectrum which displays the frequency content of the waveform. As illustrated by Figure 2.14, the peaks in this spectrum that are very closely and equally spaced for the entire frequency range are due to the vocal chord vibrations (*fundamental frequency* and its *harmonics*). The widely spaced dips and peaks that can be noticed in the contour (dotted line)of the spectrum are dictated by the shape of the vocal tract. The vocal chords contribute to the spectrum as a

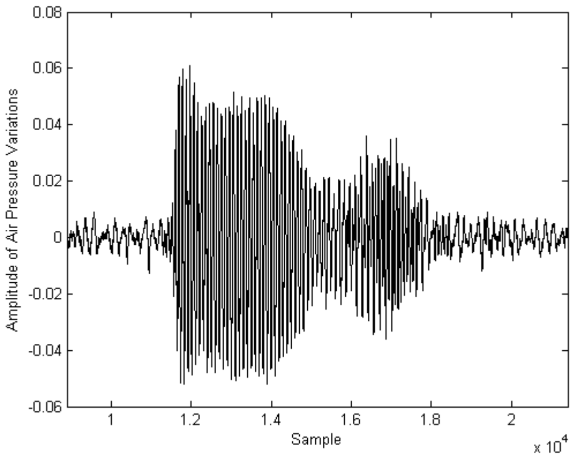

Figure 2.13: Time-domain Representation of Voice Signal

rapidly oscillating component while the vocal tract contributes as a slowly changing trend line through the oscillations [39]. Applying a DFT to this spectrum isolates the contributions of the source and filter such that the quickly-changing signal due to the source appears in the right (higher frequency range) of the resulting spectrum (which is known as *cepstrum*) and the slowly varying signal due to vocal tract manifests itself in left (lower frequency range) part of the spectrum.

Since the source and filter get separated by the cepstral analysis, this representation is most commonly used for speech and speaker analysis. However, speaker verification systems typically use features derived only from the vocal tract [10] to represent the identity of a speaker. This is because even though the difference in pitch (*fundamental frequency*) between speakers is large, it is difficult to effectively use pitch for speaker verification as people can easily change the pitch of their voice. To the contrary, lower cepstral coefficients representing the vocal tract are invariant for a given speaker.

iii) Time+Frequency domain - a spectrograph displays the amplitude of voice signal as a function of frequency and time. In this representation, the variations in amplitude are displayed by varying the intensity(bright or dark) levels in the graph which is a plot of the frequency values against time. The dark regions on a spectrogram indicate formants that represent vocal tract resonances. This representation is mainly

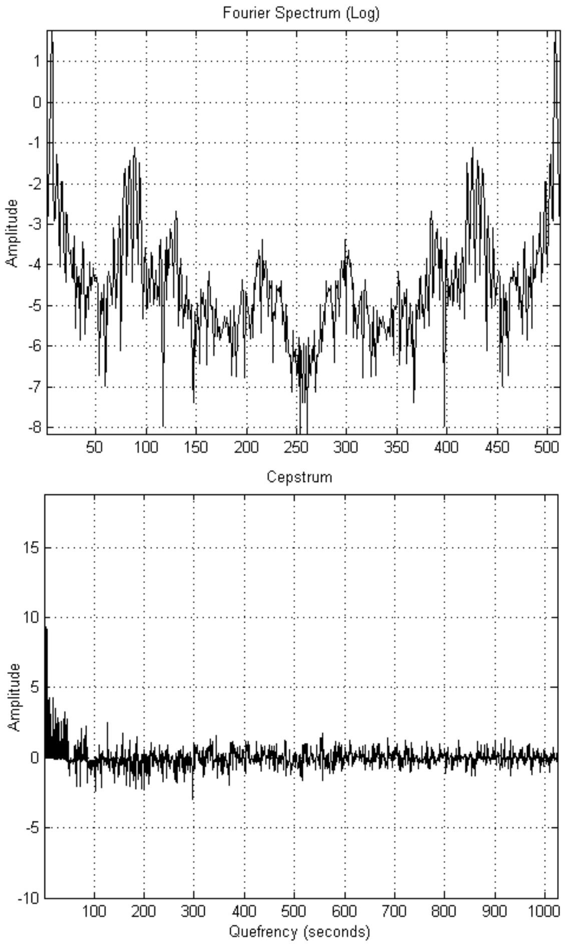

Figure 2.14: Frequency Analysis of Speech Wave

used for speech analysis and in forensics. Figure 2.15 illustrates a spectrograph.

2.5.2 Elements of Speaker Verification Systems

Automatic speaker recognition (ASR) systems aim to recognize a speaker via measurements of individual characteristics derived from the speaker's voice signal [32]. Speaker recognition requires speakers to enroll into the system prior to being recognized by the system. Speaker recognition is classified into speaker verification and speaker identification. Speaker verification is the process of verifying the claimed identity of a speaker. Speaker identification is the process of identifying the speaker of the provided voice signal from a set of enrolled speakers.

Speaker verification techniques can also be categorized as text-dependent and

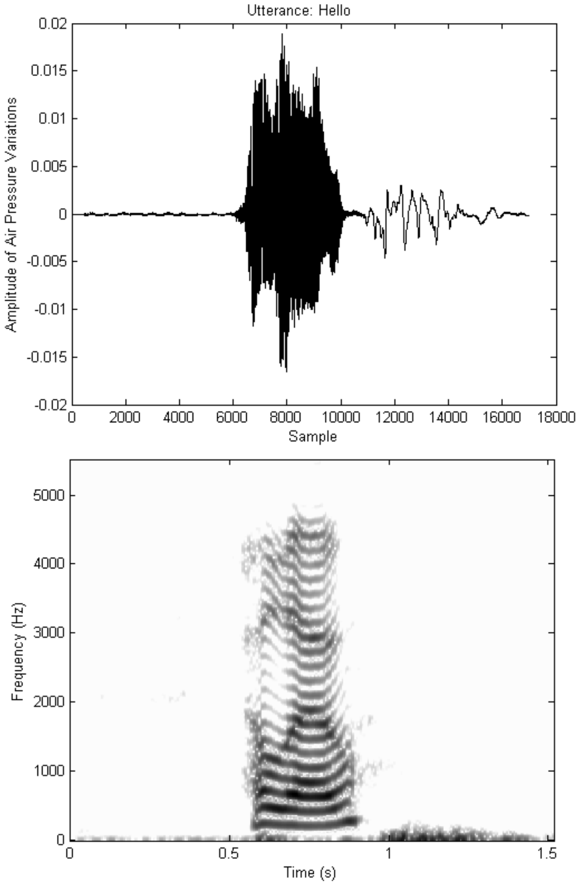

Figure 2.15: Spectrograph

text-independent techniques. In text-dependent methods, the system imposes constraints on the text utterance, for example, the claimant speaks a predefined phrase during enrollment as well as verification. In a text-independent technique the system does not rely on predetermined text thereby offering users the freedom to choose the text to be spoken. However, these systems require a lot of training/testing sessions to deliver good performance.

A generic speaker verification system consists of three modules: front-end processing, speaker modeling, and comparison, as shown in Figure 2.16. The system requires speakers to enroll into the system prior to being verified as authentic users. The enrollment process requires speakers to speak a number of words or sentences. From this acquired speech signal, the front-end processing module measures features that contain identity information. This step is also referred to as parameterization of the signal as it reduces the voice signal to a set of speaker specific parameters. The subsequent step is to create a speaker model from the extracted individual specific parameters. This step is also referred to as feature representation, as it creates a mathematical model or statistical representation of the extracted features. The generated speaker model is stored as a template which is used by the comparison module during verification. The verification process prompts the speaker to utter the same or different text used during enrollment, depending on whether it is a text-dependent or text-independent verification system. This utterance is parameterized, followed by the modeling of parameters (not all speaker verification systems employ this module during verification) and then compared against the stored template of the claimed identity of the speaker to decide if the claim is valid. A match between the newly extracted parameters and the stored speaker model verifies the speaker and a mismatch rejects the speaker. What follows is an overview of the parameterization and speaker modeling techniques.

Parametrization - Acoustic Feature Extraction Techniques

The objective of parametrization techniques is to represent the provided utterance by a sequence of feature vectors characterizing the identity of the speaker. Effectiveness of various acoustic features has been studied in [124] and [127] and the most commonly used acoustic parameters in speaker recognition systems have been voice pitch, intensity, fundamental frequency of speaker, resonant frequencies of vocal tract, vocal tract information, and spectral patterns. In order to extract the relevant

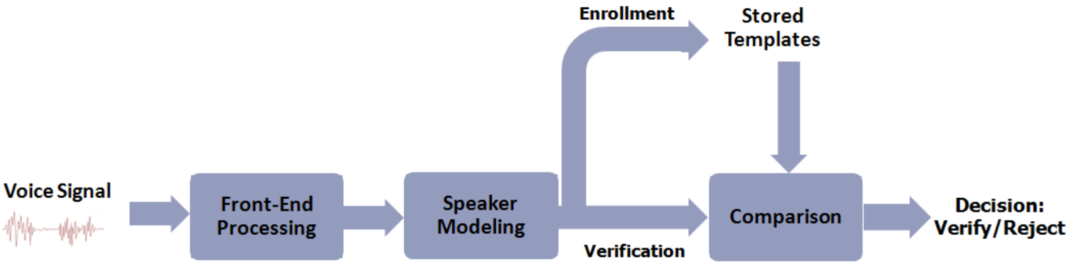

Figure 2.16: A Generic Speaker Verification System

features from a voice sample, the speech signal must first be processed to a representation that facilitates measurement of the features. The short-term spectrum of the speech signal, which is a function of time, frequency, and spectral magnitude, is the most common method of representation of the speech signal for feature extraction. Several approximations to the short-term spectrum such as linear predictive coding coefficients, reflection coefficients, cepstrum coefficients and mel-frequency cepstrum coefficients are widely used as well [112, 130, 152]. Cepstral variants such as linear frequency cepstral coefficients, mel-warped linear prediction cepstral coefficients, using discrete wavelet transform instead of fast Fourier transform for deriving the cepstrum have also been used for signal representation. The choice of a particular representation is determined by factors such as computational complexity, memory usage, and nature of the transmission channel. While linear predictive coding and linear predictive cepstral coding techniques are computationally expensive, perceptual linear predictive coding technique is more robust in presence of background noise, and mel-frequency cepstral coding is used in noise free environments. Mel-frequency cepstrum coefficients (MFCC) are by far the most prevalent technique [122] used to represent a speech signal for feature extraction in state-of-the art speaker recognition systems [21]. Therefore, the proposed approach adopts the MFCC-based features extraction technique. The Mel-Frequency Ceptrum Coding [21] is a representation of the vocal tract structure that produced the voice signal. It is based on a discrete Fourier transform of the log amplitude spectrum on a nonlinear scale of frequency. This technique will be explained in detail in Chapter 3.

Speaker Modeling - Acoustic Feature Representation Techniques

Factors such as improper user interaction with the sensor, temporary alterations of the voice itself caused by fatigue, illness, aging, and due to environmental factors the quality and consistency of captured voice biometric data is affected. Therefore, a voice sample collected from the same speaker at different time instances depicts large variability in the acquired signal (this variability is termed intra-individual variability). For this reason, the recorded voice sample cannot be directly used to uniquely represent the individual. In order to incorporate these intra-individual variations, feature representation techniques have to be used to generate a statistical model of the voice features. Speaker modeling techniques such as Gaussian mixture models (GMM), vector quantization (VQ), multi-layer perception (MLP), hidden-Markov models (HMM), artificial neural networks (ANN), support vector machines (SVM) and many other techniques are popular [121]. However, GMM outperforms other modeling techniques [121]. Therefore, state-of-the-art speaker recognition systems use GMM as the classifier owing to its better performance, probabilistic framework and training methods scalable to large data sets [11].

The approach presented in this dissertation employs GMM to generate the speaker model. This generated model is then used as a voice print to serve as the watermark. A Gaussian Mixture Model is a series of Gaussian distributions over the space of the feature vectors to statistically classify features (MFCC coefficients) using a probability based approach. Each Gaussian distribution in the GMM model is characterized by a mean, a covariance matrix and a prior probability. Chapter 3 covers the theory on GMM in detail.

A voice print does not contain the entire voice signal but it only consists of parameters related to the vocal tract, therefore reverse engineering the voice print to recreate the original voice sample is theoretically not possible. The reverse engineering process is not only challenging but also requires a lot of time, effort and technological expertise [15, 84, 107]. The cost and complexity involved in such an effort has to be far greater than the value of the information (spoken text or speaker's identity) obtained by reverse engineering. However, due to security concerns raised over the possibility of recreation of the voice signal from voice print researchers [119] propose to encrypt the voice print prior to using it for the purpose of speaker verification.

Performance Evaluation

The performance of a speaker verification system depends on various factors [121] such as - i) the quality of the acquired voice signal expressed in terms of signal-to-noise (SNR) ratio, ii) the number of voice samples used during enrollment and the duration of utterance of each voice sample used to generate speaker models, iii) the degree of intra-individual variations in the voice samples used during enrollment (generally multiple enrollment sessions are conducted at different times to accommodate variations in voice acquired at different instances), iv) the choice of feature extraction and feature-representation techniques used to formulate the speaker model, v) accurate estimation of algorithmic parameters for the employed feature extraction and representation technique, vi) the setting of threshold level used by the comparison module to reject false claimants and accept genuine claimants, and vii) the size of the speaker population which impacts the false accept rate of the system.

The voice signal can be acquired in a controlled environment with negligible background noise using a desktop microphone or a noisy environment such as a telephone set. The recording channel of the voice signal dictates the selection of parametrization and modeling algorithm. A trade-off exists between verification accuracy of the system and the enrollment-session duration of voice samples and the number of enrollment sessions to incorporate within-speaker variability. The verification accuracy is poor if the voice samples used during enrollment are of smaller duration. The verification accuracy of the system can be varied by changing the threshold - lowering the threshold causes more false rejections but results in fewer false accepts. Elevating the threshold is appropriate for low security applications as it enables fewer false rejections. However, this user convenience benefit comes at the price of higher false accept rates. The DET curve plots the FAR and FRR for various threshold levels to depict the overall performance of the system.

The size of the speaker population is determined by the database used for testing. Various databases [34] (*paid access*: TI-DIGITS, TIMIT, YOHO, XM2VT, *free for academic use*: VALID, MIT Mobile Device Speaker Verification Corpus) are available for benchmarking text-dependent speaker verification systems and provide voice recordings with varied number of enrollment-session and verification-session utterances and recorded in different acoustic environments (controlled or noisy). However, each database comes with its own set of limitations such as too few speakers, samples acquired in either quite or noisy environment but not both, insufficient amount of enrollment session voice samples, small duration for utterances that do not suffice creation of robust speaker models, lack of impostor utterances to determine rate of false accepts, lack of free academic license or are not available publicly. Our experimental evaluation of the system is therefore subject to these limitations.

Chapter 3

Methodology

Similar to biometric systems, the proposed scheme also has two steps: i) user enrollment, and ii) user authentication. The enrollment step, as depicted by Figure 3.1, acquires the voice biometric trait from the user, generates a voice print, encodes the voice print using error correcting codes and then embeds it as a watermark into the 3D mesh model.

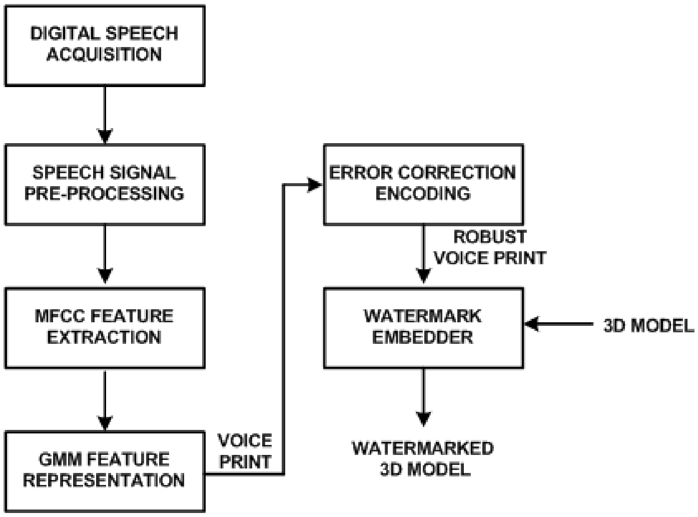
DIGITAL SPEECH ACQUISITION
SPEECH SIGNAL PRE-PROCESSING
MFCC FEATURE EXTRACTION
GMM FEATURE REPRESENTATION
VOICE PRINT
ERROR CORRECTION ENCODING
ROBUST VOICE PRINT
WATERMARK EMBEDDER
3D MODEL
WATERMARKED 3D MODEL

Figure 3.1: Enrollment

The authentication step, as portrayed in Figure 3.2, retrieves the biometric watermark from the 3D model, corrects it from any errors caused by signal processing operations on the 3D model using the error correction decoder and restores the speaker model which was used as the voice print watermark during enrollment. This step also acquires a voice sample from the user and extracts features from this sample. These extracted features are compared against the retrieved GMM speaker model to verify if the user attempting to access the 3D model is indeed the same individual whose voice print was embedded into the 3D model. The results of the verification module determines a match or mismatch of the user's voice with the embedded GMM model. Experiments in Chapter 5 demonstrate the effect of signal processing attacks on the embedded speaker model and how that subsequently impacts the verification process.

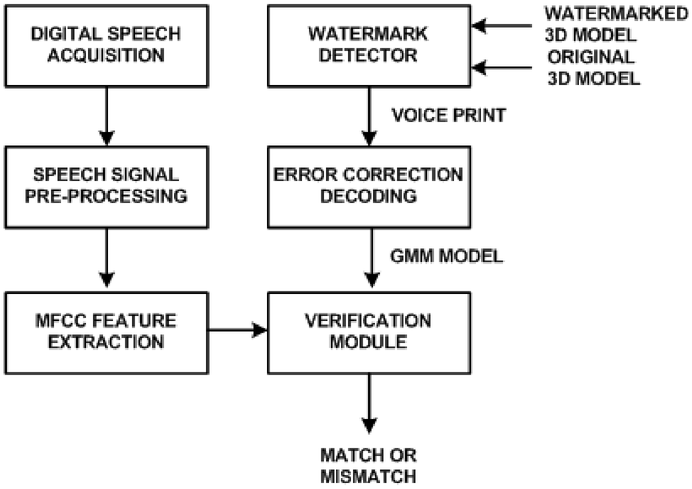

Figure 3.2: Authentication

Sections that follow provide details for each block from the enrollment and authentication steps. These sections cover each block in a substantial amount of detail and are targeted for those readers who wish to gain an in-depth knowledge of the voice print generation and watermarking process. Readers interested only in experimental results are advised to skip to Chapter 5 which outlines the overall system performance.

3.1 Voice Biometric Watermark Generation

The proposed method which we presented earlier in [93] embeds a voice biometric as a watermark in the 3D graphic content. Size of an acquired voice sample (*utterance of 10 digits, approximate duration 2-10 seconds, 32KHz sample rate, bit rate 512 kbps, 16 bit sample size, mono channel, PCM format, .wav file recording*) from a user is in the order of hundreds of kilobytes. 3D models used for experiments in this paper range in size from an order of tens of kilobytes to hundreds of kilobytes. These small 3D mesh files cannot accommodate a high payload of a *.wav* file recording for insertion as watermark. Therefore, the size of the acquired voice sample has to be reduced such that a unique and compact representation of a user's voice can be derived. For this purpose (and to incorporate variations in voice samples of a user taken at different instances of time, which will be explained later), feature extraction and representation techniques are used. These techniques measure and statistically model the features from the acquired voice sample that uniquely characterize an individual. Feature extraction from a voice sample is analogous to front-end processing or speech parametrization techniques used by speaker recognition systems [102]. Feature representation employs pattern recognition techniques to statistically model the extracted features. The following sections detail the steps involved in the formulation of the voice print.

3.1.1 Digital Speech Acquisition

Digitization is the process of converting the sound pressure wave (analog voice signal) into a format that can be stored on a digital computer. The process involves two steps - sampling and quantization. Sampling discretizes the signal in time by converting the continuously varying signal into a discrete set of values. The total number of samples extracted from an analog signal depends on the *sampling frequency* and the duration of the analog signal. Omitting parts of the analog signal that lie between the sampled points does not impact the reconstruction of the analog signal from the digital as long as Nyquist's criteria is satisfied (which states that for a bandlimited signal that contains only a certain range of frequencies, the sampling frequency should be at least twice the highest frequency contained in the analog signal). Quantization discretizes the signal in amplitude by converting the continuously varying amplitudes into a discrete set of amplitude values. Quantization is measured in terms of the number of *bits* used to represent the amplitude levels for the extracted samples from the analog signal. The resultant digital signal is defined by a series of amplitude values for discrete steps of time.

The objective of the digital speech acquisition step is to obtain the user's voice sample so that a speaker-specific voice print can be generated. Instead of randomly speaking into the microphone all users are directed to speak the same predetermined utterance because a text dependent technique allows to directly exploit voice individuality associated with each syllable. The utterance is constrained to a predetermined sequence of 10 digits - *"1 2 3 4 5 6 7 8 9 10"*.

Figure 3.3 demonstrates a speech signal captured with an ordinary PC microphone at a sample rate of 44KHz and 32-bit representation. The average file size of the digital recording for the utterance is 2.35 MB (*.wav* file format) and has a duration of 14 seconds.

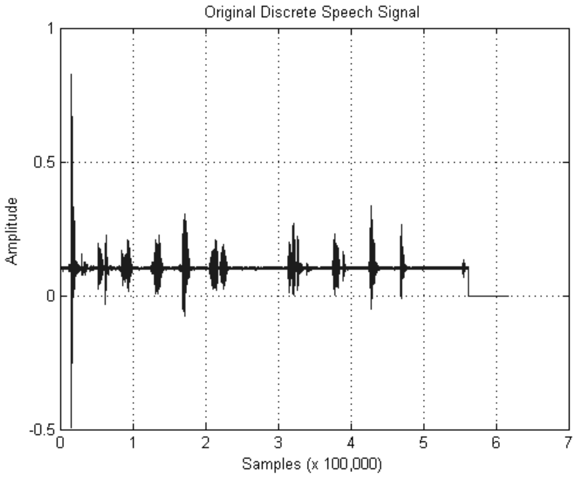

Figure 3.3: Discretized Speech Signal: 14 seconds duration, utterance "1 2 3 4 5 6 7 8 9 10"

3.1.2 Speech Signal Pre-Processing

Pre-processing of the speech signal is essential to eliminate periods of silence and areas of background noise. Pre-processing reduces the processing load of the subsequent stages of feature extraction and modeling thereby facilitating the system to be more computationally efficient. Moreover, the pre-processing step ensures that the extracted voice print is independent of the speaking rate. Slow speakers pause for a few milliseconds between uttering each digit. Also, the first or last few milliseconds of a voice recording correspond to silence or background noise because the speaker takes some time to begin speaking when recording starts and there is a minute delay before the recording can be stopped once the speaker is done uttering the 10 digits. Figure 3.4 illustrates the silence removed pre-processed frame of the original signal. The file size is reduced to 680 KB after pre-processing.

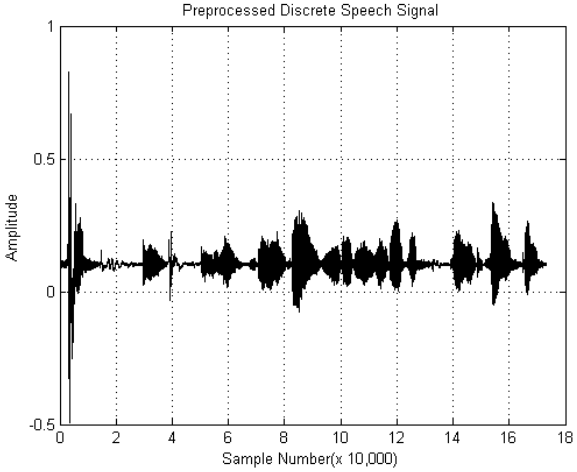

Figure 3.4: Preprocessed Discrete Speech Signal: 3 seconds duration

Speech signal can be segregated into voiced, unvoiced, and silence regions. Voiced speech is produced because of excitation of vocal tract by the periodic flow of air at the glottis. Unvoiced speech is produced when the vocal chords are not vibrating. Unvoiced regions usually have very low energy. Silence regions are where no speech is produced and therefore these regions represent the background noise. Most of the speaker specific features are present in the voiced part of speech signal. While there exist many techniques [6] such as short-time energy, auto-correlation, linear prediction coding coefficient, and Mahalanobis distance [126] to classify speech signal into voiced/unvoiced regions, we use the zero-crossing rate (ZCR) method [35] to eliminate silent regions from the speech signal.

The zero crossing count is an indicator of the frequency at which the energy is concentrated in the signal spectrum. A reasonable generalization is that if the zero-crossing rate is high, the speech signal is unvoiced, while if the zero-crossing rate is low, the speech signal is voiced. The speech signal is segmented into a non-overlapping frame of samples (frame length 1024 samples, segmentation into frames of 17.75 ms window progressing at a 8.875-ms frame rate). It is processed frame by frame until the entire speech signal is covered. ZCR for each frame with N samples is computed by:

$$ZCR = \frac{1}{N}\sum_{i=1}^{N} |sign(x_i) - sign(x_{i-1})| \tag{3.1}$$

where,

$$\begin{aligned} sign(x_i) &= \quad 1, \quad x_i \geq 0 \\ &= -1, \quad x_i \leq 0 \end{aligned} \tag{3.2}$$

A zero crossing is said to occur if successive samples have different algebraic signs. The zero-crossing rate is the rate of sign-changes along a signal, i.e., the rate at which the signal changes from positive to negative or back. Mathematically, ZCR equates to the number of time-domain zero-crossings within a defined region of signal, divided by the number of samples of that region. If the ZCR of a portion speech exceeds 50% then this portion will be labeled as unvoiced or background noise otherwise the segment is considered to be the voiced one.

3.1.3 MFCC Feature Extraction

The purpose of this step is to parametrically represent the speech waveform by converting it into a set of feature vectors. The digitized speech waveform of the speaker's 10 digit utterance is approximately of size 2-4 MB which is too high to be accommodated by graphic models of size 25 KB or so, that are used in the experiments. Even if the graphics files of much higher size are used, it is necessary to compact the waveform such that a statistical model can be created from only necessary waveform features that uniquely represent the speaker.

The speech waveform is a function of the speaker's physiological characteristics such as vocal chords and vocal tract dimensions [25] and extraction of features from the speech signal is such that they are primarily a function of speaker and not the speech. Before performing signal parameterization, it is necessary to understand how a speech wave is generated and what characteristics of this wave reflect the identity of a speaker. The next two paragraphs discuss these two aspects briefly.

Speech production mechanism is explained by a simplified source-filter model [138] according to which sounds are produced by the action of a filter (vocal tract) on a sound source (glottis or vocal chords), technically equivalent to a convolution process in signal processing. When air passes from the lungs through the vocal chords (source) it is subject to rapid variations in pressure due to vibrations of the vocal chords. Energy of this pressure wave is modified by its passage through the vocal tract (filter), which acts as an acoustic filter that suppresses energies at certain frequencies and amplifies energies at other frequencies.

The frequency and amplitude at which the air vibrates as it passes through the vocal tract is determined by vocal tract shape and length, which vary from person to person. The vocal tract dimensions are represented by a transfer function that can be obtained from the frequency amplitude spectrum of the waveform. Peaks in the spectral envelop correspond to formants which are resonant frequencies of the vocal tract. The fundamental frequency and harmonics of a speaker's spectrum reflect the frequency of vibration of the source. The amplitude of the fundamental frequency and the locations of the harmonics vary from speaker to speaker. Therefore, an acoustic waveform carries an imprint of the source and filter that produced it and is unique for every individual.

The Mel Frequency Cepstral Coding (MFCC) [21] approach to parameterize the speech signal is a cepstrum (spectrum of a spectrum) based feature representation technique. As illustrated in Figure 3.5, there are five stages to compute MFCC: Windowing, Fourier Analysis, Mel-Filter Bank, Log Magnitude Spectrum, Cepstrum.

Stage 1 - Windowing: A speech signal is non-stationary because its characteristics are not constant over long periods of time. However, when speech signal is examined over short periods of time (5 to 100 milliseconds), its characteristics are fairly constant

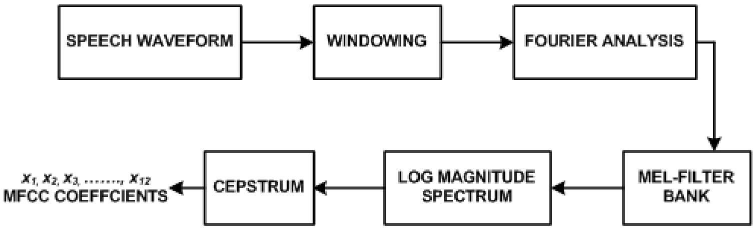

Figure 3.5: MFCC Block Diagram

and the signal can be considered as a stationary signal. To extract this stationary part of the signal, a Hamming window is used (see Figure 3.7, 3.8, and 3.9).

A symmetric Hamming window is given by:

$$w[n] = \begin{cases} 0.54 \text{ - } 0.46\cos(\frac{2\pi n}{L-1}) & , 0 \leq n \leq L-1 \\ 0 & , \text{otherwise} \end{cases}$$

Multiplying the window function with the time-varying speech signal not only forces the signal to be periodic (which is a requirement for Fourier analysis) but also reduces the leakage in the frequency domain which results in the signal energy spreading over a wider frequency range as opposed to the actual signal frequency that lies in a narrow frequency range. This leakage is a result of applying a Fourier transform to non-periodic signals. Using a window that is shaped so that it approaches zero at the beginning and the end, molds the signal into a periodic form thereby reducing the leakage.

The Hamming window of width 1024 samples that extracts 17.75 milliseconds windows (frames of length 1024 samples) from the original signal and is overlapped for 512 samples such that the offset between successive windows is 8.875 milliseconds is illustrated by Figure 3.6. There are a total of 337 frames for the pre-processed signal, shown in Figure 3.4.

Stage 2 - Fourier Analysis: The next stage extracts the energy of the signal in different frequency bands by applying the Discrete Fourier Transform (DFT) for each windowed signal i.e. frame. A plot of the magnitude against the frequency is visualized by the spectrum shown in Figure 3.10. This spectrum reveals the frequency components for the pre-processed signal. For k frames of an original signal, the DFT

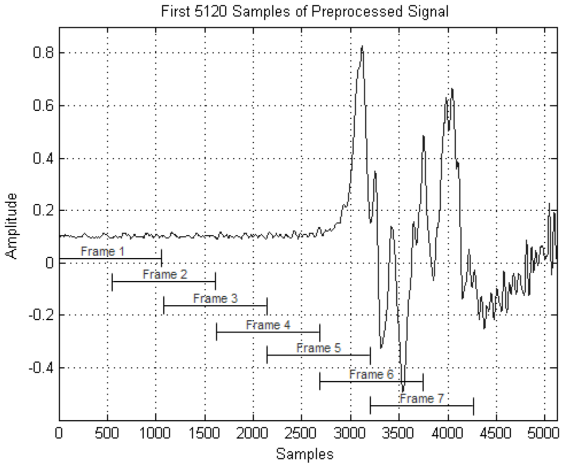

Figure 3.6: Extracting Frames from Preprocessed Discrete Signal

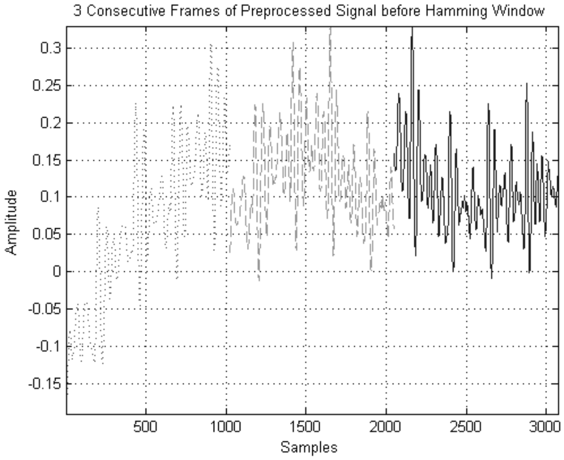

Figure 3.7: Frames of the Preprocessed Discrete Signal before Windowing

is given by the following equation:

$$X[k] = \sum_{n=0}^{N-1} x[n] e^{-j \frac{2\pi}{N} kn} \tag{3.3}$$

where N represents the discrete frequency, $X[k]$ is a complex number representing the magnitude and phase of that particular frequency component of the original signal.

Stage 3 - Mel-Filter Bank: The sensitivity of the human ear is not the same for all frequencies. The ear is less sensitive to frequencies higher than 1 KHz. The melody scale approximates the frequency response of the human ear and places less emphasis

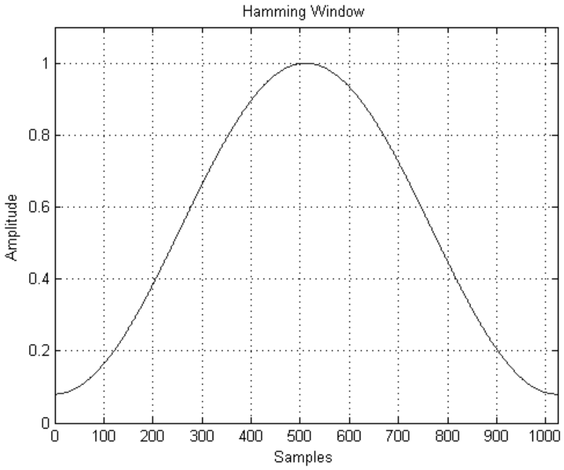

Figure 3.8: Hamming Window

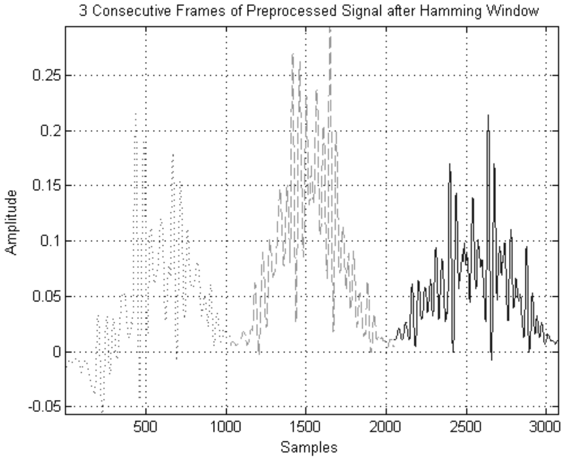

Figure 3.9: Frames of the Preprocessed Discrete Signal after Windowing

on the higher frequencies. This stage warps the Fourier spectrum on a melody scale by applying a mel-filter bank to the spectrum. Mel-filters are linearly spaced below 1KHz and logarithmically spaced above 1KHz in the filter bank. These filters are triangular shaped. Each filter from the bank collects energy from its respective frequency band. The *mel* frequency can be computed from the acoustic frequency f by using the following equation:

$$mel(f) = 1127 \ln(1 + \frac{f}{700}) \tag{3.4}$$

We use 39 filters in the filter bank. Figure 3.11 represents the mel-filter bank used to capture energies from the Fourier spectrum of the windowed original signal.

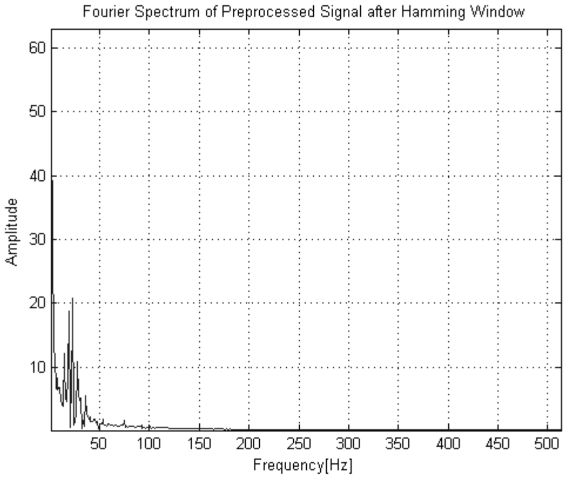

Figure 3.10: Fourier Spectrum of one Frame of Windowed Preprocessed Discrete Signal

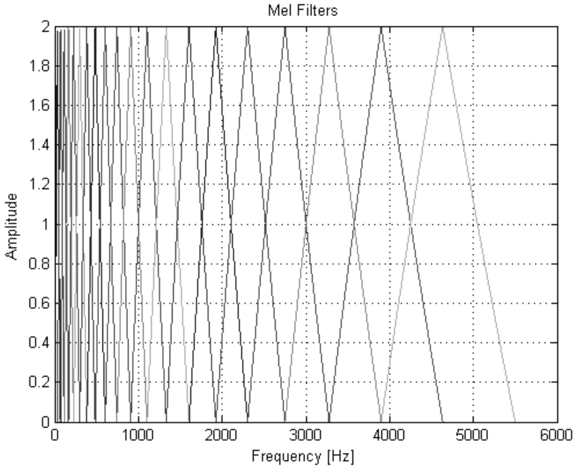

Figure 3.11: Mel Bank of Filters

Stage 4 - Log Magnitude Spectrum: This stage takes the logarithm of the *mel*-spectrum energy values in order to non-linearly compress the filter bank energies in accord with the human auditory response. Human response is less sensitive to small differences in amplitude at high amplitudes than at low amplitudes. Using a log also makes the extracted features less sensitive to variations in energy of original signal arising out of the speaker speaking closely into or being further away from the microphone while recording the speech. Figure 3.12 depicts the transformation of the *mel*-spectrum to log scale.

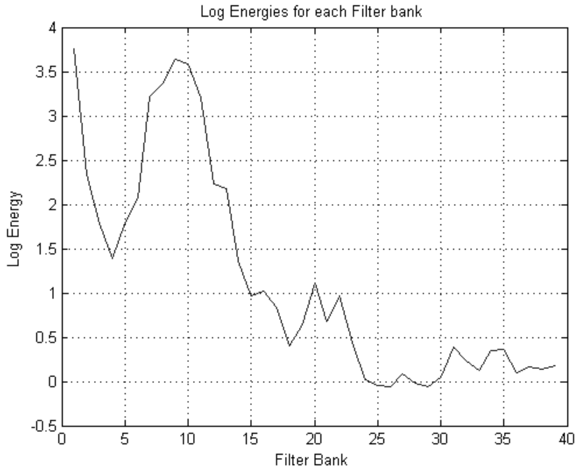

Figure 3.12: Log of Mel Spectrum

Stage 5 - Cepstrum: This stage takes the inverse DFT of the log magnitude of the spectrum of a windowed frame of the original signal to get a cepstrum, which is shown in Figure 3.13. The inverse DFT is computed by the equation below:

$$c[n] = \sum_{n=0}^{N-1} \log \left(\left| \sum_{n=0}^{N-1} x[n] e^{-j\frac{2\pi}{N}kn} \right| \right) e^{j\frac{2\pi}{N}kn} \tag{3.5}$$

The cepstral representation characterizes the vocal tract (lower cepstral values) and the source (higher cepstral values) [19]. Peaks in the lower frequency components of the cepstrum represent the formants while peaks in the higher frequency components are caused by the fundamental frequency and harmonics.

MFCC feature extraction takes the first 12 cepstral values that represent the vocal tract filter distinctly separated from information about the vocal source. Each frame of the original signal is represented by a 12-dimensional feature vector consisting of MFCCs i.e., $x = x_1, x_2, x_3, \ldots x_{12}$. Figure 3.14 illustrates the MFCC cepstral features.

3.1.4 GMM Feature Representation

The 12 *mel* cepstral feature vectors representing spectral information are extracted from the speech waveform every 17.75 milliseconds. Each of the 337 frames are represented by 12 MFCC features. A data density plot (histogram) of the first MFCC

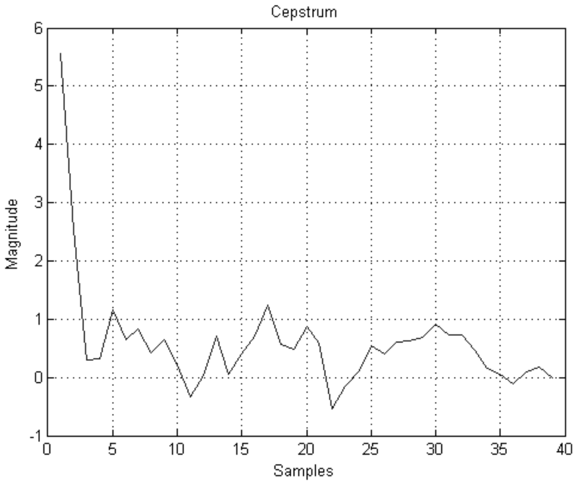

Figure 3.13: Cepstrum

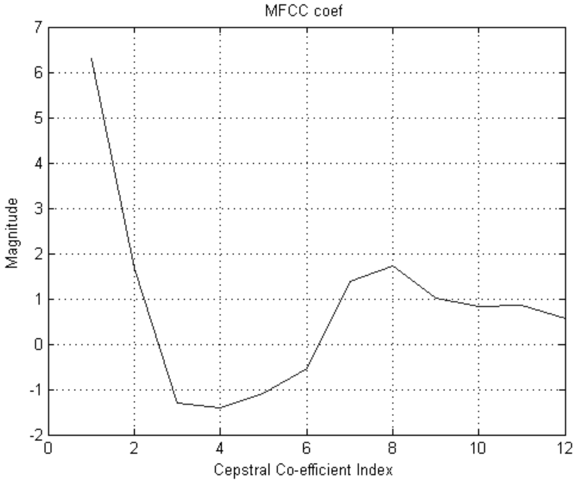

Figure 3.14: First 12 Mel-Frequency Cepstral Coefficients

feature is shown in Figure 3.15 by the grey bars. The data with such a representation is said to have a non-normal distribution. Figure 3.16 demonstrates the histogram of data which has a normal distribution, it can be approximated by a Gaussian (bell-shaped curve). Since each MFCC cesptral feature may not have a normal or Gaussian distribution, the extracted MFCC features are modeled by a weighted mixture of Gaussian distributions as shown in Figure 3.15. Such a model is known as a Gaussian mixture model (GMM).

Each Gaussian is parametrized by a mean μ and variance σ^2 value. The mean defines the position of the center of the Gaussian and the variance defines the width

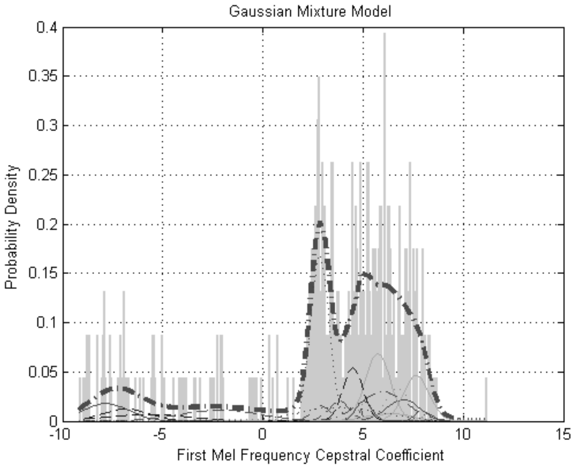

Figure 3.15: Gaussian Mixture Model with 20 Gaussians for the first MFCC

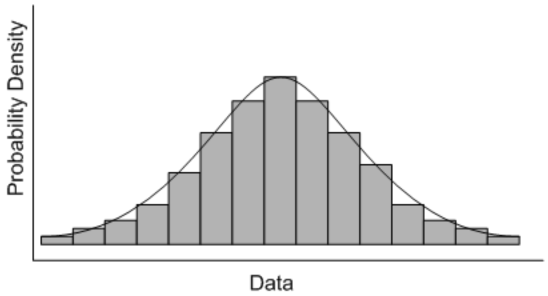

Figure 3.16: Data with normal distribution approximated by a Gaussian

of the Gaussian. Figure 3.17 demonstrates Gaussian distributions with different parameters μ and σ^2.

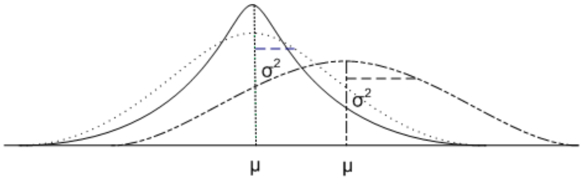

Figure 3.17: Gaussian distributions with different mean μ and variances σ^2

A univariate Gaussian represents one-dimensional data. Figure 3.18 shows multiple univariate Gaussians that are averaged to represent an arbitrary function with a non-normal data distribution using a GMM for 1-dimensional data set. However, the MFCC feature set is 12-dimensional, with 337 values for each dimension. Hence, we use a mixture of multivariate Gaussians to model the multi-dimensional feature set.

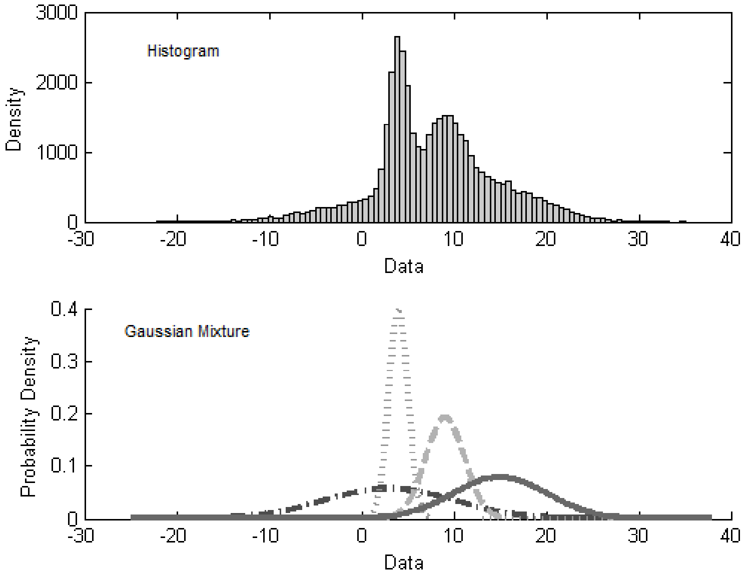

Figure 3.18: Gaussian Mixture Model of Univariate Gaussian distributions to approximate 1-dimensional feature set

Each individual multivariate Gaussian in the mixture model is parameterized by a mean vector $\vec{\mu}$ and covariance matrix Σ for the N-dimensional feature vector x_n. A model for M Gaussian mixtures, with each mixture having weight $P(k)$ is given by the equation:

$$p(x_n) = \sum_{k=1}^{M} P(k)p(x_n|k) \tag{3.6}$$

where,

$$p(x_n|k) = \frac{1}{(2\pi)^{\frac{N}{2}} |\Sigma|^{\frac{1}{2}}} e^{-\frac{1}{2}(x_n-\vec{\mu})^T \Sigma^{-1}(x_n-\vec{\mu})} \tag{3.7}$$

represents the Gaussian distribution with $|\Sigma|$ and Σ^{-1} are the determinant and inverse of the covariance matrix, $(x_n - \mu)^T$ is the transpose of the matrix $(x_n - \mu)$ and the covariance matrix Σ is a diagonal matrix representing the variance of each dimension only and all non-diagonal elements are zero (since the MFCC features have a nice property of being uncorrelated).

However, for a given non-normal distribution i.e. data set of MFCC features (Figure 3.15), the question arises which Gaussian accounts for which part of the distribution. Since it is not known which features from the MFCC set correspond to which Gaussian, it is difficult to estimate the location (mean) and width (variance) of each Gaussian in the mixture model. Learning approaches (such as neural networks) and iterative techniques have been used to find which Gaussians correspond to which data points and to determine what are the parameters for the individual Gaussian distributions in the mixture model. In our approach, we use Expectation Maximization(EM) [22] which is an iterative approach that is dominantly used to estimate the best possible value of parameters (means, variances and mixture weights) for each Gaussian in the distribution.

The EM approach is an optimization technique that estimates parameters for each Gaussian in the mixture model. It starts off by choosing Gaussian models with an initial set of parameters μ_k, Σ_k for $k = 1, \ldots M$ Gaussian distributions and assigning equal initial probabilities (i.e. mixture weights that characterize which Gaussian is accountable for which part of the data distribution) $P(k) = \frac{1}{M}$ to each Gaussian model. Given this initial guess of parameters, the estimation step computes posterior estimates for the mixture weights $P(k|x_n)$ (i.e. probability for each data point x_n to belong to the Gaussian mixture (μ_k, Σ_k). Given posterior estimates for the mixture weights, the Gaussian distribution parameters that maximize the expectation of the joint density for the data and the mixture weights is computed. The estimation and maximization steps are re-iterated to improve the initially set probabilities until a convergence to a good fit of Gaussians for representing the distribution is obtained. Maximizing the expectation and the parameter reestimating steps give no guarantee of how good the estimates will be, however, it has been proven that the estimates are guaranteed to improve or at least not worsen with each iteration.

For the set of parameters $\theta = \{P(k), \mu_k, \Sigma_k\}$ that need to be optimized using the EM algorithm, the GMM with M multivariate weighted Gaussians is denoted by the following equation:

$$p(x_n, \theta) = \sum_{k=1}^{M} P(k, \theta) p(x_n | k, \theta) \tag{3.8}$$

where:

- $p(x_n, \theta)$ is the probability density function for the GMM,
- θ is the set of estimated parameters with the constraint $\sum_{k=1}^{M} P(k) = 1$,
- $P(k, \theta)$ is the weight of the kth Gaussian or the probability that x_n is being generated by Gaussian (μ_k, Σ_k), and
- $p(x_n | k, \theta)$ is the value of the kth Gaussian at x_n assuming mean μ_k, variance Σ_k and represents the conditional probability density function for x_n conditioned on x_n being generated by the kth Gaussian.

The posterior probability $P(k|x_n)$ can be computed from $p(x_n|k)$ by Bayes' formula:

$$posterior = \frac{prior * likelihood}{evidence} \tag{3.9}$$

$$P(k|x_n, \theta_{posterior}) = \frac{P(k, \theta_{prior}) p(x_n | k, \theta_{prior})}{p(x_n, \theta_{prior})} \tag{3.10}$$

Substituting Equation 3.8 in the denominator, we get the following:

$$P(k|x_n, \theta_{posterior}) = \frac{P(k, \theta_{prior}) p(x_n | k, \theta_{prior})}{\sum_{k=1}^{M} P(k, \theta_{prior}) p(x_n | k, \theta_{prior})} \tag{3.11}$$

The next step is to estimate the true probability densities by maximizing the logarithm of the joint density for x_n and k. Unknown probability density $p(x_n, \theta)$ can be decomposed as joint and conditional densities:

$$p(x_n, \theta) = \sum_{k=1}^{M} P(x_n, k|\theta) = \sum_{k=1}^{M} P(k|\theta) p(x_n | k, \theta) \tag{3.12}$$

Expression for the log of joint density is written as:

$$J = \log P(x_n, k|\theta) = \log[P(k|\theta)p(x_n|k, \theta)] \tag{3.13}$$

Expectation of the log joint density is written as:

$$Q(\theta_{prior}, \theta_{posterior}) =$$
$$\sum_{n=1}^{N} \sum_{k=1}^{M} P(k|x_n, \theta_{prior}) \log p(x_n, k|\theta_{posterior}) \tag{3.14}$$

where,

the first term $P(k|x_n, \theta_{prior})$ is given by Equation 3.11,

the second term is determined by Equation 3.12 and the initial/subsequent guess/estimates for $P(k|\theta)$,

θ_{prior} is the set of parameters used to determine the distribution and

$Q(\theta_{prior}, \theta_{posterior})$ is the objective function that is maximized by assigning its partial derivatives taken over each of the parameters of θ to zero.

The new estimates for parameters μ_k, Σ_k and $P(k|\theta_{posterior})$ are computed by the following equations:

$$\mu_k = \frac{\sum_{n=1}^{N} P(k|x_n, \theta_{prior}) x_n}{\sum_{n=1}^{N} P(k|x_n, \theta_{prior})} \tag{3.15}$$

$$\Sigma_k = \frac{\sum_{n=1}^{N} P(k|x_n, \theta_{prior})(x_n - \mu_k)(x_n - \mu_k)^T}{\sum_{n=1}^{N} P(k|x_n, \theta_{prior})} \tag{3.16}$$

$$P(k|\theta_{posterior}) = \frac{1}{N} \sum_{n=1}^{N} P(k|x_n, \theta_{prior}) \tag{3.17}$$

In approximately 10 iterations the algorithm finds the means and covariances of Gaussians that correctly estimate the probabilities of which Gaussian represents which data points. Figure 3.15 illustrates the GMM for the 12 MFCC coefficients.

The speaker model (voice print), is the aggregate of the parameter values $\lambda = \{P(k), \mu_k, \Sigma_k\}$ of the Gaussian mixture model.

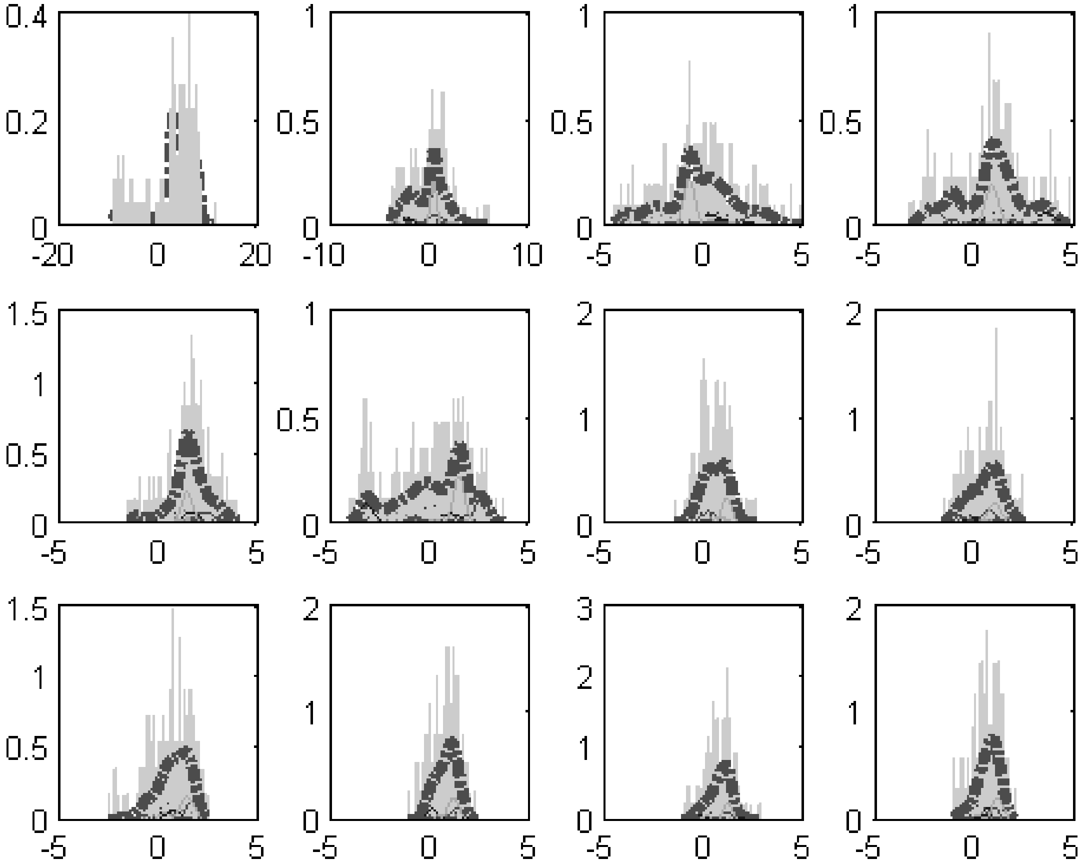

Figure 3.19: Gaussian Mixture Models with 20 Gaussians for all 12 MFCCs

3.1.5 Error Correction Encoding

The 3D model acts as a host that carries the watermark and can be subject to signal processing operations such as noise. Therefore, this host is considered as a noisy communication channel via which the embedded voice print data is transmitted and gets corrupted, as per Shannon's theory of communication [131]. In order to ensure the integrity of the voice print data, error correcting codes are used to encode the watermark. We selected Reed-Solomon codes [118] for error correction. Reed-Solomon codes are an important subclass of the non-binary BCH (Bose-Chaudhari-Hocquenghem) [111] codes and operate over the Galois Field [74] of arithmetic. Reed-Solomon codes are chosen because they have a simply-implemented decoding procedure, can detect and correct large numbers of missing bytes of data, and require the least number of extra error correcting code bytes for a given number of data bytes. In addition, this coding scheme provides superior burst error correcting capability while maintaining an excellent ability to correct random errors [142].

Reed-Solomon (RS) coding scheme generates a N-byte codeword from a K-byte message. A t-error correcting RS code with symbols from Galois Field GF(2^m) has the following parameters:

- Block length: $N = 2^{m-1}$ bytes
- Message size: K bytes
- Parity-check size: $N - K = 2t$ bytes

For example, when $t = 2$, four redundant check bytes will be appended to the K message byte, $m_0, m_1, \dots m_{k-1}$, to form a RS codeword of size $N = K + 4$. The check bytes are computed from the message byte using the following equation:

$$C(x) = M(x) * x^{2t}|g(x)| \tag{3.18}$$

where:

- $M(x) = m_0x^{k-1} + m_1x^{k-2} + \dots + m_{k-1}x + m_k$ is the message polynomial,
- $C(x) = c_0x^3 + c_1x^2 + c_2x^1 + c_3$ is the check polynomial, and $g(x) = (x+\alpha_1)(x+\alpha_2)(x+\alpha_3)(x+\alpha_4)$ is the generator polynomial

The Reed-Solomon code is performed in the Galois Field GF(2^8), where α is the primitive element that satisfies the primitive binary polynomial:

$$p(x) = x^8 + x^4 + x^3 + x^2 + 1 \tag{3.19}$$

The codeword N constitutes a robust voice print since the error correction encoding adds redundancy to the voice print data to enable it to withstand attacks. This voice print is used as the watermark, which is denoted by W.

3.2 3D Mesh Model Watermarking Algorithm

3.2.1 Watermark Embedder

The proposed technique estimates local curvature variation of the surfaces in the 3D mesh model and is similar to related work in that it employs surface normals based approach. The curvature or smoothness of a surface is used as a 3D perceptual measure to embed the watermark. Smooth surfaces can imperceptibly accommodate a watermark as opposed to flat surfaces or edges (sharp curves). The variation in the direction of surface normals is used to measure the smoothness of a surface. Figure 3.20 outlines the steps of the watermarking algorithm.

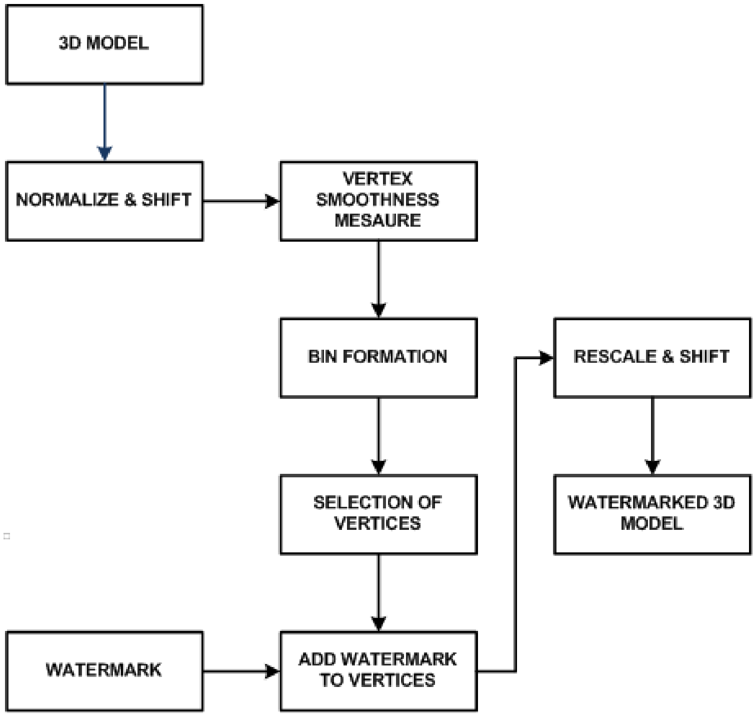

Figure 3.20: Watermarking Process

Normalizing and Shifting of 3D Model

Normalization of the 3D model is a pre-processing step that makes the watermark retrieval process invariant to changes in the orientation, translation, and scale of the watermarked 3D model. For translation invariance, the center of mass (the mean vector of all vertices) is shifted to the origin of the rectangular co-ordinate system [67]. For rotation invariance [133], the eigenvectors of the 3D model are used to represent the principal component axes of the model and are aligned to coincide with the co-ordinate axes. To achieve scale invariance, the average distance of the vertices from the center of mass is computed to determine the scale factor [77], which is used during the retrieval process to normalize the model and compensate for scaling.

Finding Vertex Smoothness Measure

The mesh model is collection of triangular facets that approximate the 3D object. Figure 3.21 shows the mesh structure of a textured *Horse* model.

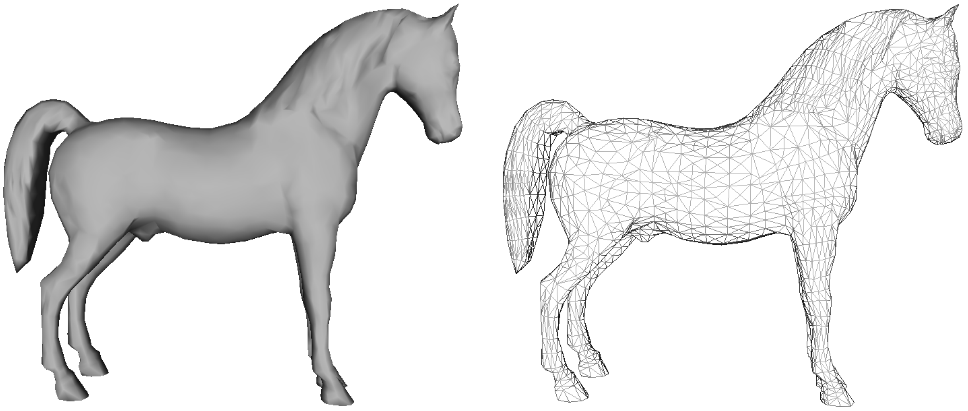

Figure 3.21: 3D Model of *Horse* and the Mesh Representation

Figure 3.22 highlights the 1-ring neighborhood of a set of vertices in the model. All the vertices that a vertex under consideration is connected to, is called the 1-ring neighborhood of a vertex. The curvature for each vertex's 1-ring neighborhood surface is estimated to determine whether the vertex can accommodate the watermark without causing any perceptual distortion to the model.

Figure 3.23 demonstrates the direction of the normals (in blue) to each face of the model. Since only the face normals in the 1-ring neighborhood of each vertex of the model are considered, the smoothness measure is local.

The following steps are implemented to compute the local smoothness measure: *Step 1:* Consider a vertex v from the mesh model as shown in Figure 3.24. Let M

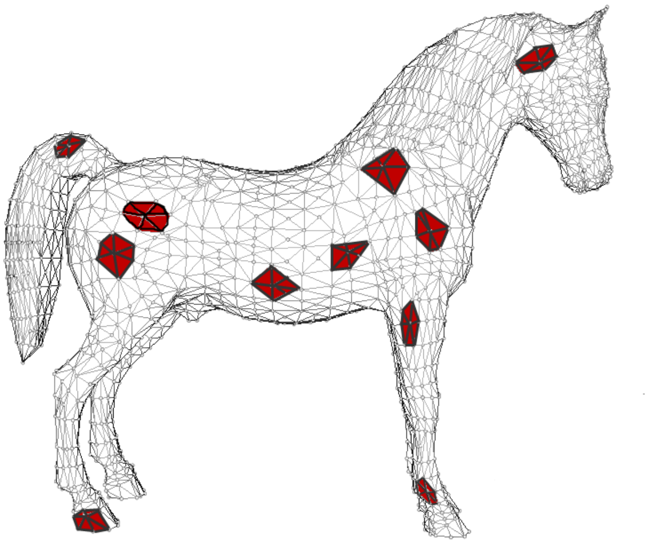

Figure 3.22: 1-Ring Neighborhood(highlighted in red) of Vertices

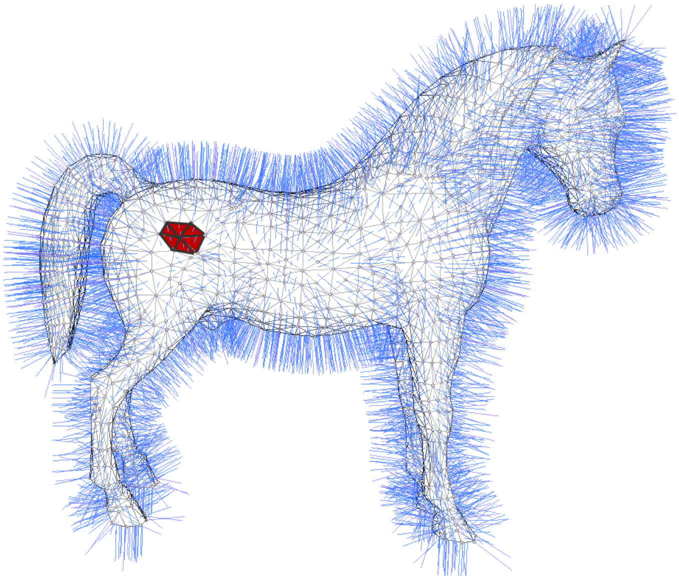

Figure 3.23: Face Normals(in blue)

be the number of its adjacent faces ($M = 6$ for the vertex v in Figure 3.24). The normals N_i to each face F_i which is formed by v and its neighboring vertices v_i is computed by taking the cross-product of the two edges of the face.

Step 2: Shift the face normals to pass through v. Find the eigen normal N of all the normals passing through v by computing the eigen-vectors from the eigen-

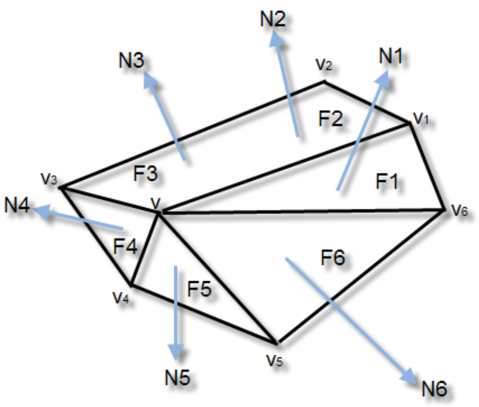

Figure 3.24: Eigen Normal N derived from 6 Face Normals

decomposition of the covariance matrix of all these surface normals. The eigen-vector corresponding to the maximum eigen-value constitutes the eigen-normal, as shown in Figure 3.25.

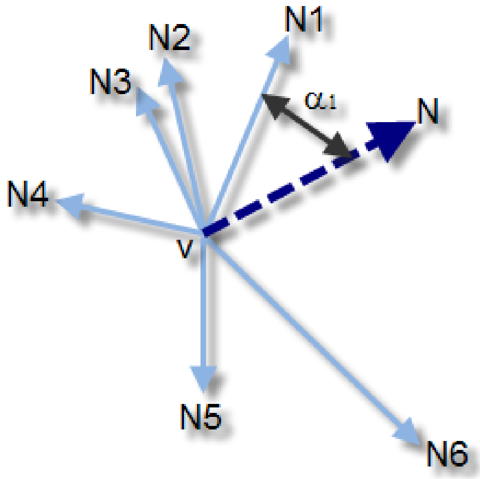

Figure 3.25: Normals Shifted to Pass Through Vertex v

Step 3: Now compute angles α_i between each pair of N_i and N. Figure 3.25 shows an angle α_1 between the eigen vector N passing through a vertex v and a normal N_1 to a face which has v as one of is vertices.

$$\alpha_i = \cos^{-1}\left(\frac{N_i N}{|N_i||N|}\right) \tag{3.20}$$

Step 4: Compute the average of all the angles α_i to give the local smoothness measure.

$$\alpha_{avg} = \frac{1}{m}\sum_{i=1}^{M}\alpha_i \tag{3.21}$$

Similarly, the algorithm is implemented at all the vertices in the mesh, to obtain the local smoothness measure for the entire model. If the region around the considered vertex is flat, the angles α_i will be small in magnitude since the face normals will be almost parallel to the eigen normal. If the region represents a peak, the angle between the face normal and the eigen normal through the vertex, α_i will have a larger magnitude and so the smoothness measure's magnitude will be higher. Thus, this parameter α_i represents local geometry or shape of a surface or region.

The illustration of this method is shown in Figure 3.26. The color scale starts with blue and ends with red, where red represents the most rough surface. Toolbox graph [66] has been used to display the models in *MATLAB*.

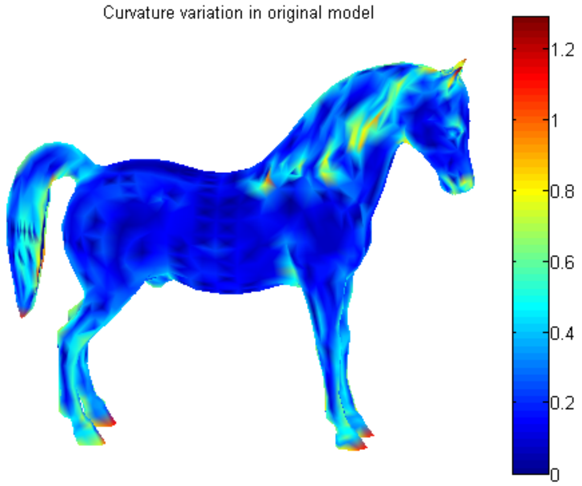

Figure 3.26: Curvature Variation in the *Horse* Model

Bin Formation

Based on the observed values of smoothness measure obtained for the vertex under consideration, the degree of smoothness variation is scaled to lie between 1 and 8.

These scaled values are labeled into three bins. This scaling is done on the basis that the bins between 1 and 2 have a low smoothness measure, bins between 3 and 6 are have a moderate smoothness measure, and bins between 7 and 8 have a high smoothness measure. Thus, different regions of vertex smoothness measure are classified in the model. The decision of choosing 8 bins (instead of 3) was made to allow room for the algorithm for manipulation of the number of bins selected for embedding the watermark. Preliminary experiments suggested that 8 bins provide sufficient granularity of curvature variation to adjust appropriate bins for watermarking should the algorithm fail to achieve imperceptibility while embedding the voice print in all bins with moderate smoothness measure. In scenarios where the watermark caused perceivable distortions in the 3D model, the number of selected bins with moderate smoothness measure were lowered and the scaling factor (discussed in later sections) was decreased by an order of 10^{-1}. Figure 3.27 shows the model and color bar indicating bins with pseudo colors (blue for the lowest variation and red for the highest variation).

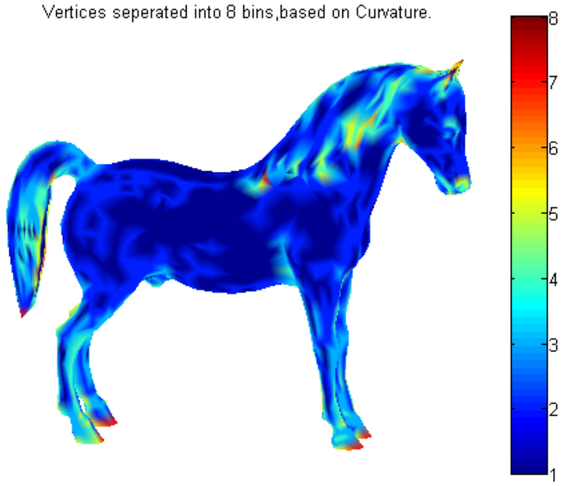

Figure 3.27: Bin Formation in Original Models

Selection of vertices for watermark insertion

Vertices lying in the regions which have moderate smoothness are selected to allow imperceptible distortions in the final watermarked model. High values of the smoothness measure represent very sharp changes such as edges. Low values correspond to smooth or flat surfaces. Watermark insertion in these extreme high or low smoothness regions is perceptible due to response of the Human Visual System. Figure 3.28 shows the selected vertices (in dark red) in the model.

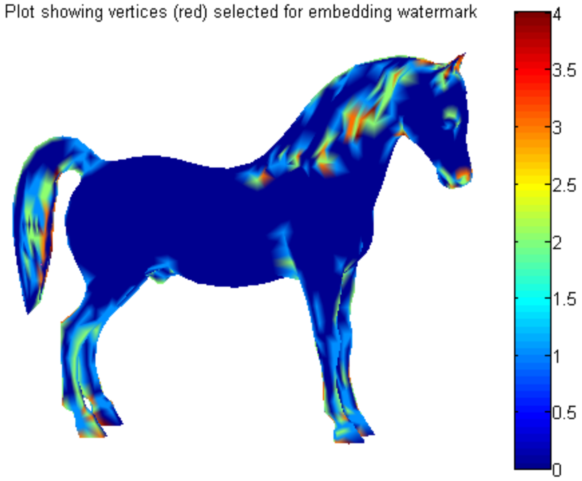
Plot showing vertices (red) selected for embedding watermark
4
3.5
3
2.5
2
1.5
1
0.5
0

Figure 3.28: Vertices Selected for Watermarking (in red)

Insertion of watermark

The robust voice print W is inserted as the watermark in the selected vertices. Watermark embedding is performed by altering the co-ordinate (x, y, z) of a vertex according to the following formula:

$$v\acute{}(x, y, z) = v(x, y, z) + KW \tag{3.22}$$

where,

$K = ScalingFactor$,

$W = WatermarkSequence$. The corresponding watermarked vertex is denoted by $v\acute{}$.

A scaling factor of 10^{-4} is used to embed the watermark values in the fourth decimal place of the vertex coordinate. The watermark is embedded in x,y,z co-ordinates therefore it is replicated thrice in the 3D model, thereby employing a secondary level of redundancy in addition to the Reed Solomon error correction encoding.

Rescaling and Shifting

Finally, the model is re-shifted and re-oriented to its initial location in the co-ordinate system. The watermark is inserted in the geometry of the model and modifies only the locations of vertices, without changing the connectivity of vertices. As it can be seen from Figure 3.29, there is minimal perceptible distortion between the original model and the watermarked model.

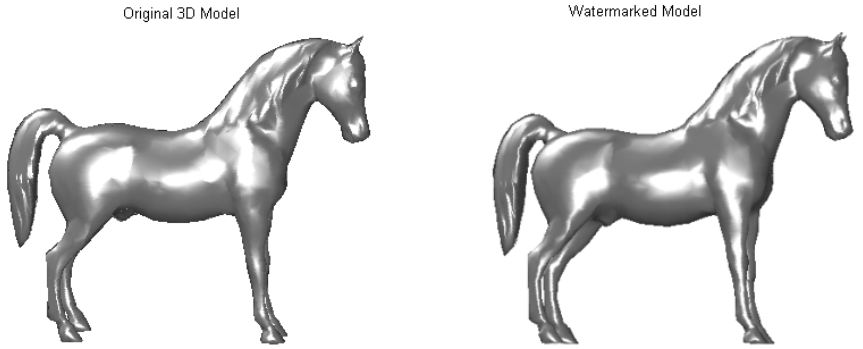

Figure 3.29: The Original and Watermarked Model of *Horse*

3.2.2 Watermark Detector

The watermark retrieval process requires the semi-blind key as well as the watermarked model to extract the watermark. Figure 3.30 outlines the extraction process.

Prior to watermark retrieval, the center of mass of the watermarked 3D model is determined and subtracted from the center of mass of the original model to determine the translation on the x,y and z coordinates of the watermarked vertices. The model is then shifted to compensate for this translation. The extent of scaling in the x, y and z directions is computed by dividing the average distance of the x, y, and z

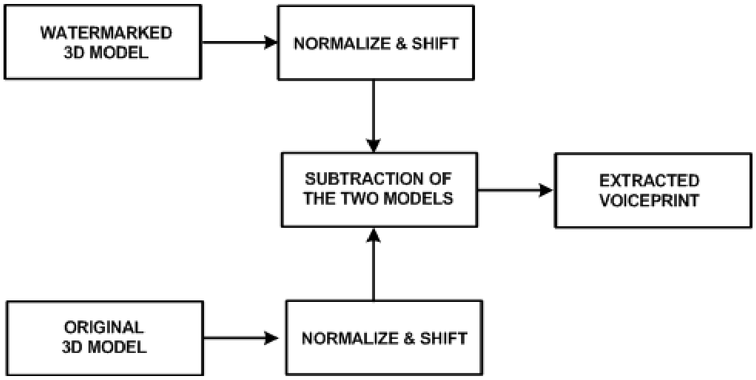

Figure 3.30: Watermark Extraction Process

coordinates of the watermarked and original vertices from the center of mass of the respective models. The normalization process [133] then re-scales and re-aligns the model after determining the degree of rotation.

3.2.3 Error Correction Decoding

Error correcting codes are applied to retrieve the voice print from the extracted watermark. The extracted watermark is decoded by the Reed-Solomon decoder and the original voice print data is recovered depending on the extent of damage caused to the watermark. The decoder can either correct errors (half as many as parity/check bytes appended to the original voice print) or fail to make corrections, in which case the verification module assists in determining the extent of damage and whether the extracted voice print can still be used to verify the user.

3.2.4 Verification Module

This step measures - i) the extent of similarity between the embedded and extracted watermark, and ii) whether the MFCC features extracted from a newly acquired voice sample from the user represent the same speaker whose voice print has been embedded as the watermark.

The correlation coefficient *Corr* that gives the extent of similarity between the embedded watermark W and the recovered watermark W' is computed by:

$$Corr = \frac{\sum WW' - \left(\frac{\sum W \sum W'}{n}\right)}{\sqrt{\left(\sum W^2 - \frac{(\sum W)^2}{n}\right)\left(\sum W'^2 - \frac{(\sum W')^2}{n}\right)}} \tag{3.23}$$

where, n is the size of the watermarks.

This correlation coefficient is a number between -1 and +1 which measures the degree to which two variables are linearly related. If there is perfect linear relationship with positive slope between the two variables, the correlation coefficient will be +1. If there is a perfect linear relationship with negative slope between the two variables, the correlation coefficient will be -1. A correlation coefficient of 0 indicates that there is no linear relationship between the variables.

The acoustic likelihood measure of the extracted MFCC features from the user's voice sample acquired at access time, with the extracted voice print(i.e. the speaker model embedded into the 3D model) is computed by:

$$LogLikelihood = \log[P(k|\theta)p(x_n|k,\theta)] \tag{3.24}$$

The value of this log likelihood measure suggests if the extracted features from the acquired voice sample match the speaker model represented by the GMM embedded as the watermark. When a speaker's GMM is evaluated for a set of MFCC features, only that speaker's features contribute significantly to the likelihood value. If this value falls within a threshold of ±1 (which allows for intra-individual variations in voice) of the original log likelihood measure derived during the enrollment phase, then the user is authenticated and allowed to access the 3D model. Changing the value of the threshold results in different FRR and FAR, as demonstrated by the experiments in Chapter 5.

3.3 Proposed Digital Rights Management Model

A high-level overview of the proposed DRM system framework is outlined in Figure 3.31. This process model [95] shows the basic processes in the DRM system and the logical work flow from creation to consumption of the graphic file.

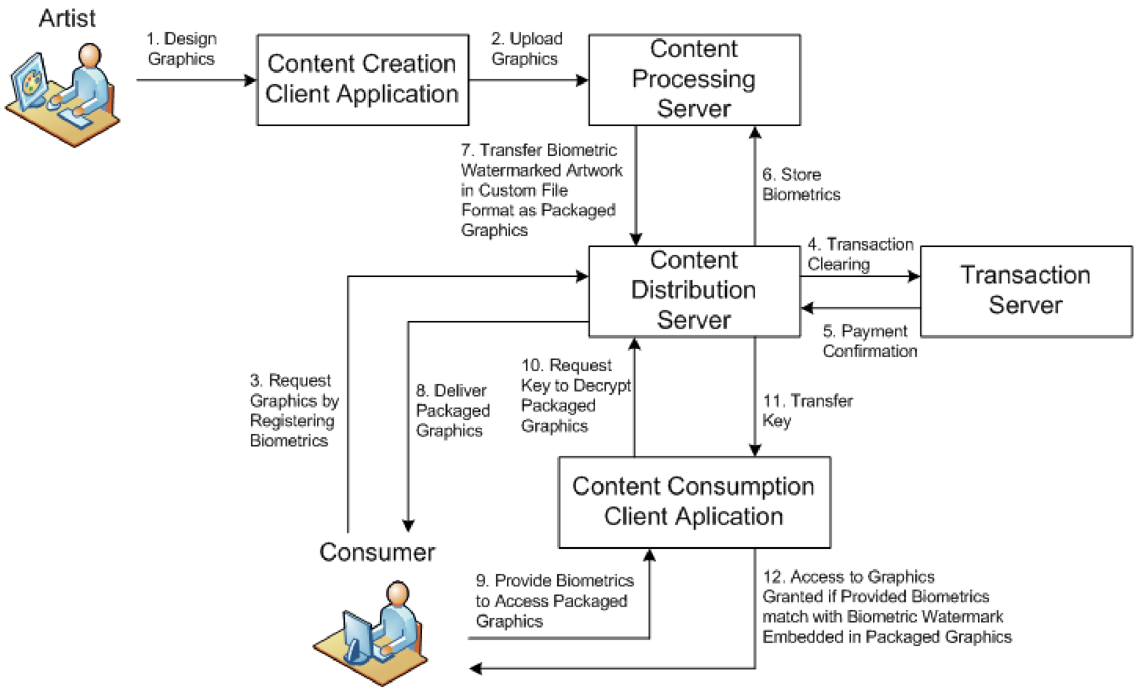
Artist
1. Design Graphics
Content Creation Client Application
2. Upload Graphics
Content Processing Server
7. Transfer Biometric Watermarked Artwork in Custom File Format as Packaged Graphics
6. Store Biometrics
Content Distribution Server
4. Transaction Clearing
Transaction Server
5. Payment Confirmation
3. Request Graphics by Registering Biometrics
8. Deliver Packaged Graphics
10. Request Key to Decrypt Packaged Graphics
11. Transfer Key
Content Consumption Client Aplication
Consumer
9. Provide Biometrics to Access Packaged Graphics
12. Access to Graphics Granted if Provided Biometrics match with Biometric Watermark Embedded in Packaged Graphics

Figure 3.31: DRM System Block Diagram

DRM framework is composed of two stages - i) enrollment (represented by steps 3-8 in Figure 3.31) and ii) authentication (represented by steps 9-12 in Figure 3.31). The consumer provides his biometric images during enrollment, prior to purchasing the graphics. The system inserts the biometric image of the consumer as watermark into the purchased 3D graphics, wraps the watermarked graphic in a custom file format so that the graphic file cannot be accessed outside the system, and encrypts these contents using a consumer-specific key. This packaged content is then distributed to the consumer. When the consumer attempts to access the graphics file, the authentication stage prompts the consumer to provide his biometric image and compares this newly acquired biometric image with the biometric image embedded as watermark to verify the consumer's legitimacy. Based on the computed similarity measure between the acquired and embedded biometric images, the system authenticates the user to access the graphics. A predefined threshold value is set for the similarity measure to distinguish a genuine user from an illegitimate user. An illegitimate user's biometric provided at access time does not match with a genuine user's biometric embedded as the watermark, so the system denies access to the graphics.

If the biometric watermark can't be retrieved from the graphic file, the system denies access to the graphic file. Therefore, the system does not rely on the assumption that the biometric watermark is intact and has not been destroyed by hackers. This feature discourages consumers from tampering with the packaged graphics. If illegal copies of the artwork are redistributed by a legitimate user, the biometric watermark travels with the artwork and secures it from illegitimate usage. This is because the custom file format prevents consumers from accessing the file outside the DRM system, and the authentication stage of the system sieves legitimate users from illegitimate users. Therefore, the biometric watermark protects the graphics content from being used by anyone other than the valid user.

If the system is compromised and the artwork is distributed and accessed by anyone other than the legitimate user, the embedded biometric serves as a tracer. The pirated graphic file is examined for the embedded biometric watermark. If the biometric watermark has not been tampered with, it assists in tracing back illegitimate redistribution to the traitor in the distribution chain and suing the responsible individual for piracy. Privacy concerns over sharing one's biometric trait along with the purchased protected graphic content on peer-to-peer(P2P) networks, prevents large scale piracy of the artwork.

In the event of compromised biometrics, since a biometric trait cannot be revoked, the framework has the provision to support multiple biometrics so the compromised trait is replaced by an alternative trait. Furthermore, upon receiving notification of compromised biometrics from the user, the server de-activates the user-specific key thereby locking out access to files previously encrypted with this key and issues a new key for the user. This new key is used to encrypt files previously purchased by the user, so only the legitimate user is able to access these files in spite of the compromised biometrics.

3.3.1 DRM System Architecture

The architectural design of the system, see Figure 3.32, has been motivated by various DRM system architectures [9, 28, 31, 37, 59, 62, 75, 89, 113, 116]. The system utilizes a client-server protocol for implementation as shown in Figure 3.32 and involves a custom file format associated with a DRM enabled graphics design/consumption application. 3D graphics files are sold in various formats , such as *3ds (3D Studio), mb (Maya), lwo (Lightwave), c4d (Cinema 4D).* A file format's (e.g. *3ds*) native graphics design software (e.g. *3D Studio*) is not equipped with DRM functionalities. Embedding biometric watermarks in existing file formats requires the associated graphics design software to incorporate a DRM plug which enforces access control. Graphics designed and sold prior to installation of this plug-in are DRM-free and are not protected from piracy. Biometric watermarks from protected graphics can be easily removed by using DRM-free versions of the same graphic. Since backwards compatibility and DRM can't go hand in hand, it necessitates the need for a custom 3D graphic file format and a customized graphics design application equipped with DRM modules. The custom file format enables access control by notifying a graphics consumption application that a file is DRM enabled. The custom file format is a just way to bind the graphics to the DRM system in order to prevent users from bypassing the access control mechanism. The custom file format also assists in content editing, logging, and system renewability.

The proposed DRM system has five components: Content Creation, Content Processing, Transaction Management, Content Distribution, and Content Consumption. Functionality of each component is specified below.

Content Creation

Artists use a graphics design application to create the artwork. The design software has DRM capabilities after installation of a DRM plug-in. Alternatively, a proprietary DRM system based on a proprietary 3D file format can be developed that supports design of the graphics in multiple native formats (*3ds, mb, lwo*) which then undergo

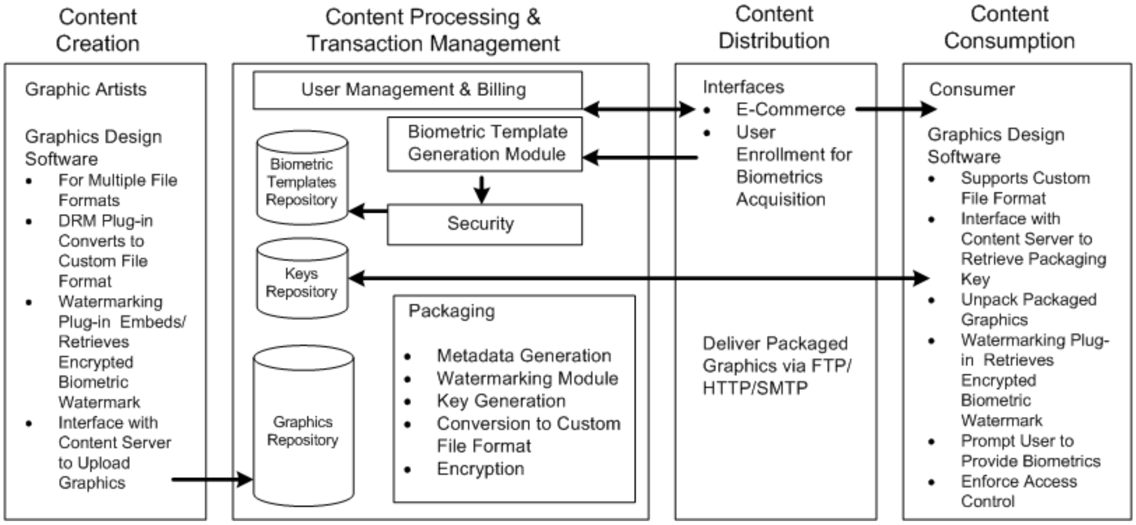
Content Creation
Content Processing & Transaction Management
Content Distribution
Content Consumption
Graphic Artists
Graphics Design Software
For Multiple File Formats
DRM Plug-in Converts to Custom File Format
Watermarking Plug-in Embeds/ Retrieves Encrypted Biometric Watermark
Interface with Content Server to Upload Graphics
User Management & Billing
Biometric Template Generation Module
Biometric Templates Repository
Security
Keys Repository
Packaging
Metadata Generation
Watermarking Module
Key Generation
Conversion to Custom File Format
Encryption
Graphics Repository
Interfaces
E-Commerce
User Enrollment for Biometrics Acquisition
Deliver Packaged Graphics via FTP/ HTTP/SMTP
Consumer
Graphics Design Software
Supports Custom File Format
Interface with Content Server to Retrieve Packaging Key
Unpack Packaged Graphics
Watermarking Plug-in Retrieves Encrypted Biometric Watermark
Prompt User to Provide Biometrics
Enforce Access Control

Figure 3.32: DRM System Components

DRM compliant format conversion. Figure 3.32 illustrates the functionalities of this component. The plug-in for the artists will include the watermark embedder, detector and matcher components, and an interface to connect to the graphics repository on the content server.

Content Processing

The user enrollment interfaces provided by the content distribution component (see Figure 3.33) securely transfer the acquired biometric trait of the user to the biometric template generation module on the content server. This module generates a biometric print from the biometric samples provided by the user. Due to privacy concerns [57], the template is encrypted and then stored in the biometric templates repository along with an associated user identifier. The packaging module is responsible for conversion of graphics to custom file format representation. This module populates meta data in a header with default values. The graphic content is watermarked with an encrypted version of the biometric template. A key is generated for the user, stored in the key repository, and linked with the user's biometric template. The packager encrypts the content along with the meta data using this key so that the content is scrambled and made unreadable. The packaged content is ready for distribution to the user.

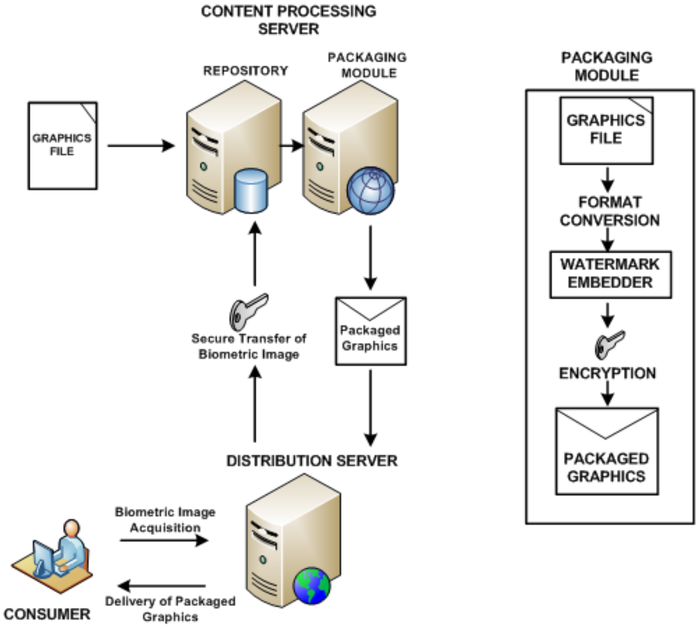

Figure 3.33: Content Processing

Transaction Management

This component handles the user registration, commerce, and billing activities. It includes a module for interaction with an external payment service to handle the financial aspects of the purchase transaction.

Content Distribution

The main function of this component is trading and registration of the user. It maintains a website which acts as the interface between the consumer and the content provider. It provides interfaces to register the user, accept payment information, capture user's biometric samples and securely transfer the acquired information to the *Transaction Management* component. Distribution of the packaged graphics to the clients is also handled by this component. Distribution is carried out by providing download interfaces using either HTTP, FTP, or SMTP protocols. Content is delivered over a secure transmission channel.

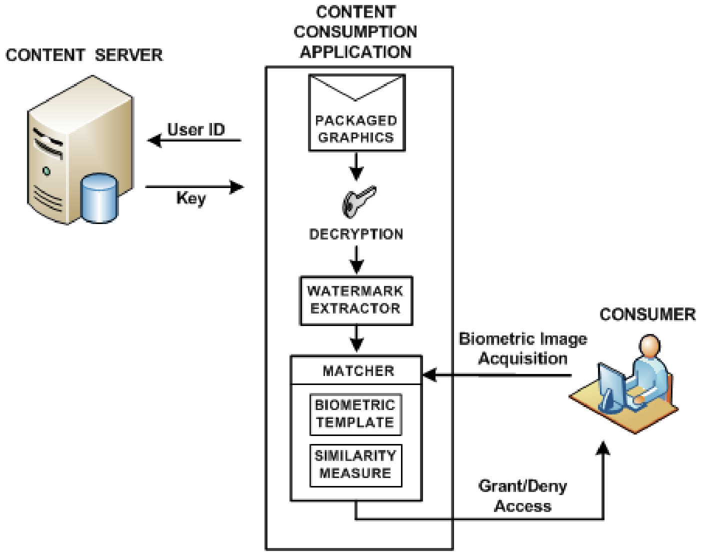

Figure 3.34: Content Consumption

Content Consumption

Figure 3.34 outlines the content consumption component of the proposed DRM system. The client-side DRM enabled graphics consumption software is responsible for authorizing rightful users to access the purchased graphics. When an attempt is made to access the file by the end user, the 3D content consumption application prompts the consumer to provide his/her biometric trait. The DRM plug-in installed at the client application generates a biometric template from the acquired sample, encrypts it and then sends it to the server along with the user identifier to request the key associated with the user to decrypt the file contents. The plug-in used by the consumer application will only have the watermark detector and matcher component. The encrypted biometric template is compared with the extracted biometric watermark to validate legitimacy of the user. A match between the captured biometric template and the embedded template grants access to the user, while a mismatch locks down the graphic file. If the watermark detector is unable to retrieve the watermark it denies access to the file. The plug-in provides access management by tracking save as, modify and save, cut, copy, paste operations on the graphics file. It keeps track of the user activity in regards to modifying and copying the graphics to new files and updates the header of the graphics file with appropriate logging information. This logging assists the plug-in to maintain the presence of the biometric watermark in the graphics content regardless of modifying or saving of the graphics to a new file. If the system is compromised and the file is distributed and accessed by anyone other than the legitimate user, the embedded biometric serves as a tracer. The pirated graphic file is examined for the embedded biometric watermark. If the biometric watermark has not been tampered with, it assists in tracing back illegitimate distribution to the traitor in the distribution chain and suing the responsible for piracy.

The system employs a locking and logging mechanism and handles security issues by using encryption to address the privacy and maintain anonymity of users. The robustness of the system is based on the performance characterization of biometrics which has been discussed in detail in [106].

3.3.2 Custom File Format

Figure 3.35 illustrates the proposed file format which includes a header and the watermarked graphics content. The header comprises of 7 fields that serve as meta data.

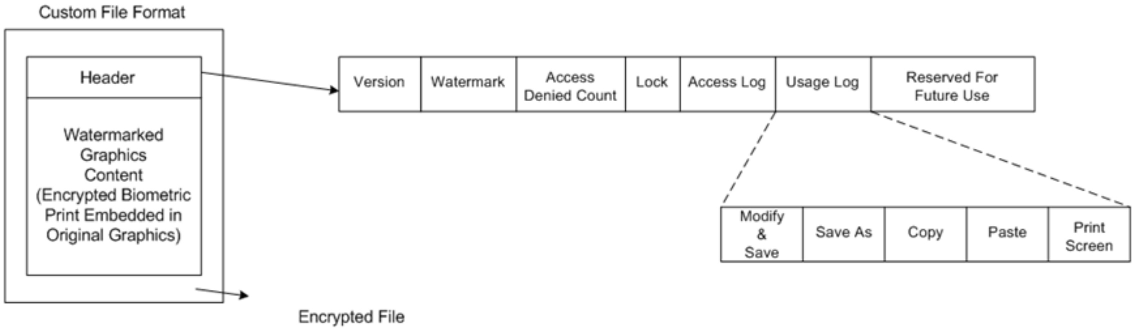

Figure 3.35: Header Fields

The field for version number is used to allow future modifications to the file format. To avoid a file from being watermarked twice, the watermark field indicates whether the file has been watermarked or not. The number of times access is denied to a file based on the provided biometrics, is stored in the access denied count field. This is to prevent illegitimate users from circumventing the system by repeated trial and error attempts. The user is allowed 3 attempts to access the file using biometric authentication and then the Lock flag is set to disable the file. Access log stores the number of attempts required to access the file for monitoring user activity, the date, time and PC's hardware identifier for the last successful access. The first time a user accesses a file on a PC, the user is prompted to provide biometric samples. The biometric print is encrypted and cached on the local store. Subsequent accesses on the same PC utilize a locally cached copy of the biometric print. Each time the user tries to access the file from a different PC, the hardware ID in the header is checked to prompt the user for biometric sample acquisition. Activities of the user in terms of modifying and copying the graphic content are recorded in the usage log field to notify the system for taking incremental protection measures to watermark the modified or copied file. Analogue attacks are addressed by the system by monitoring the screen capture flag. Reserved field is included to accommodate tags for future use such as multiple watermarks, reseller watermarks, transfer of watermark, and interoperability. Table 3.1 provides the description and values for the header fields.

3.3.3 Security Aspects of the DRM System

Security Model

The primary security goal of the DRM system is to prevent illegitimate access to the legally distributed 3D graphics. The secondary goal of the system is to trace illegally accessible graphics back to the buyer responsible for unauthorized redistribution. According to Kerckhoff's principle, the strength of a system should lie entirely in the difficulty in determining the key and not in the secrecy of the algorithm. The proposed system utilizes a consumer-specific key to encrypt/decrypt the custom file format. The custom file format merely serves as a container for the raw graphics data and the purpose of the key is to make it difficult for the adversary to segregate this raw graphics data that is wrapped in the custom file format. The system is breached if this key is accessible to the adversary, for the unprotected graphics data can be

Table 3.1: Header Fields of Custom File Format

Byte	Description	Value
0:	Version	1, For current implementation
2:	Watermark	0 - File is not watermarked, 1 - File is watermarked
3:	Access Denied Count	Number of Times Access to File is Denied
10:	Lock	0 - File is Unlocked, 1 - File is Locked For Access
11-51:	Access Log	Number of Attempts Required to Access the File Date, Time and Machine's Hardware Identifier for Last Successful Access
52-56:	Usage Log	00000 Default Value
52		1 - File is Modified and Saved,
53		1 - File is Saved As New Copy,
54		1 - Copy (Ctrl-C Key pressed),
55		1 - Paste (Ctrl-V Key Pressed),
56		1 - Screen Capture (PrtScrn Key is Pressed)
57 - 300		Reserved For Future Use

separated from the decrypted custom file format. Therefore, the system completely relies on the secure storage of this key in order to protect the data.

The security assumption made by the system is that the communication between the artist, the DRM client and servers, and the consumer takes place through a secure channel in order to protect information from eavesdropping when it is transmitted.

Trust Model

- To ensure that the content server receives artwork from a genuine artist, the system requires the artist to provide his digital certificate. Prior to uploading the graphics to the content server. the artist signs and encrypts the graphics. The server validates the integrity of the uploaded content by verifying the artist's signature and then decrypts the content for further processing. This validates the content to be genuine and establishes trust between the artist and content server.

- To obtain the user-specific key from the content server to decrypt the packaged graphics, the content consumption client application requires that the buyer must authenticate to prove his identity to the server by providing a user ID.

- The user's authentication data and biometric data are only available to the user.
- The system will not share a user's personal data with third parties.
- The framework handles security issues associated with biometric data by using encryption to address the privacy and maintain anonymity of users.

Threat Model

Security Issues For The Server

The Content Server is prone to hacking. An adversary can exploit security flaws in the server to obtain control over any one of the server repositories that store the biometric templates, keys and unpackaged graphics, the packaging module and defeat the system.

Security Issues For The Communication Channel

The communication channel is considered to be under the complete control of an adversary who can break weak cryptography, exploit weak keys, knows the communication protocol, controls the network, can break into servers with security flaws, download original content.

Security Issues For The Client's Side

- The adversary has complete control over the user side and can hack the DRM client consumption application. The client side watermark extractor or matcher component can be replaced by an attacker-supplied component.
- The user-specific key acquired from the server is temporarily stored on the client's machine to decrypt the packaged graphics, and is vulnerable to exposure.

- It is possible to make an analogue copy of the output (e.g. reconstructing the 3D model from 2D images captured from the display screen). This can be prevented by limiting the number of allowed screen captures.

- Attacks against the rendering application that replace part of the rendering application so that once the content is decrypted, it can be captured and saved.

- A major threat to the system is compromised biometrics that lead to spoofing attacks. When a user's biometric trait is compromised (i.e. an adversary obtains the biometric of a legitimate user without his consent or knowledge), the adversary fraudulently gains access to the protected graphics file with the legitimate biometric trait. Biometric-based authentication systems have been criticized due to this vulnerability, since a biometric trait cannot be revoked. The proposed framework addresses this security issue by supporting the use of multiple biometric traits such that if one biometric trait is compromised, it can be replaced by an alternative trait. Furthermore, since the DRM system is an online system, the server deactivates the key generated for a user whose biometric has been compromised thereby locking out access to files previously encrypted with this key and issues a new key for the user. This new key is used to encrypt files previously purchased by the user, so only the legitimate user is able to access these files in spite of the compromised biometrics.

Chapter 4

Software Engineering Design Principles

This chapter outlines the system assumptions, requirements, specifications along with software engineering design principles concerned with the modularization and detailed interfaces of the system elements.

4.1 System Assumptions

The system operation is based on the following assumptions:

1. The biometric trait is present in the user (which means that the user has a voice).

2. The user is willing to offer his/her voice biometric samples to the system for legitimate access control of watermarked 3D models.

3. The user is cooperative and utters the predetermined phrase while providing voice samples during both enrollment and authentication phases. The system does not check the validity of the spoken phrase should the user intentionally change the spoken text.

4. The voice samples are acquired in a quite environment.

5. The acquired voice samples represent a single speaker audio stream. The system does not support multi-speaker streams.

6. The user will not share voice recordings of the spoken phrase with others. The security of the system is based on this assumption so that prerecorded voice samples of legitimate user do not circumvent the system.

7. The system ignores variations such as different pitch that alters the speaking manner, noisy voice samples due to the environment or communication channel (voice acquired over telephone), speaking under stress or during sickness (cough, cold, fatigue), and attempted mimicry.

8. The file formats that will be used are *.wav* for sound file input, *.off* format for 3D mesh models, ascii *.txt* representation for the biometric voice print.

9. The input *.off* file size is restricted to the range of 15KB - 2000KB. Most 3D files smaller than 15KB are unable to accommodate a watermark that houses a voice print (minimum size 1.17KB). 3D files over 2000KB require longer processing times (over a couple of minutes) on a desktop PC.

4.2 Requirements Specification

The purpose of the requirements specification is to describe the functionality that the Biometric Watermarking System (BWS) will support. The system requirement can be categorized as non-functional and functional.

4.2.1 Non-Functional Requirements

The non-functional requirements are associated with the usability, reliability, performance of the system, and system specifications.

Usability: BWS must meet usability goals set in regards to:

- Effectiveness: The system must always accept legitimate users and may falsely accept non-genuine users depending on the FAR for a specific user.

- Efficiency: The system must not require an inordinate amount of the users' effort for enrollment and authentication.

- Satisfaction: The system must be perceived as *easy to use* by the users.
- Learnability: The system must not require an inordinate amount of effort for novice users to learn how to use it.

Performance: Watermarking and Accessing 3D Files: A model should be watermarked and the user authenticated in a *reasonable* amount of time. Actual processing time for a model will depend on variables such as file size and user interaction.

- Time should not exceed 120 seconds per 3D model 95% of the time for files less than 500KB.

Reliability: The system must have the ability to operate correctly over time, including consistent stability of the system at all times.

Hardware and Software Requirements: The hardware and software requirements of the system are outlined in Figure 4.1.

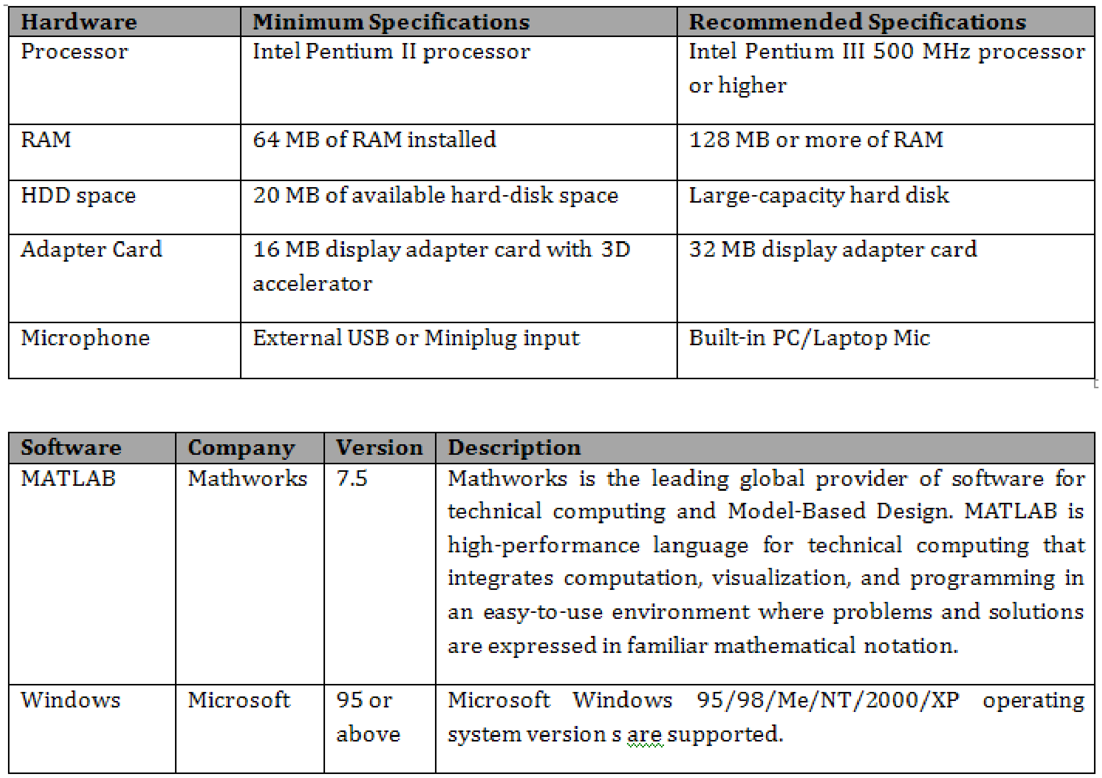

Hardware	Minimum Specifications	Recommended Specifications
Processor	Intel Pentium II processor	Intel Pentium III 500 MHz processor or higher
RAM	64 MB of RAM installed	128 MB or more of RAM
HDD space	20 MB of available hard-disk space	Large-capacity hard disk
Adapter Card	16 MB display adapter card with 3D accelerator	32 MB display adapter card
Microphone	External USB or Miniplug input	Built-in PC/Laptop Mic

Software	Company	Version	Description
MATLAB	Mathworks	7.5	Mathworks is the leading global provider of software for technical computing and Model-Based Design. MATLAB is high-performance language for technical computing that integrates computation, visualization, and programming in an easy-to-use environment where problems and solutions are expressed in familiar mathematical notation.
Windows	Microsoft	95 or above	Microsoft Windows 95/98/Me/NT/2000/XP operating system version s are supported.

Figure 4.1: Hardware and Software Requirements

4.2.2 Functional Requirements

This section has a list of all specific requirements that are to be implemented by BWS. Each functional requirement has been assigned a reference number, starting with the characters - DT, PR, for traceability to other system artifacts.

Data Requirements

- Graphics File Format (F_DT_01): BWS must support the Open File Format (*.off*) for 3D models.
- Characteristics and quality of the recorded voice (F_DT_02): A 2 channels stereo sound signal with a bit rate of 1411kbps, sample size of 16 bits and an audio sampling rate of 44 KHz is captured in *.wav* format.

Process Requirements

- Imperceptible watermark (F_PR_01): The system embeds a voice print of the user into a 3D model such that watermarked 3D mesh model looks like the original model and it should not reveal any clues of the presence of the watermark.
- Semi-Blind watermarking technique (F_PR_02): The system does not require the original unmarked model to extract the watermark from the watermarked media but makes use of a key, that stores the locations and original values of the vertices that are modified by the watermarking scheme, in addition to the original watermark.
- Semi-Fragile watermark (F_PR_03): A semi-fragile watermark is inserted into the host model and can withstand certain attacks (noise, cropping, smoothing) but not all. The watermarking scheme does not support 3D content editability, mesh subdivision, decimation and remeshing operations.
- Text and speaker dependent voice print (F_PR_04): The voice capture process is text dependent as all the speakers have to speak a predetermined text. The speech waveform is then converted to a parametric representation i.e. feature

vectors. Extraction of features is done such that they are primarily a function of speaker.

- Variable speaking rate (F_PR_05): The voice print extracted from the recording has to independent of the length of duration of recorded voice sample (talking speed of the speaker). The system achieves insensitivity to speaking rate by pre-processing the acquired voice sample to eliminate silence thereby accommodating slow, moderate, and fast speakers which generate voice samples of different duration.

- Constant size voice print (F_PR_06): Since the voice print is derived from the Gaussian mixture model of the mel-frequency cepstral co-efficients of the voice signal, the voice print always assumes a fixed size of values irrespective of who the speaker is.

- Access Control Decision (F_PR_07): BWS will determine if a user for a 3D model is authentic or not. The system provides a decision on whether to accept or reject the user based on the comparison of the voice sample provided by the user during authentication with the voice print generated during user enrollment.

4.3 System Design

Figure 4.2 demonstrates a high-level layered architecture of the system. There are six functional layers - Voice Acquisition, Watermark Generation, Watermark Embedding, Voice Parametrization, Watermark Detection, and Access Control. The system is divided into two sub-systems - Enrollment and Authentication subsystems.

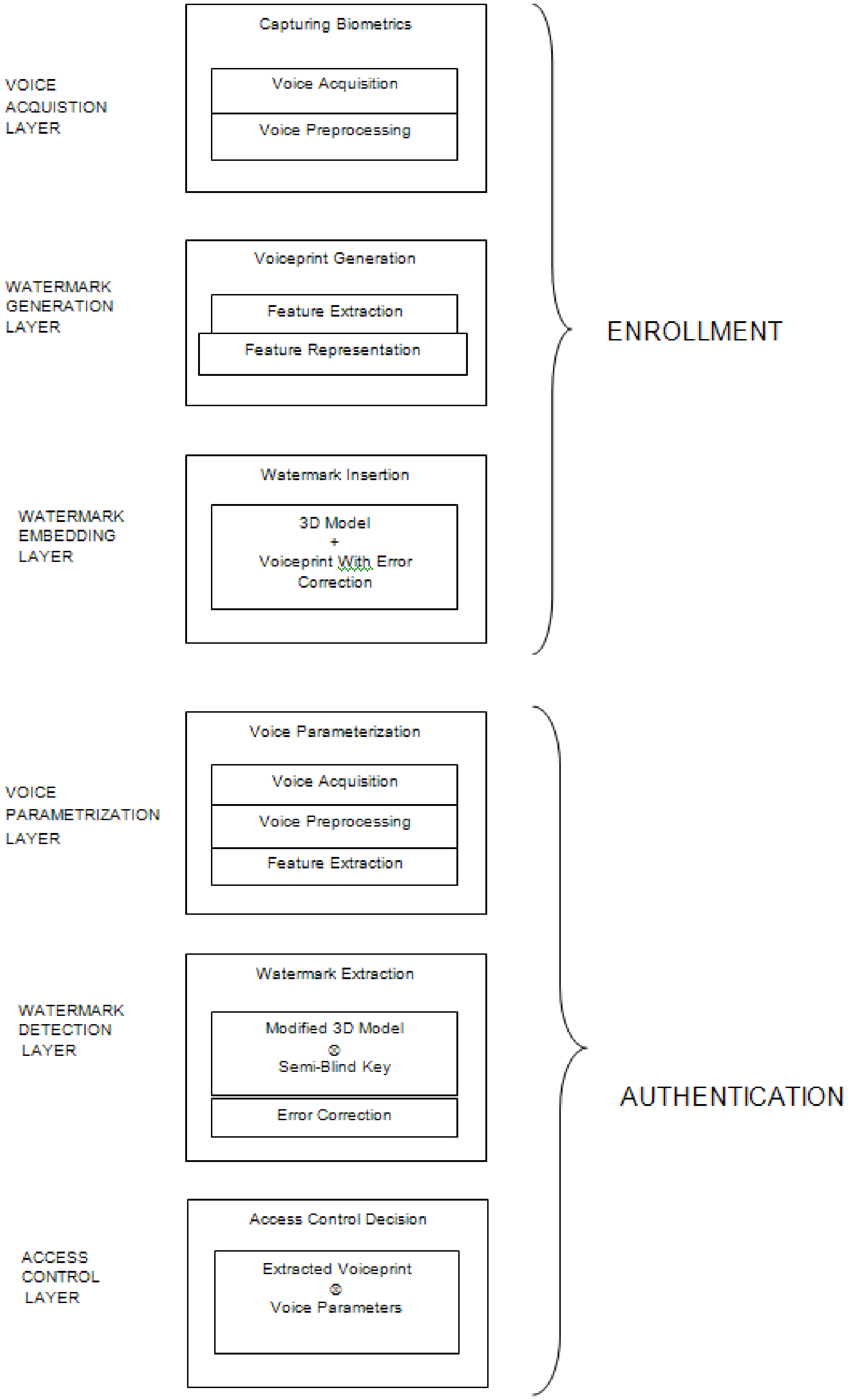

Figure 4.2: System-Level Layered Architectural Diagram

Enrollment Sub-System

- Voice Acquisition Layer - This module is responsible for acquiring the voice samples of an individual and preprocessing the waveform to eliminate silence areas.

- Watermark Generation Layer - This module is responsible of generating a voice print from the speech waveform by extracting feature vectors and representing those features using a GMM.

- Watermark Embedding Layer - This module generates a watermarked model by embedding the voice print as a watermark into the 3D graphic model after employing error correcting codes to safeguard the voice print.

Authentication Sub-System

- Voice Parametrization Layer - This module extracts the MFCC features from the newly acquired pre-processed voice sample for comparison against the voice print embedded into the watermarked 3D mesh model.

- Watermark Detection Layer - This module extracts the watermark and attempts to correct any modifications that the voice print may have been subject to by an attack.

- Access Control Layer - This module is responsible for authentication of the user by comparing the user's extracted voice features against the extracted voice print. This layer either grants or denies access to the graphics based on the obtained likelihood measure between voice features and the GMM-based voice print.

4.4 Use Cases

The system has 10 use cases (see Figure 4.3). Each use case is assigned a reference number, starting with the characters UC, for traceability to other system artifacts.

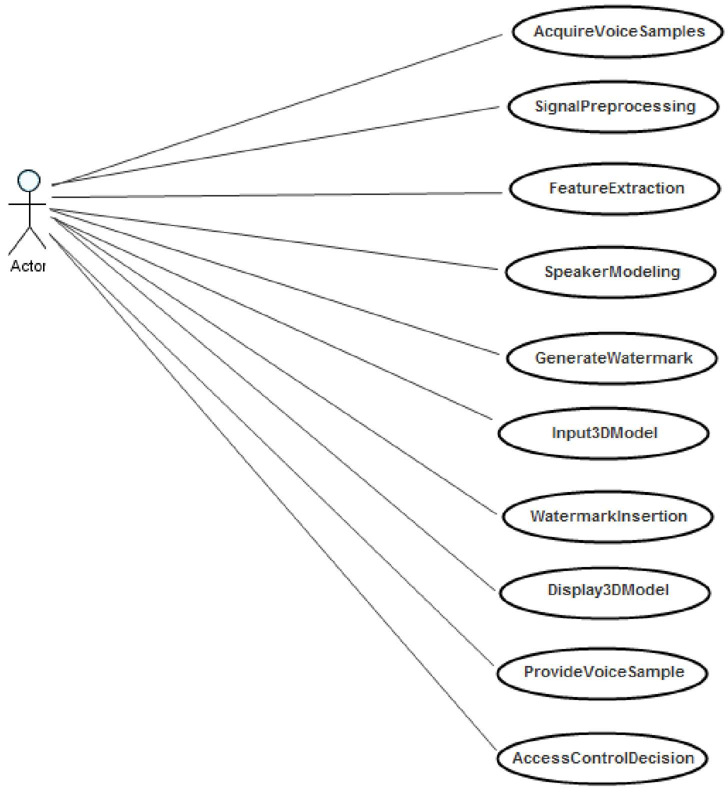

Figure 4.3: Use Case Diagram

- AcquireVoiceSamples (UC01): The user provides the system with voice samples in .wav format for a predefined utterance. The user presses the *Provide 3 Voice Samples* button to upload the .wav files into the system.

- SignalPreprocessing (UC02): The system eliminates silent regions from the waveform when the user presses the *Voice Signal Pre-Processing* button. This step enables the voice print formulation process to be independent of the pace at which the predetermined phrase was spoken during the voice acquisition phase. The display area is updated with the representation of processed signal.

- FeatureExtraction (UC03): The user presses the *MFCC Feature Extraction* button to extract features representing the identity of the user.

- SpeakerModelling (UC04): The user presses the *GMM Speaker Model* button to instruct the system to use the extracted features in the previous step for generating a GMM that constitutes the user's voice print.

- GenerateWatermark (UC05): The user presses *Generate Watermark* button to encode the voice print using error correction routines in order to protect its data from attacks.

- Input3DModel (UC06): The user presses the *Input 3D Mesh Model* button to upload the 3D model for watermarking. The display area is updated with a rendering of the graphic file.

- WatermarkInsertion (UC07): The user presses the *Watermark Insertion* button to enable the system to inserts the watermark into the previously selected 3D model.

- Display3DModel (UC08): The user pushes the *DRM Protected 3D Model* button to display the watermarked model in the bottom right axis on the interface.

- ProvideVoiceSample (UC09): The user presses the *Provide Voice Sample* button to upload a voice sample with the predetermined utterance. The system preprocesses this voice sample and extracts user specific features from it.

- AccessControlDecision (UC010): The user presses the *Access Control Decision* button for the system to provided a decision regarding granting or denying access to the graphics file. The access control decision is displayed in the center bottom area of the authentication interface panel.

4.5 Requirements Traceability Matrix

Figure 4.4 shows the mapping between the functional requirements and the corresponding use cases which implement the requirement. This traceability matrix is used to check if the requirements are being met.

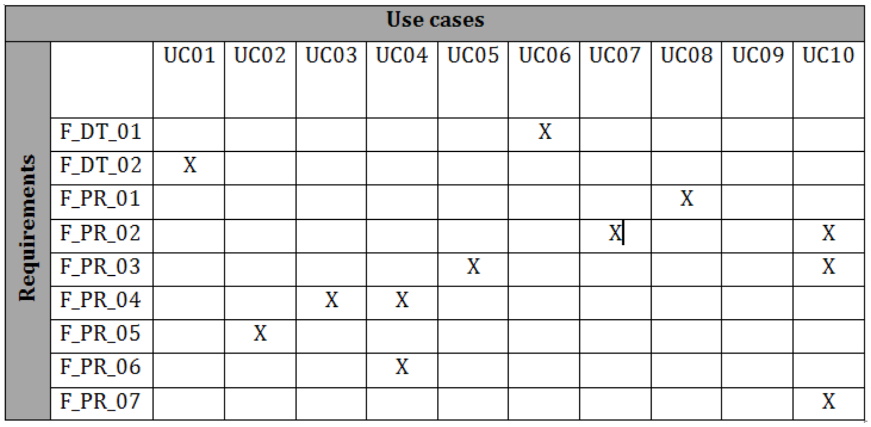

	Use cases									
Requirements	UC01	UC02	UC03	UC04	UC05	UC06	UC07	UC08	UC09	UC10
F_DT_01						X				
F_DT_02	X									
F_PR_01								X		
F_PR_02							X			X
F_PR_03					X					X
F_PR_04			X	X						
F_PR_05		X								
F_PR_06				X						
F_PR_07										X

Figure 4.4: Requirements Traceability Matrix

4.6 User Interface

Figure 4.5 illustrates the main GUI of the system. The GUI provides an interface with buttons and axes to interact with the user and display intermediate phases of the biometric watermarking process. The GUI is divided into two sections to represent the two phases of the system - Enrollment and Authentication. For the enrollment phase, the end user only needs to interact with the system using the first button (*Provide 3 Voice Samples*) which prompt the user to upload his voice samples, the *Input 3D Mesh Model* button which prompts the user to upload the 3D model that needs to be watermarked, and the last button (*DRM Protected 3D Model*) which inserts the voice biometric watermark into the uploaded 3D model and provides a rendering of the watermarked 3D model in the right bottom display area. The remaining intermediate buttons have been provided to enable - i) users to understand the various steps involved in the biometric watermarking process and ii) visualize the intermediate steps of signal pre-processing, MFCC feature extraction and GMM speaker modeling. The right panel does not provide an interface for the intermediate steps of watermark extraction solely for the purpose of giving users a feel of the simplicity of interacting with the system during the authentication phase. Figure 4.6 depicts one of the intermediary steps that displays the speech waveform in red, representing the pre-processed voice signal.

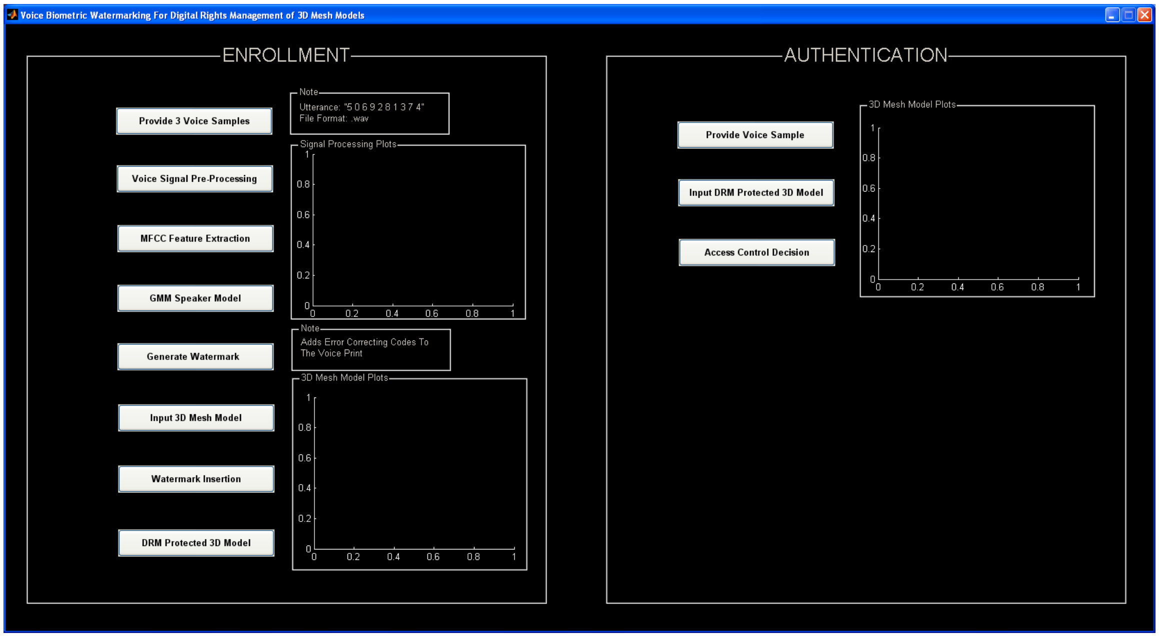

Note
Utterance: "5 0 6 9 2 8 1 3 7 4"
File Format: .wav

Note
Adds Error Correcting Codes To The Voice Print

Figure 4.5: Main GUI - The left panel provides an interface for user enrollment. The right panel provides an interface for user authentication.

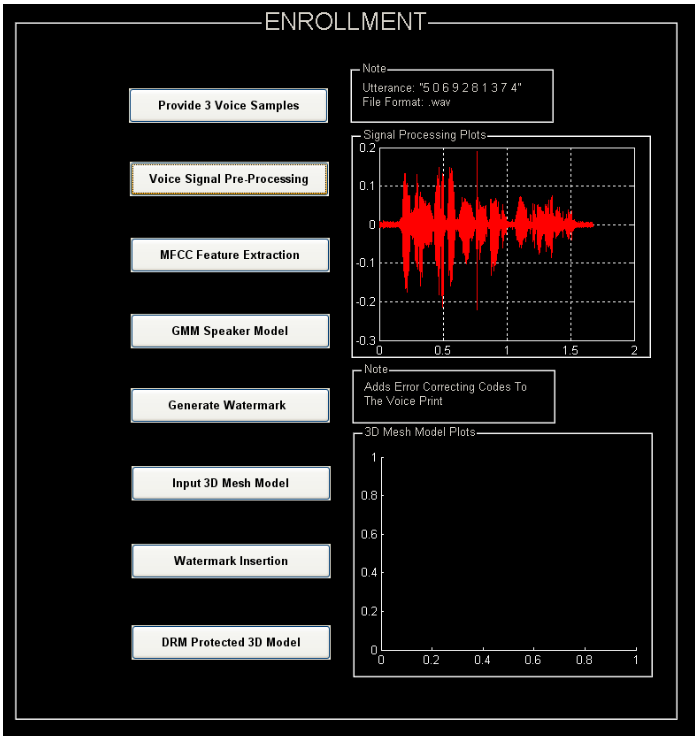

Note
Utterance: "5 0 6 9 2 8 1 3 7 4"
File Format: .wav

Note
Adds Error Correcting Codes To The Voice Print

Figure 4.6: Voice Signal Preprocessing - The axis on the upper left corner shows a plot of the voice signal (in red) after silence removal.

Figure 4.7 portrays a plot of the 12 MFCC coefficients of the first frame from the acquired voice sample.

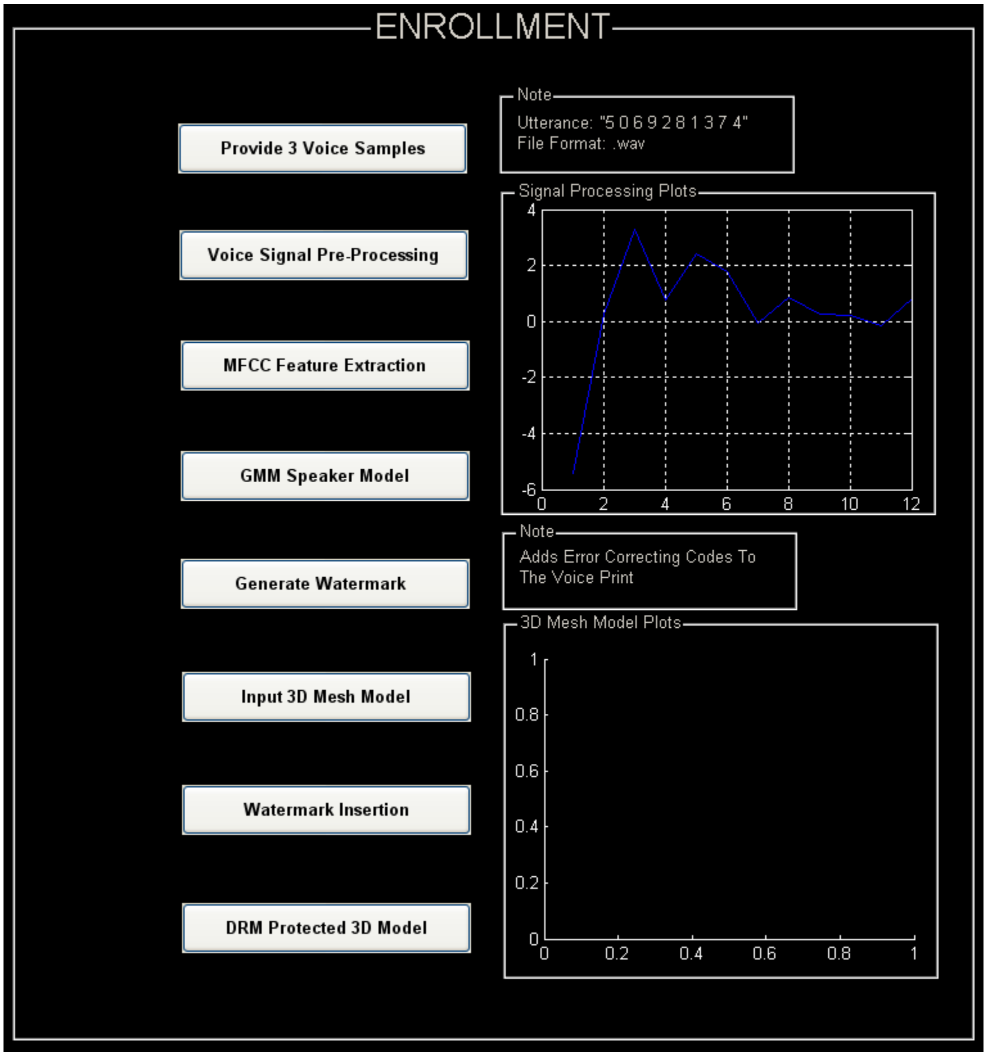

Utterance: "5 0 6 9 2 8 1 3 7 4"
File Format: .wav

Adds Error Correcting Codes To
The Voice Print

Figure 4.7: MFCC Feature Extraction - The axis on the upper left corner plots the 12 MFCC coefficients corresponding to the first frame of the first voice sample provided by the user.

Figure 4.8 enables users to see the GMM in one dimension plotted for the first MFCC coefficient acquired from all the frames of the enrollment voice samples.

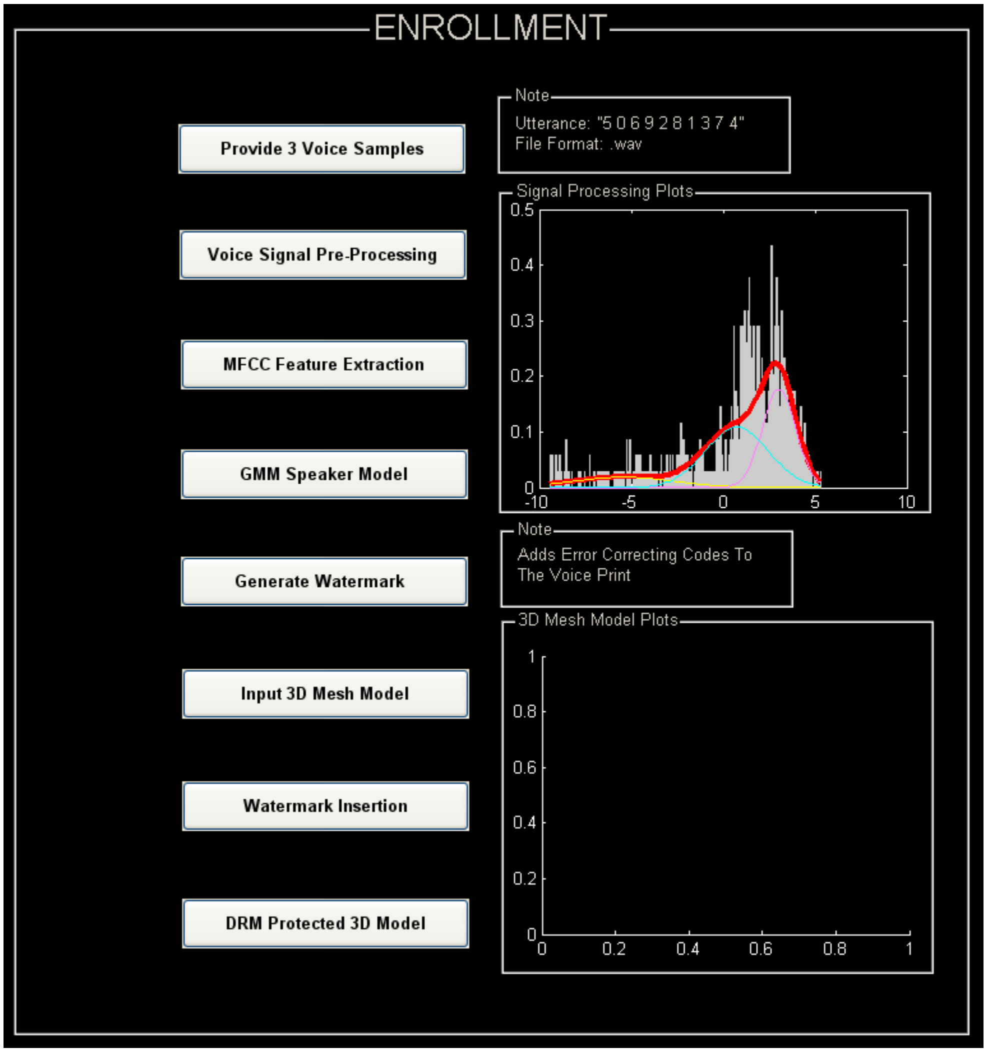

Note

Utterance: "5 0 6 9 2 8 1 3 7 4"
File Format: .wav

Note

Adds Error Correcting Codes To The Voice Print

Figure 4.8: GMM Speaker Model - The axis on the upper left corner plots the Gaussian mixture model for the first MFCC coefficients of all the frames from the three voice samples..

When the user pushes the *Input 3D Mesh Model* button, the system pops up a file selection window that lets the user select the *.off* 3D model that needs to be watermarked (see Figure 4.9). The selected model is then displayed in the bottom right corner of the left panel in the GUI.

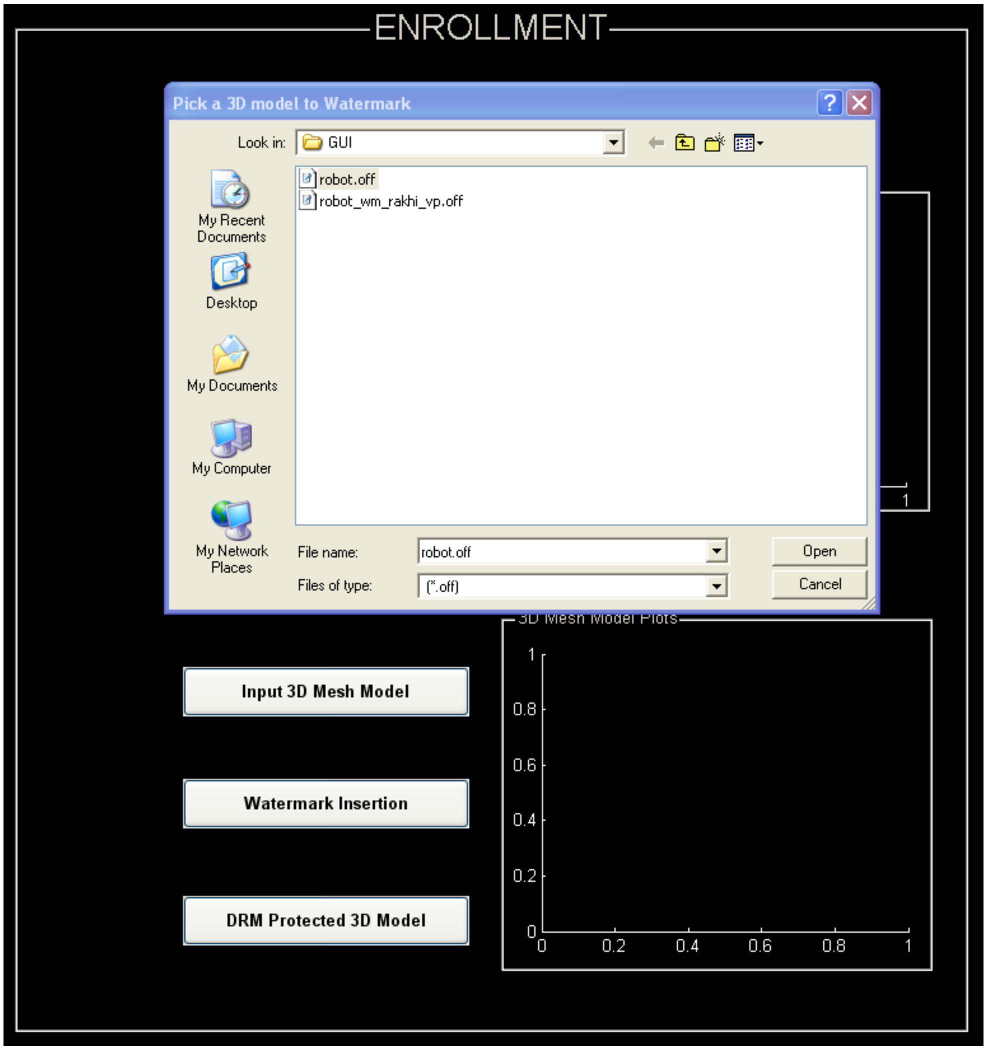

Pick a 3D model to Watermark

Look in: GUI

robot.off
robot_wm_rakhi_vp.off

File name: robot.off

Files of type: (*.off)

Figure 4.9: Input 3D Mesh Model - The system prompts the user to provide the 3D model that needs to be watermarked.

Figure 4.10 demonstrates the 3D model watermarked using the voice signal plotted in red.

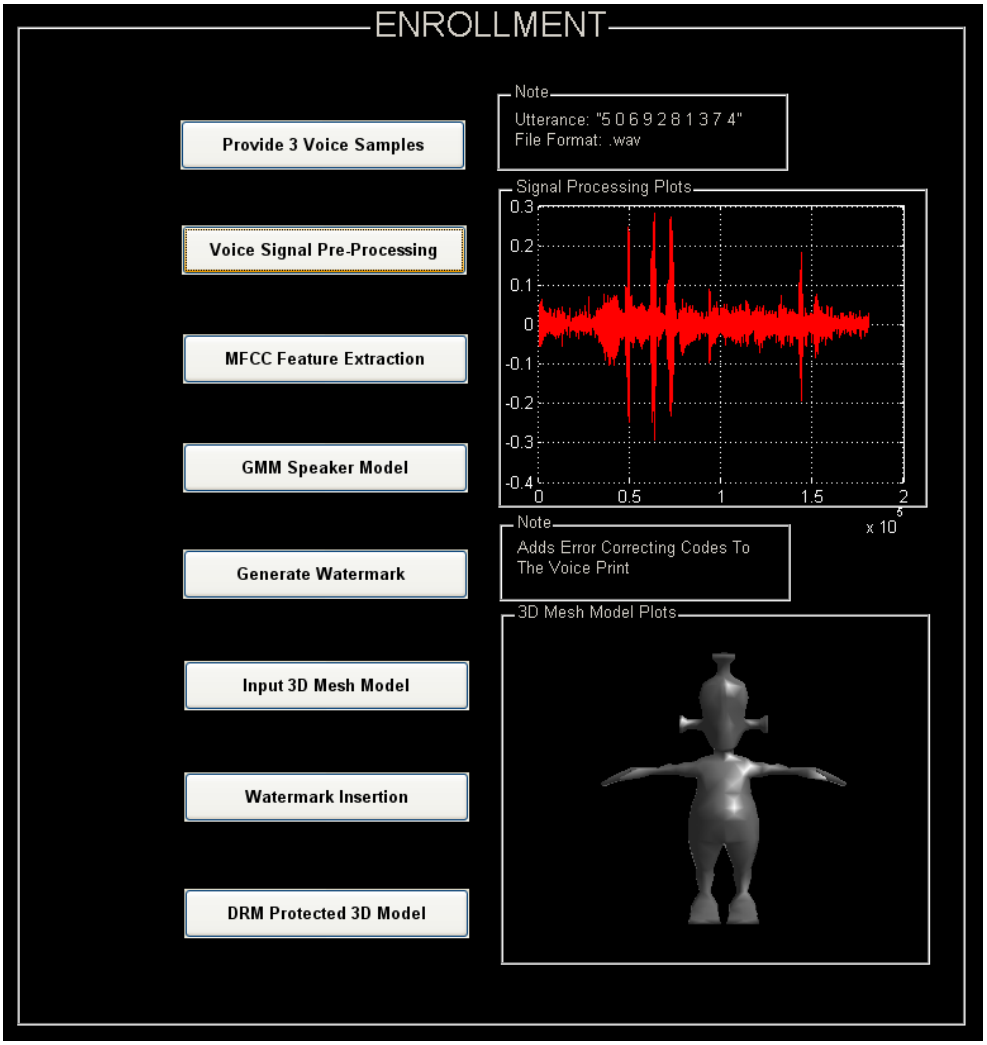

ENROLLMENT

Note

Utterance: "5 0 6 9 2 8 1 3 7 4"
File Format: .wav

Note

Adds Error Correcting Codes To The Voice Print

Figure 4.10: DRM Protected 3D Model - The axis on the upper left corner shows a plot of the voice signal used for generating the voice print. The bottom right display area shows the watermarked 3D model.

Figure 4.11 illustrates the system access control decision for a given voice sample and watermarked 3D model, which are provided by the user in the right authentication panel of the main GUI.

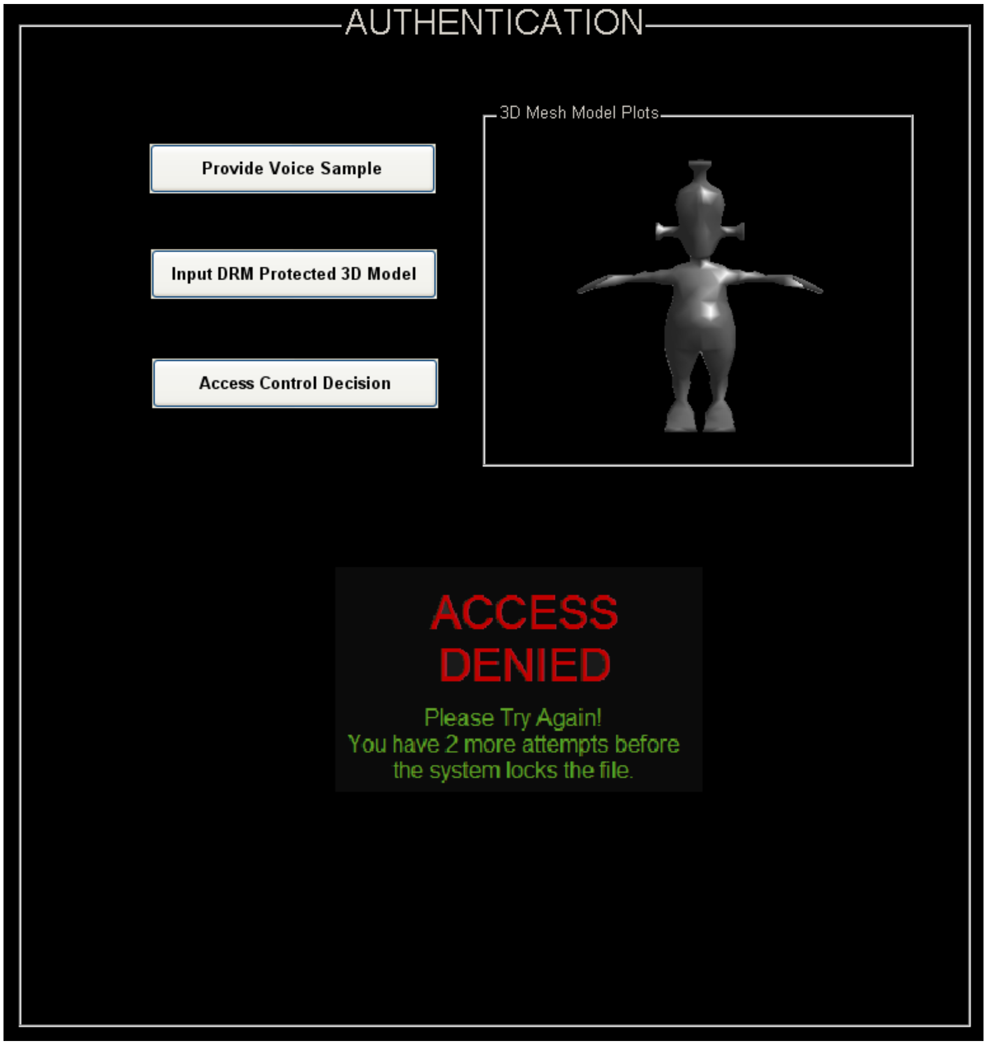

ACCESS DENIED

Please Try Again!
You have 2 more attempts before the system locks the file.

Figure 4.11: Access Control Decision - The user has only 3 verification attempts to gain access to the 3D mesh model. Since the FRR of the system is 0.6667 (computed for a total of 3 verification attempts), the system is guaranteed to grant access to legitimate user within the three trials.

Figure 4.12 displays the system's decision to grant access to a DRM protected (biometric watermarked) 3D model.

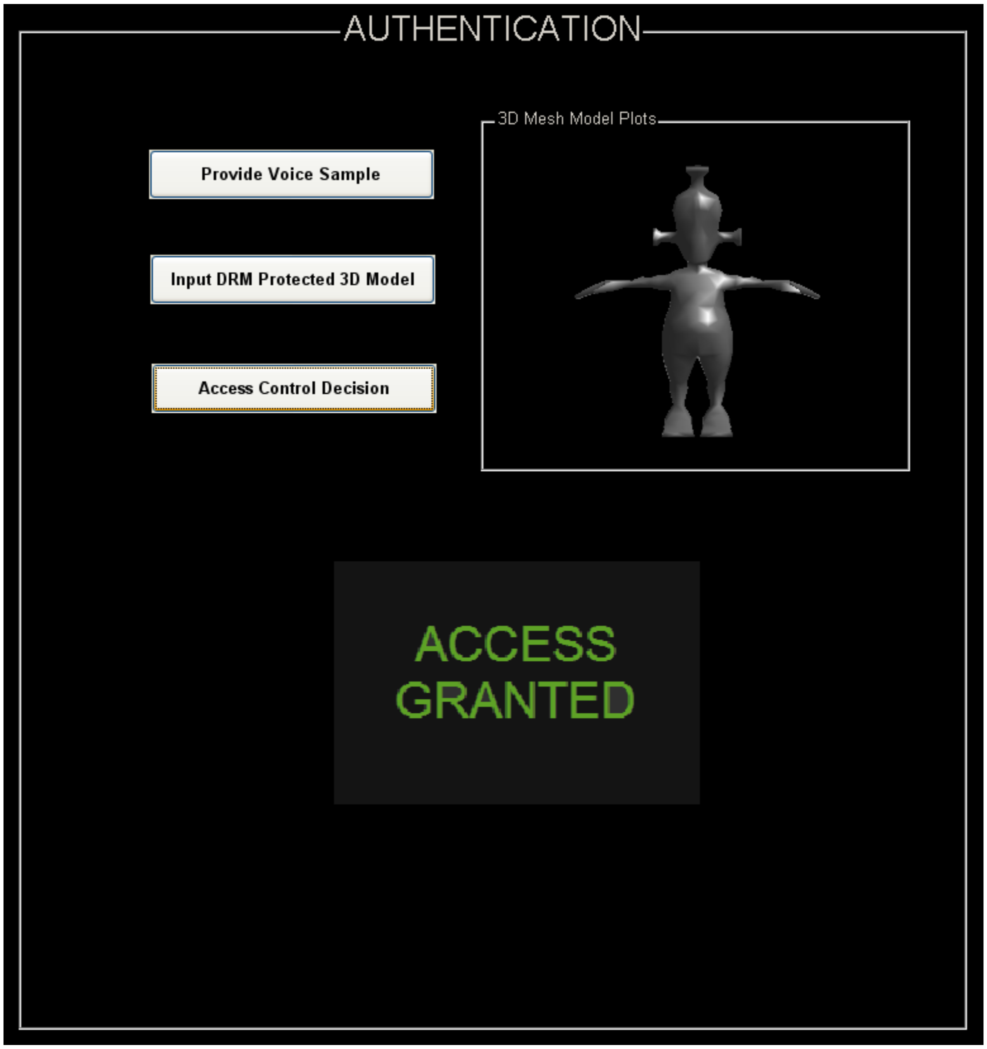

ACCESS GRANTED

Figure 4.12: Access Control Decision - A legitimate user is granted access to the watermarked 3D model upon providing a voice sample.

Chapter 5

Experimental Results

Evaluation of System Performance

The proposed scheme embeds a biometric system within a watermarking system. Therefore, this chapter lists several experiments which are performed to: i) evaluate the effectiveness of the watermarking scheme, ii) determine parameters for the voice biometric system, and iii) test the feasibility of the overall system with the objective of determining the extent of attacks the biometric watermark can withstand to correctly verify the legitimacy of a user.

5.1 Effectiveness of the Watermarking Scheme

Watermarking algorithms are evaluated in terms of *perceptibility*, *embedding capacity*, and *robustness* of the watermark to attacks. *Perceptibility* is the perceivable distortion caused to the 3D model after embedding the watermark. It is measured by the Hausdorff distance between the original and watermarked model. *Embedding capacity* is the amount of data that can be embedded as watermark into the 3D model. It is expressed in terms of the count of vertices that are modified to accommodate the watermark. Generally, the size of the watermark, commonly referred to as the payload size, also indicates the embedding capacity. *Robustness* is the ability of the watermark to withstand attacks such as affine transformations, cropping, additive noise, vertex reordering, mesh simplification, remeshing, mesh smoothing, and watermark removal. It is expressed in terms of a correlation coefficient which indicates the similarity measure between the embedded watermark and the extracted watermark that has been affected by the aforementioned attacks..

5.1.1 Perceptibility and Embedding Capacity

The 3D mesh models used for our experiments are shown in Figure 5.1. Table 5.1 lists the perceptibility measure and the capacity of the proposed watermarking technique.

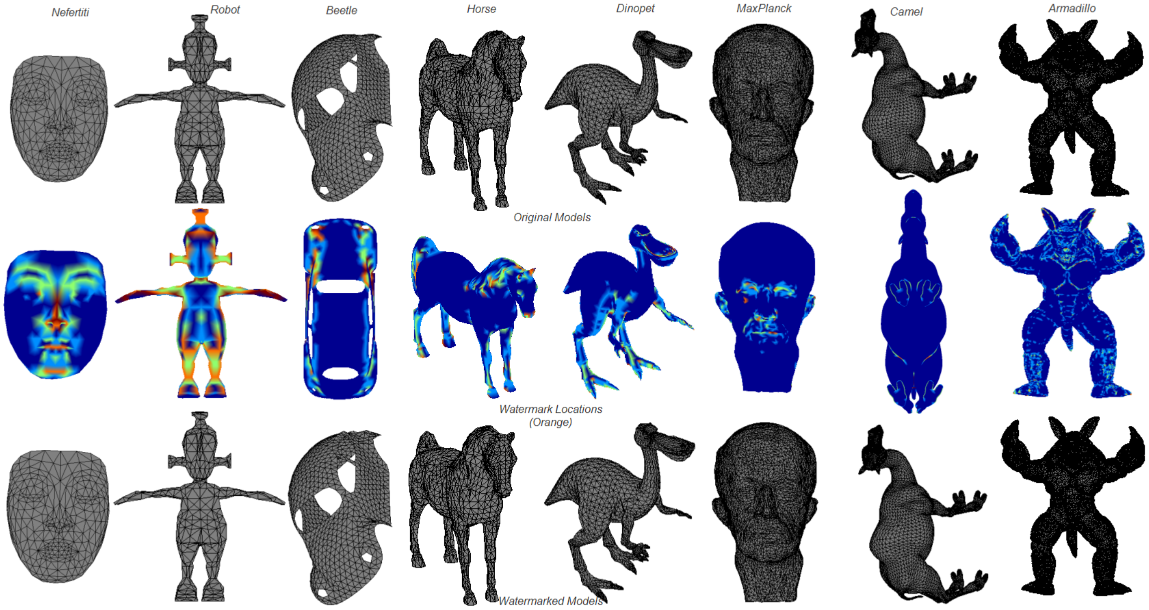

Figure 5.1: Original and Watermarked 3D Models

Table 5.1: Comparison Of Original Model With Watermarked Model

Model	Total	# of	Hausdorff Distance		
Name	# of	Watermarked	Max	Mean	RMS
	Vertices	Vertices	Dist.	Dist.	Dist.
Nefertiti	299	127	0.018535	0.001203	0.002547
Robot	600	255	0.038651	0.005788	0.009253
Beetle	988	230	0.040023	0.002398	0.005490
Horse	2450	765	0.041686	0.004004	0.007774
Dinopet	4500	1275	0.03904	0.002267	0.005113
MaxPlanck	7399	510	0.041861	0.000754	0.003323
Camel	9770	765	0.041082	0.001153	0.003884
Armadillo	26002	6630	0.043971	0.002279	0.005451

The Hausdorff distance(H) measures the distance of two meshes in 3D space from each other. It is defined by:

$$H(M_1, M_2) = max \left\{ \begin{array}{l} sup_{v \in M_1} inf_{v^{'} \in M_2} d(v, v^{'}), \\ sup_{v^{'} \in M_2} inf_{v \in M_1} d(v, v^{'}) \end{array} \right.$$

where,

- M_1 and M_2 are the two meshes,
- $d(v, v^{'})$ is the Euclidean distance between vertex v and $v^{'}$ in the 3D space,
- *sup* represents the supremum [125] and inf the *infimum* [125].

For our experiments, Hausdorff distance is computed using the *Metro* [12] tool. *Metro* measures the surface error incurred by watermarking by calculating the maximum, mean, and root-mean-square errors between original and watermarked meshes.

An attack on a 3D model attempts to destroy or remove the watermark while minimizing the distortion or usability of the model. 3D models are prone to operations such as translation, rotation, scaling, cropping, mesh smoothing, and noise addition which tend to destroy the watermark depending on the level and extent of the operation. It is desired that the watermark is preserved despite such operations. Therefore, the embedded watermark should be robust enough to withstand such attacks. The efficiency of the presented scheme is evaluated by simulating noise, cropping, and smoothing attacks on the watermarked models. The following experiments solely test the robustness of the 3D watermarking scheme and do not incorporate any level of error correction for the embedded watermark. The following sections present the summary of experiments and results for the *Horse* model. The value of the correlation coefficient lies between 0(no match) and 1(perfect match).

5.1.2 Robustness

Smoothing

Smoothing has a considerable effect on the watermarked model. A smoothing operation filters out high-frequency components of the model and attenuates the roughness of the surface. This results in degradation of the watermark. Figure 5.2 shows the effect of Laplacian and Taubin($\lambda = 0.5, \mu = -0.53$) smoothing on the *Horse* model. Table 5.2 lists the values of the correlation coefficient.

Table 5.2: Smoothing Attacks

Laplacian Smoothing	1 step	2 steps	3 steps
Correlation Value	0.0443	0.0984	0.1082
Taubin Smoothing	3 steps	10 steps	30 steps
Correlation Value	0.0550	0.0423	0.0338

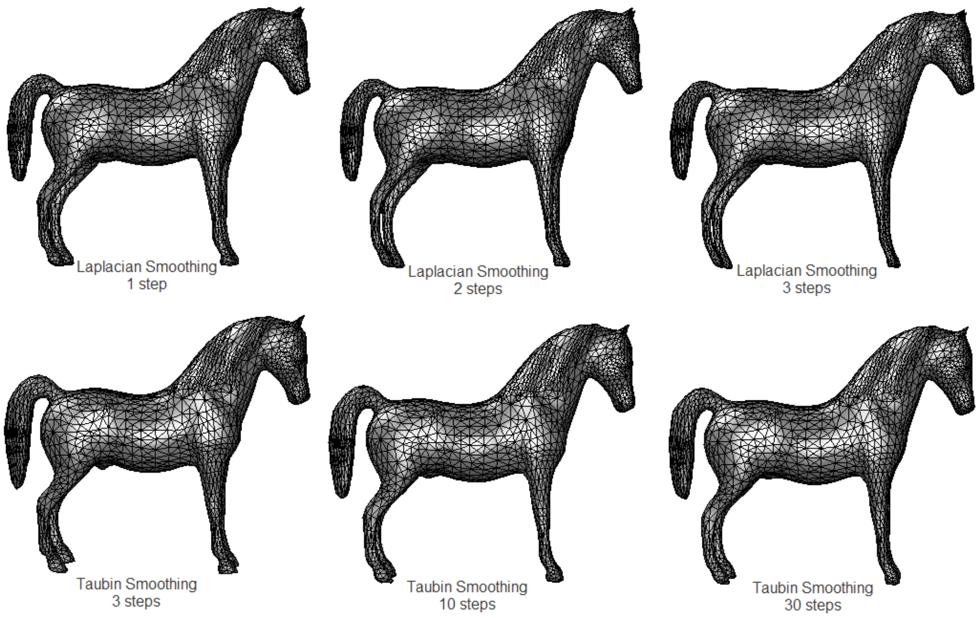

Figure 5.2: Smoothing operation on *Horse* model

Noise

This attack is simulated by adding normally distributed random numbers i.e. Gaussian noise with varied mean and variances, to the coordinates of the vertices of the watermarked 3D mesh model. Table 5.3 lists the impact of noise on the extracted watermark. The noise level expressed in % is the extent of vertices that are modified by noise. A 100% level indiciates additive noise for all vertices of the mesh model. Figure 5.3 and 5.4 shows the result of noise attacks on the *Horse* model.

Table 5.3: Noise Attacks

Proportion of Vertices Affected by Noise	10%	30%	50%	70%	100%
Correlation Value (Gaussian Noise: Mean 0 Variance 0.5477)	0.8441	0.4821	0.4187	0.3020	0.1819
Correlation Value (Gaussian Noise: Mean 1 Variance 2)	0.7749	0.5062	0.0482	0.0417	0.1302

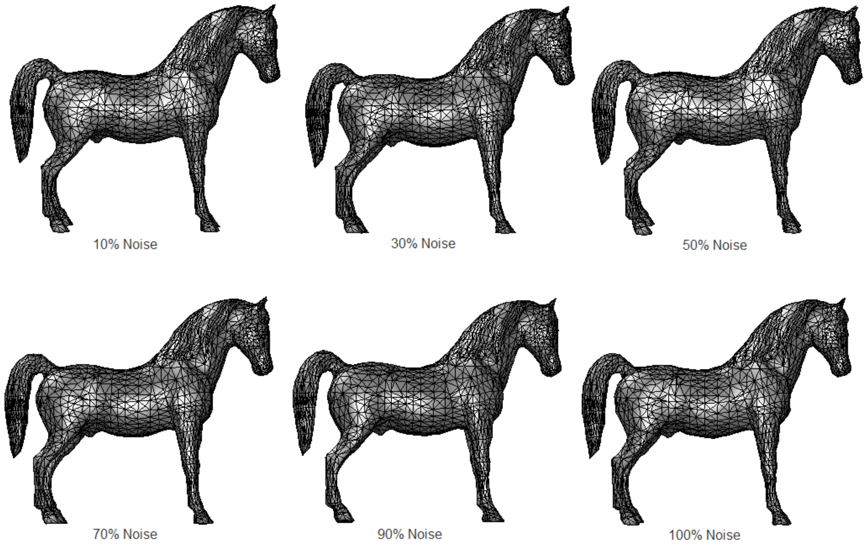

Figure 5.3: Gaussian Noise (Mean 0, Variance 0.5477) added to *Horse* model

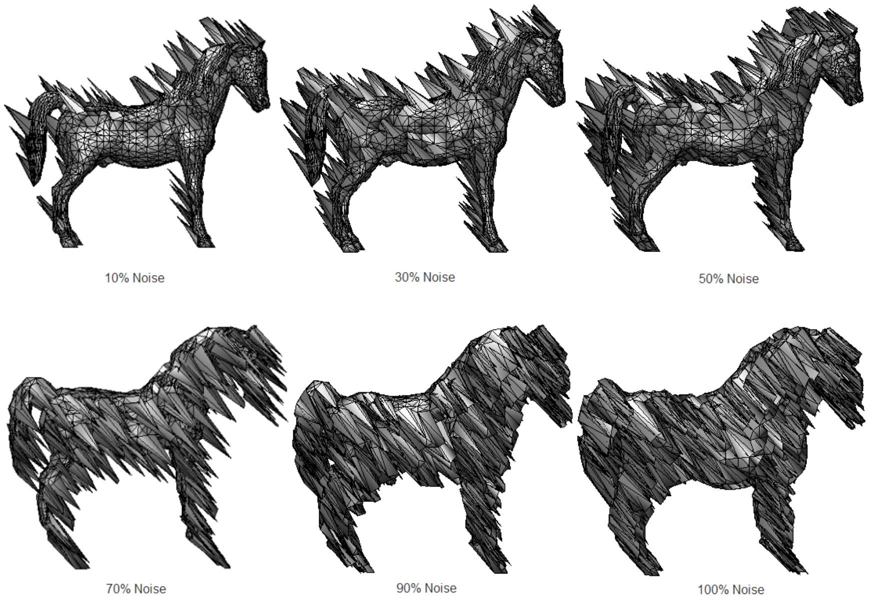

10% Noise 30% Noise 50% Noise

70% Noise 90% Noise 100% Noise

Figure 5.4: Gaussian Noise (Mean 1, Variance 2) added to *Horse* model

Scaling, Translation, and Rotation

The implementation is completely invariant to geometric attacks such as uniform scaling and affine transformations. Since the 3D model is normalized prior to the watermark insertion, the change in the position, scale and orientation of the model does not affect the relative orientation of the normals at the vertices and thus the local smoothness measure for each vertex remains unchanged. Thus our algorithm gives 100% correlation between original and extracted watermarks, as outlined in Table 5.4. Figures 5.5, 5.6, and 5.7 show the watermarked 3D model subject to these geometric transformations.

Table 5.4: Geometric Attacks

Transformation	X	Y	Z	X,Y,Z
Translate	5 units	10 units	5 units	(5,10,5) units
Correlation Value	1.0	1.0	1.0	1.0
Rotate	45°	90°	75°	(45°,90°,75°)
Correlation Value	1.0	1.0	1.0	1.0
Scale	0.25	0.5	0.75	1.5
Correlation Value	1.0	1.0	1.0	1.0

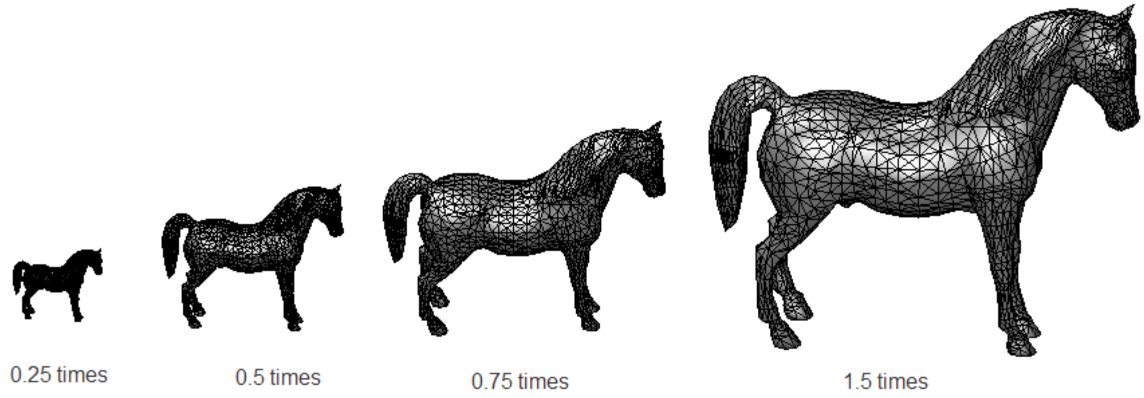

Figure 5.5: Scaling of Watermarked *Horse* model

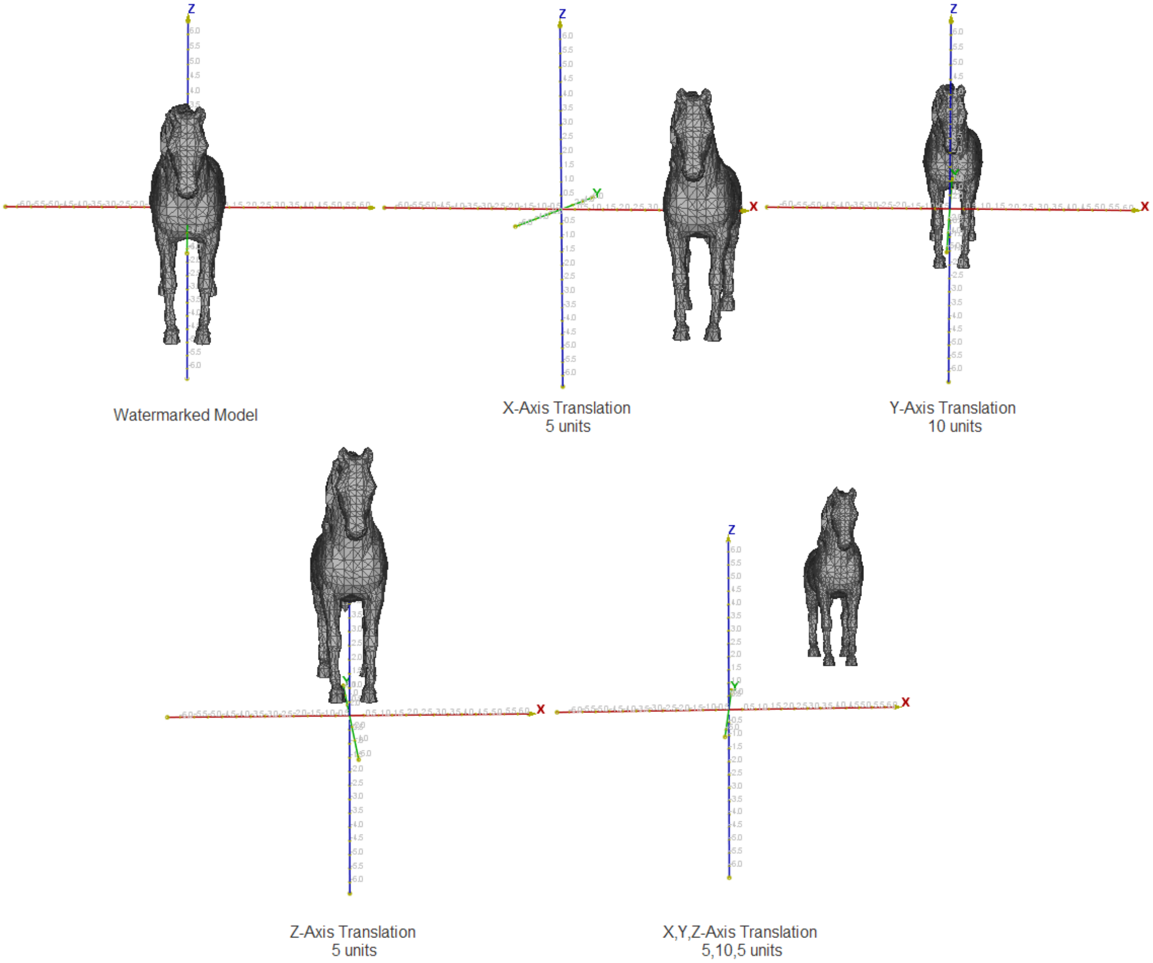

Figure 5.6: Translation of Watermarked *Horse* model

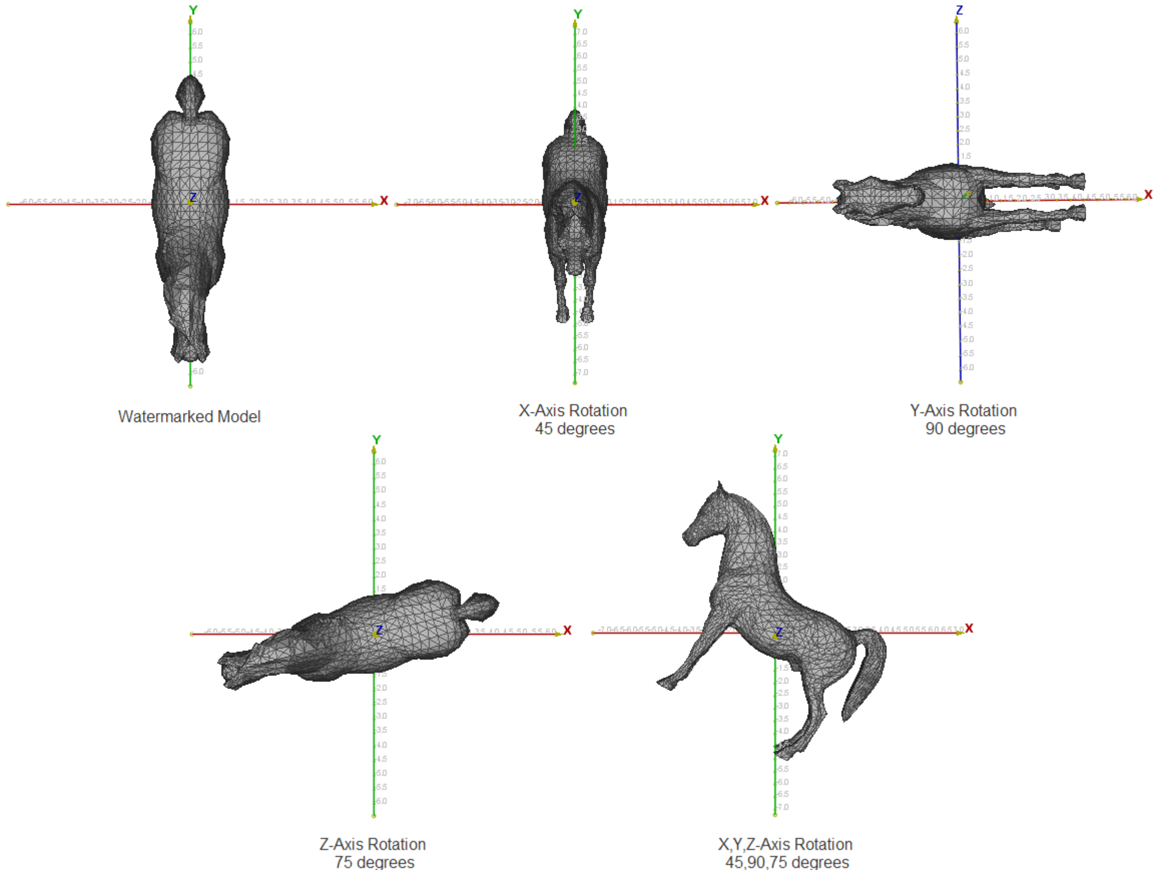

Figure 5.7: Rotation of Watermarked *Horse* model

Cropping

Cropping refers to removal or chopping off a part or parts of a model. The amount of watermark destroyed depends upon the extent and location of cropping. This necessitates adequate presence of the watermark in various regions. Figure 5.8 shows the *Horse* model cropped at varied levels in the x, y, and z-directions. Table 5.5 reflects the similarity measure between the embedded and extracted watermark against different cropping levels. However, 10% cropping in the y-direction removes the tail portion of the *Horse* where most of the watermark is embedded, so the correlation value is significantly lowered.

Table 5.5: Cropping Attacks

Cropping Ratio	10%	30%	50%	70%
Correlation Value Cropping along X-Axis	0.7013	0.2144	0.1755	0.0133
Correlation Value Cropping along Y-Axis	0.1596	0.1504	0.0411	0.0574
Correlation Value Cropping along Z-Axis	0.9992	0.4378	0.1412	0.0842

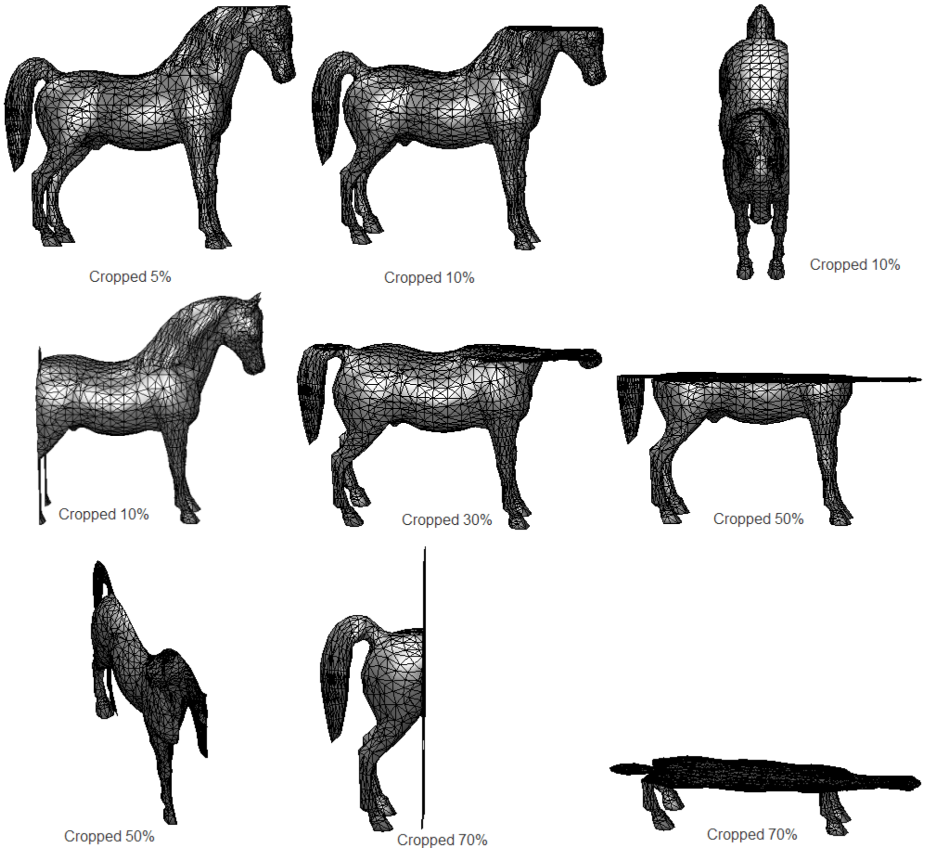

Figure 5.8: Cropped *Horse*

5.2 Parameter Evaluation of Voice Biometric System

For our experiments, the VALID database [23] was used. The database has a total of 106 subjects with 5 voice samples acquired from each subject in a controlled environment. Each speaker utters the sentence - *5 0 6 9 2 8 1 3 7 4*. The file sizes of voice recordings range from 173 KB to 696 KB with a duration of 2.5 seconds - 10 seconds, thereby incorporating slow, moderate and fast speakers. The *.wav* files are acquired at a sampling rate of 32KHz with bit rate 512kbps, sample size 16-bit, 1 Channel (mono) mode and PCM format.

To get optimum performance from the speaker verification (voice biometrics) module various experiments are conducted to tune algorithmic parameters, determine threshold for verification, and determine the required number of voice samples to generate a robust speaker model (voice print) formulation using MFCC and GMM. The performance measures of a biometric verification system are the False Acceptance rate(FAR) and the False Rejection rate(FRR). False acceptance is the case where an illegitimate user is granted access by the system. False rejection is the case where a genuine user is denied access by the system. FAR and FRR are computed by:

$$FAR = \frac{NumberofFalseAcceptances}{NumberofVerificationAttempts} \tag{5.1}$$

$$FRR = \frac{NumberofFalseRejections}{NumberofVerificationAttempts} \tag{5.2}$$

Determination of Threshold and Number of Voice Samples

Experiments were conducted using either 1, 2 or 3 voice samples for generating the GMM model. Figure 5.9 illustrates the FRR when 1 voice sample was used for generating the speaker model and the remaining 4 used for verification. Since the duration of just 1 sample was not sufficient to incorporate intra-individual variations, it mostly resulted in a rejection of all the remaining 4 voice samples for the test subjects. While the database has 106 test subjects, the reference numbers assigned to the subjects span a range of 1 through 122 leaving some reference numbers as void, which explains the cross marks on the x-axis indicating an FRR of 0.000 for these dummy reference numbers. Figure 5.10 depicts the performance of the speaker verification module at threshold values between 0.5 and 10 with increments of 0.5.

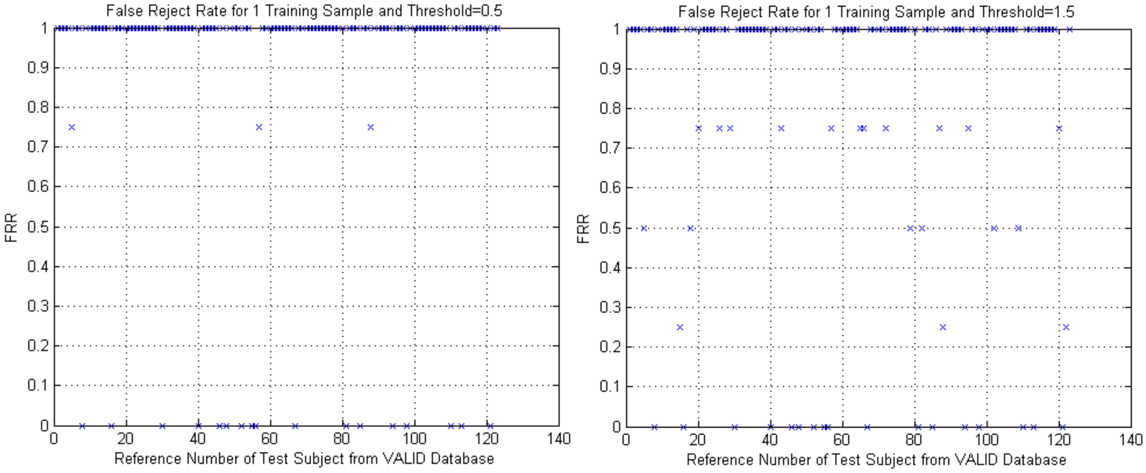

Figure 5.9: Plot of False Reject Rates for various Test Subjects with 1 voice sample used to generate the speaker model

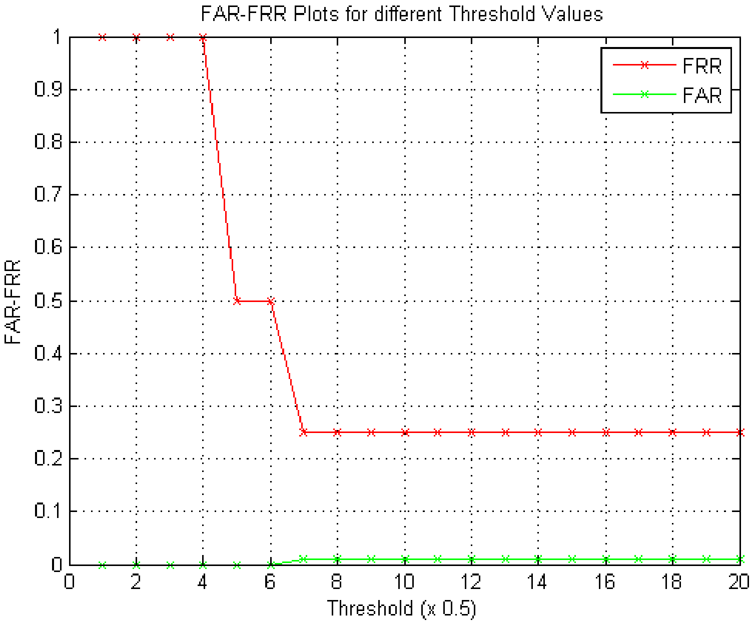

Figure 5.10: FAR and FRR plots for Test Subject 2 at various threshold values when 1 voice sample was used to generate the speaker model

The FRR improved when 2 voice samples were used for creating the speaker model. Figure 5.11 depicts the FRR at threshold values of 0.5 and 1.5, with some test subjects still having significantly higher false reject rates of 0.5 and above (which means that out of 4 verification attempts the user is falsely rejected by the systems at least twice). The FRR and FAR plots for a single test subject at different thresholds are shown in Figure 5.12.

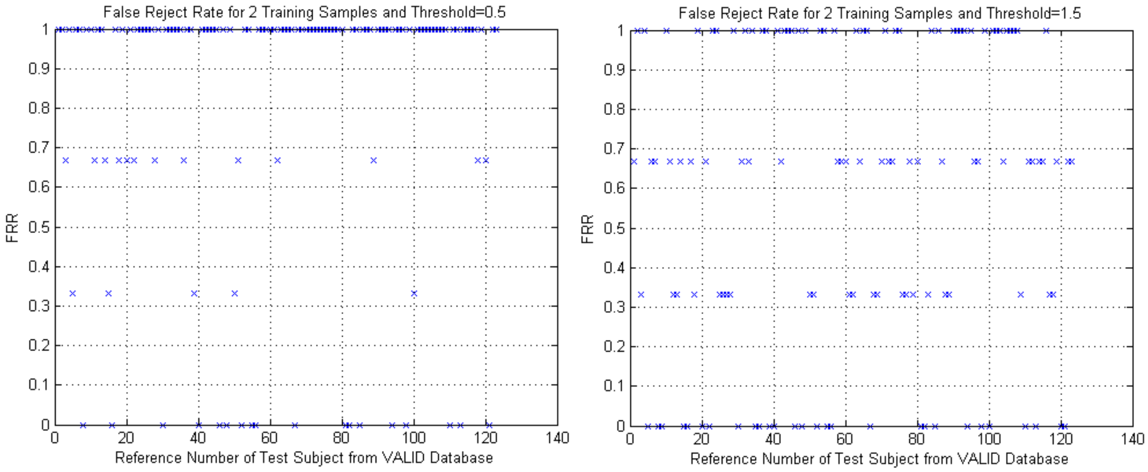

Figure 5.11: Plot of False Reject Rates for various Test Subjects when 2 voice samples are used to generate the speaker model

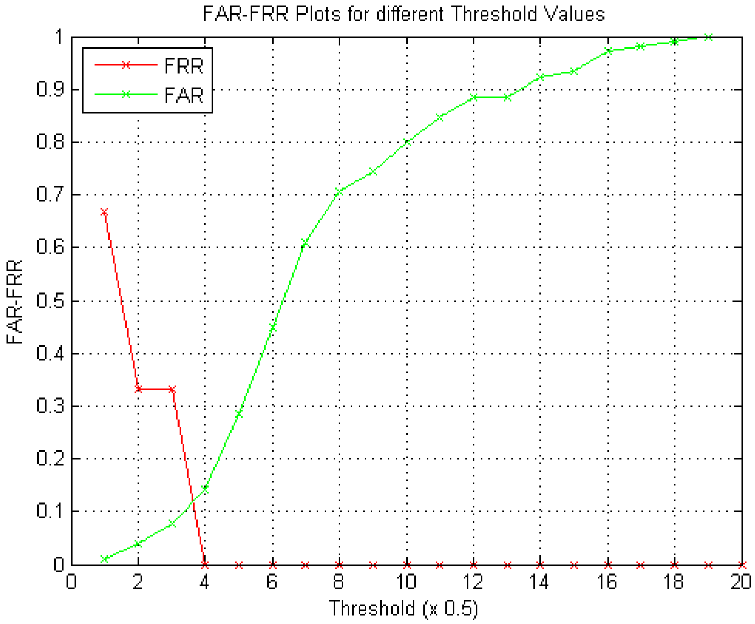

Figure 5.12: FAR and FRR plots for Test Subject 2 at various threshold values when 2 voice samples are used to generate the speaker model

When 3 voice samples were used to create the speaker model, FRR for all test subjects was less than 1.0 (at threshold 1.5, see Figure 5.13), indicating that no test subject from the dataset would be rejected by the system after 3 verification attempts. A plot of the FRR and FAR for various threshold values and different test subjects is shown in Figure 5.13. It was observed that FRR depends on the number of voice samples available for generating GMM speaker model - more the number of samples, the better the speaker model is thereby lowering the FRR. Experiments also show that lowering the threshold causes more false rejections but results in fewer false accepts. From Figure 5.14, it can be concluded that a threshold value of 1.5, where the FAR and FRR curves intersect, is the optimal value to be used for the aggregate system that integrates the speaker verification module with the 3D watermarking module.

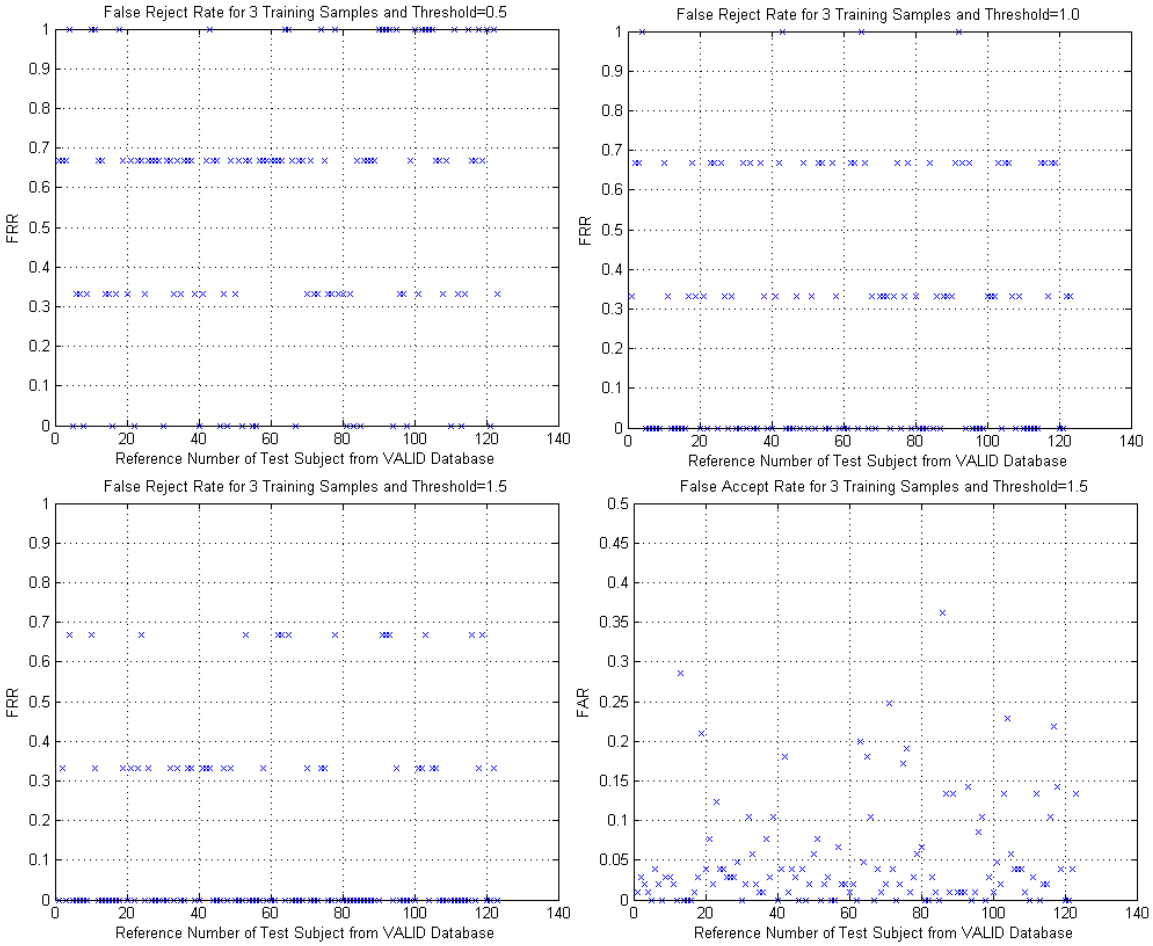

Figure 5.13: Plot of False Reject Rates for various Test Subjects when 3 voice samples are used to generate the speaker model

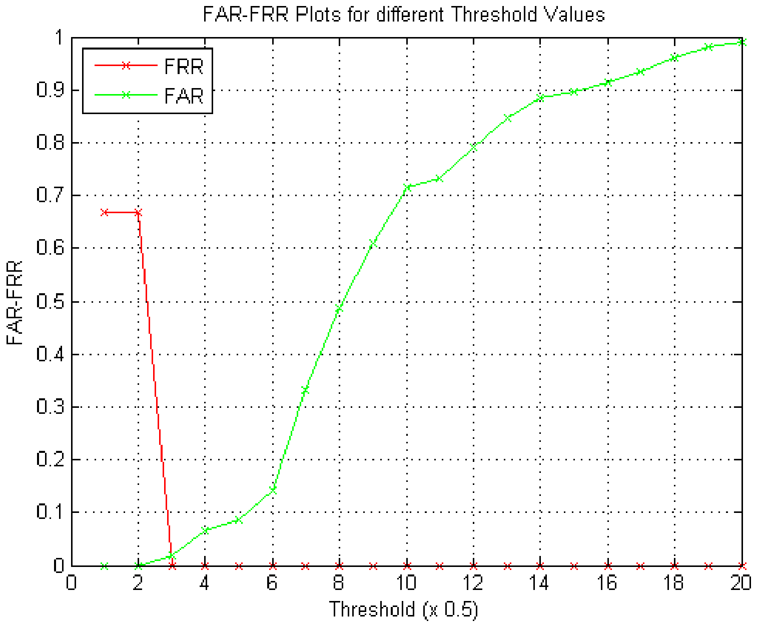

Figure 5.14: FAR and FRR plots for Test Subject 2 at various threshold values when 3 voice samples are used to generate the speaker model

For user enrollment, we use the first 3 out of the 5 voice samples from the dataset to generate the speaker model. The MFCC features extracted from the frames derived from each of the 3 voice samples are concatenated to train the GMM. For user verification, the last 3 voice samples are used of which 2 are unused samples from the dataset and 1 sample overlaps with the enrollment samples. The speaker model generating algorithmic parameters are determined by experiments shown in Table 5.6 which lists the False Reject Rate(FRR) and False Accept Rate(FAR) for different frame lengths, number of MFCC co-efficients extracted from each frame, and order of the GMM (which is the number of Gaussians used to model the speaker). To evaluate the effect of the frame length on FRR, the number of MFCC co-efficients is fixed at 12 with an order of 3 for the GMM.

Tuning Algorithmic Parameters

The next set of experiments are based on a frame length of 512, GMM model order of 3 and vary the number of extracted MFCC co-efficients for each frame from 8 to

100. Using 12 MFCC coefficients gives optimal performance. The order of GMM is varied from 1 to 36, and it was observed that this order does not have a significant impact on the FRR. Therefore a GMM order of 3+ can be used for experiments since FAR is 18% or lower.

Table 5.6: Experiments on Voice Print Generation Algorithmic Parameters (N=number of MFCC Coefficients, M=GMM order)

Frame Length	N	M	FRR			FAR		
(#samples)			min	max	mean	min	max	mean
128	12	3	0.0000	0.3333	0.0136	0.0095	0.9810	0.4057
256	12	3	0.0000	0.3333	0.0136	0.0095	0.9143	0.3123
512	12	3	0.000	0.6667	0.0488	0.0095	0.6952	0.1807
1024	12	3	0.000	1.000	0.1274	0.0095	0.6190	0.1182
512	12	1	0.000	0.6667	0.0244	0.0095	0.9238	0.3237
512	12	2	0.000	0.6667	0.0379	0.0095	0.9238	0.2320
512	12	3	0.000	0.6667	0.0488	0.0095	0.6952	0.1807
512	12	6	0.000	0.6667	0.0949	0.0095	0.5333	0.1053
512	12	12	0.000	0.6667	0.1518	0.0095	0.3714	0.0437
512	12	15	0.000	0.6667	0.2141	0.0095	0.2857	0.0388
512	12	18	0.000	0.6667	0.2304	0.0095	0.2667	0.0312
512	12	24	0.000	0.6667	0.3144	0.0095	0.2000	0.0202
512	12	36	0.000	0.6667	0.4065	0.0095	0.0952	0.0126
512	8	3	0.000	0.6667	0.0244	0.0095	0.9048	0.2821
512	12	3	0.000	0.6667	0.0488	0.0095	0.6952	0.1807
512	16	3	0.000	0.6667	0.0678	0.0095	0.6095	0.1160
512	39	3	0.000	1.000	0.2710	0.0000	0.4571	0.0616
512	100	3	0.000	1.000	0.7534	0.0095	0.3143	0.1162

The FRR and FAR are determined for all the test subjects from the dataset and the table outlines the minimum, maximum and mean values of FRR and FAR derived from voice samples of 106 test subjects. Results show that the GMM order improves the FAR (a higher order of GMM lowers the FAR) at the expense of increasing the FRR (while maintaining the upper limit of 0.6667) for various test subjects (mean of FRR for 106 test subjects increases as GMM order increases) because a higher number of Gaussians in the mixture model result in over fitting of the data. Conclusively, a order as high as 36 for the GMM, maintains the FRR at 0.6667 which means that the user is guaranteed to be authenticated by the system within 3 verification attempts.

The frame length primarily affects the FRR (increasing in frame lengths increases the FRR) but from the table it can be observed that a higher frame length also lowers the FAR. Although frame lengths 128 and 256 give the lowest FRR for 3 verification attempts, we choose 512 since the corresponding FAR is relatively lower. The number of MFCC coefficients change both FRR and FAR significantly with 12 coefficients striking a good balance between FRR and FAR. For experiments conducted to test the overall system performance presented in the next section, the voice print generation process uses a frame length of 512, 12 MFCC co-efficients per frame and 3 or higher number of Gaussians in the GMM depending on the size of the 3D model.

5.3 Overall System Performance

The overall performance of the voice biometric 3D watermarking system is evaluated in the case of no attacks and varied levels of noise, cropping and smoothing attacks. All the experiments are conducted using the following parameters:

1. Out of 5 voice samples for *Test Subject 2* from the *VALID* dataset, the first 3 voice samples are used for enrollment and the last 3 samples are used for verification.

2. Value of threshold used to compute the likelihood of extracted features with the speaker model (i.e voice print) is 1.5.

3. 12 MFCC coefficients are used to generate the voice print.

4. The MFCC feature extraction process employs a frame rate of 512 samples with a frame overlap of 256 samples.

5. 3D mesh models of various sizes (ranging from small(15KB-60KB), medium(140KB-450KB), large(640KB-1700KB)) and varied geometry (surface curvature) are selected for experiments.

6. The Reed Solomon error correction encoding and decoding processes impose a restriction on the number of bits in the message (voice print) m and codeword

(watermark) length n such that $n = 2^m - 1$. The system requires the 3D model to have an embedding capacity of at least n for a chosen value of m. Since a GMM requires at least 3 Gaussians (which generates a voice print of length 75) to attain low FRR and FAR, the codeword length n should be greater than 75 to accommodate redundancy through error correcting bytes. Given this criteria, values of m must be 7 or higher such that a codeword of size 127 or higher is generated. Since the watermark embedding capacity of a 3D model drives the size of the codeword and is entirely dependent on the geometry of the model and not the size of the model (i.e. total number of vertices), therefore the value of m may vary from model to model.

7. The order of the GMM varies according to the watermarking embedding capacity of the model and can lie anywhere between 3 and 15. The order of the GMM model increases the size of the voice print since each Gaussian in the model is parameterized by its weight (1 value), μ (12 values for 12 MFCC coefficients), and Σ (12 values for 12 MFCC coefficients) - a total of 25 values, thereby decreasing the level of error correction that can be utilized for the watermark.

No Attacks

In the case of no attacks, Figure 5.15 shows the FRR and FAR plots for the system. The False Accept Rate(FAR) is obtained by comparing voice prints of 106 test subjects from the database against the extracted voice print. The FRR is computed using 3 verification attempts. These plots were generated for the voice print extracted from the watermarked *Nefertiti* model (total number of vertices=299, watermarked vertices=127, GMM order=3, m=7) for every test subject. These plots are not identical to Figure 5.13 as one would expect since the likelihood measure generated for the GMM of a speaker is not a fixed value and it varies each time a speaker model is generated due to variation in the initialization of the parameters by the EM algorithm that incorporates random values for the covariance matrix. FRR and FAR are highly dependent on the value of this likelihood measure and therefore can vary for a GMM model of the same speaker generated at a different instances of time.

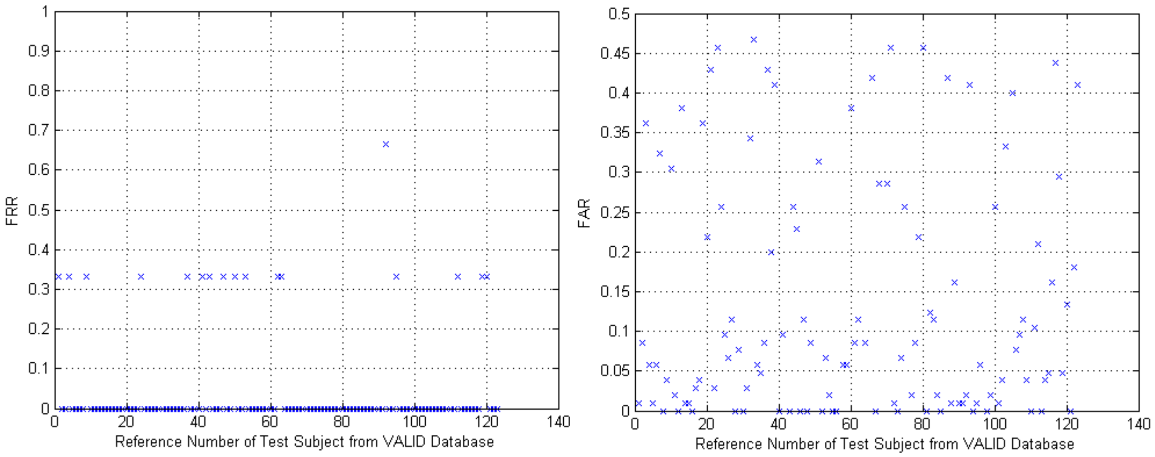

Figure 5.15: System performance when the watermarked 3D model is not subject to any attacks

Attacks

Table 5.7 illustrates the maximum tolerance limit of the system to mesh smoothing, cropping and additive noise attacks on the embedded watermark in order to accept a legitimate user. The robustness of the watermark depends on the level of redundancy employed by the error correction encoding. The payload (watermark) size minus the voice print size indicates the number of parity bytes or the level of redundancy. Results from these experiments indicate that larger size models with higher embedding capacity can afford a higher level of redundancy for the payload and can withstand an increased level of cropping and noise attacks up to 20%-49%. However, the system's tolerance of 20% levels of noise and cropping is highly dependent on the location of the noise and cropping attacks. For example, since no watermark is inserted in the forehead region of the *MaxPlanck* model (see Figure 5.1), no information is lost when the forehead is cropped, thus offering a higher tolerance of 45% noise and cropping irrespective of its relatively smaller payload capacity. To the contrary, even though *Camel* has a higher payload capacity it can not withstand higher levels of cropping which alter the vertices accomodating the watermark.

Table 5.7: Measure of Overall System Performance

3D Model	Model Size	Voiceprint Size	Payload Size	Maximum Tolerance For User Acceptance		
				Smoothing Attack (Taubin)	Cropping Attack (Level %)	Noise Attack (Level %)
Nefertiti	17KB 299 vertices	1.17KB 75 values	1.98KB 127 values	5 steps $\lambda = 0.0005$	26%	20%
Robot	35KB 600 vertices	1.17KB 75 values	3.98KB 255 values	40 steps $\lambda = 0.0005$	27%	35%
Beetle	56KB 988 vertices	1.17KB 75 values	3.58KB 230 values	200 steps $\lambda = 0.001$	36%	25%
Horse	145KB 2450 vertices	1.17KB 75 values	11.9KB 765 values	5 steps $\lambda = 0.0025$	44%	40%
Dinopet	278KB 4500 vertices	1.17KB 75 values	19.9KB 1275 values	5 steps $\lambda = 0.005$	49%	45%
MaxPlanck	438KB 7399 vertices	1.17KB 75 values	7.97KB 510 values	2 steps $\lambda = 0.002$	40%	45%
Camel	646KB 9770 vertices	1.17KB 75 values	11.9KB 765 values	35 steps $\lambda = 0.005$	28%	45%
Armadillo	1662KB 26002 vertices	1.17KB 75 values	99.6KB 6630 values	60 steps $\lambda = 0.005$	49%	45%

Smaller models can not resist such high levels of noise or cropping attacks since the embedded speaker model suffers damage to the extent that it rejects a genuine user. Further research is required in the direction of high embedding capacity watermarking algorithms for small size 3D models. The next three sections provide an in-depth analyses of the impact of noise,cropping and smoothing attacks on the watermarked models.

Impact of Noise Attack

In the case of additive Gaussian noise (Mean 0, Variance 1.2247), Tables 5.8-5.21 list the effect of various noise levels on the test subject's verification decision by the system. For smaller 3D models (*Nefertiti, Beetle,* and *Robot*), a GMM of order 3 and 5 was used to ensure that whole voice print could be embedded in the model with small degree of error correction. Due to the high embedding capacity, *Horse* and *Dinopet* models could afford 9 and 15 order GMMs respectively. *Maxplanck* had relatively lower payload capacity and therefore used 6 Gaussians to model the GMM for the same test subject. Although *Camel* and *Armadillo* model could accommodate a much higher order GMM, we used a GMM of 3 Gaussians for a codeword size of 255 that was inserted within the model multiple times. Experimental results indicated that keeping the order of GMM down to 3 did not impact the FAR, FRR but it did improve the system tolerance owing to the higher degree of error correction employed in the watermark in place of the additional Gaussian parametric values.

Table 5.8: 3D Model *Nefertiti*- Impact of Gaussian Noise on Voice Biometric Watermark of Length 127 (m = 7) that Accommodates a Voice print of Size 75 (GMM order 3)

Proportion of Vertices Affected by Noise	10%	15%	20%	25%	30%	50%	100%
Correlation Value x dimension y dimension z dimension	 1.0000 1.0000 1.0000	 1.0000 1.0000 1.0000	 1.0000 1.0000 1.0000	 0.6006 0.3208 0.4097	 0.4976 0.2143 0.2887	 0.3409 0.1529 0.2159	 0.1055 0.0468 0.0230
Error Correction (# of corrected) values)	14	20	23	Failed	Failed	Failed	Failed
FRR	0.0000	0.0000	0.0000	1.0000	0.3333	1.0000	1.0000
FAR	0.0857	0.0857	0.0857	0.0000	0.3048	0.0000	0.0000

Even though the embedding capacity of Robot was twice that of Nefertiti, the system did not show any significant improvement in surviving higher noise levels (see Table 5.9). Therefore, we experimented with a lower order GMM and observed a significant improvement in noise tolerance. Lowering the number of Gaussians in the GMM allowed for increased redundancy of the voice print values in the watermark enabling a higher degree of error correction on the extracted watermark. Table 5.10 indicates the improvement in performance from noise tolerance of 20% to 35%.

Table 5.9: 3D Model *Robot*- Impact of Gaussian Noise on Voice Biometric Watermark of Length 255 (m = 8) that Accommodates a Voice print of Size 125 (GMM order 5)

Proportion of Vertices Affected by Noise	10%	15%	20%	25%	30%	50%	100%
Correlation Value							
x dimension	1.0000	1.0000	1.0000	1.0000	0.3167	0.1986	0.1901
y dimension	1.0000	1.0000	1.0000	1.0000	0.2625	0.2209	0.1612
z dimension	1.0000	1.0000	1.0000	1.0000	0.1754	0.1205	0.0499
Error Correction (# of corrected) values)	28	36	47	63	Failed	Failed	Failed
FRR	0.0000	0.0000	0.0000	0.0000	1.0000	1.0000	1.0000
FAR	0.0952	0.0952	0.0952	0.0952	0.0000	0.0000	0.0000

Table 5.10: 3D Model *Robot*- Impact of Gaussian Noise on Voice Biometric Watermark of Length 255 (m = 8) that Accommodates a Voice print of Size 75 (GMM order 3)

Proportion of Vertices Affected by Noise	10%	20%	30%	35%	40%	50%	100%
Correlation Value							
x dimension	1.0000	1.0000	1.0000	1.0000	0.4637	0.4215	0.3109
y dimension	1.0000	1.0000	1.0000	1.0000	0.1200	0.0971	0.0025
z dimension	1.0000	1.0000	1.0000	1.0000	0.3229	0.3214	0.1689
Error Correction (# of corrected) values)	24	51	76	85	Failed	Failed	Failed
FRR	0.0000	0.0000	0.0000	0.0000	1.0000	1.0000	1.0000
FAR	0.1619	0.1619	0.1619	0.1619	0.0000	0.0000	0.0000

Even though *Beetle* is larger in size than *Robot* it has a lower tolerance to noise (see Table 5.11) than *Robot* because the watermark (codeword of size 255) is truncated to 230 to match the embedding capacity of the model. The 25 truncated values lower the redundancy in the error correcting codeword (watermark) thereby affecting the tolerance of the system to noise attacks.

Table 5.11: 3D Model *Beetle*- Impact of Gaussian Noise on Voice Biometric Watermark of Length 230 that Accommodates a Voiceprint of Size 75 (GMM order 3)

Proportion of Vertices Affected by Noise	10%	15%	20%	25%	30%	50%	100%
Correlation Value							
x dimension	1.0000	1.0000	1.0000	1.0000	0.4361	0.3961	0.1621
y dimension	1.0000	1.0000	1.0000	1.0000	0.4380	0.3412	0.1677
z dimension	1.0000	1.0000	1.0000	1.0000	0.4953	0.3981	0.0586
Error Correction (# of corrected) values)	47	61	71	79	Failed	Failed	Failed
FRR	0.0000	0.0000	0.0000	1.0000	1.0000	1.0000	1.0000
FAR	0.3143	0.3143	0.3143	0.3143	0.0000	0.0000	0.0000

Table 5.12: 3D Model *Horse*- Impact of Gaussian Noise on Voice Biometric Watermark of Length 765 (m =8), Voiceprint size is 225 (GMM order 9, voiceprint is split into 3 equal parts with each part having a codeword of size 255, the 3 codewords concatenate to form the watermark)

Proportion of Vertices Affected by Noise	10%	20%	30%	35%	40%	50%	100%
Correlation Value							
x dimension	1.0000	1.0000	1.0000	0.6006	0.2224	0.1349	0.0588
y dimension	1.0000	1.0000	1.0000	0.3208	0.2786	0.2352	0.1225
z dimension	1.0000	1.0000	1.0000	0.4097	0.2746	0.2222	0.0127
Error Correction (# of corrected) values)	64	137	213	253	Failed	Failed	Failed
FRR	0.3333	0.3333	0.3333	0.3333	1.0000	1.0000	1.0000
FAR	0.0095	0.0095	0.0095	0.0095	0.0000	0.0000	0.0000

Results from Table 5.12 indicated a low noise level tolerance for the system for models with embedding capacity higher than 255 which motivated us to try a variation in the watermark pattern by concatenating the codeword of 255 values (with 75 voice print values) to see if performance could be improved. The GMM order of 3 yielded better performance, as shown in Tables 5.13, 5.15, and 5.17.

Table 5.13: 3D Model *Horse*- Impact of Gaussian Noise on Voice Biometric Watermark of Length 765 (m =8), Voiceprint size is 75 (GMM order 3, voiceprint is split into 3 equal parts with each part having a codeword of size 255, the 3 codewords concatenate to form the watermark)

Proportion of Vertices Affected by Noise	10%	20%	30%	40%	45%	50%	100%
Correlation Value							
x dimension	1.0000	1.0000	1.0000	1.0000	0.2064	0.1708	0.0978
y dimension	1.0000	1.0000	1.0000	1.0000	0.4333	0.2506	0.1492
z dimension	1.0000	1.0000	1.0000	1.0000	0.3839	0.2108	0.0550
Error Correction (# of corrected) values)	85	164	229	300	Failed	Failed	Failed
FRR	0.0000	0.0000	0.0000	0.0000	1.0000	1.0000	1.0000
FAR	0.3333	0.3333	0.3333	0.3333	0.0000	0.0000	0.0000

Table 5.14: 3D Model *Dinopet*- Impact of Gaussian Noise on Voice Biometric Watermark of Length 1275 that Accommodates a Voiceprint of Size 375 (GMM order 15)

Proportion of Vertices Affected by Noise	10%	20%	25%	30%	35%	50%	100%
Correlation Value							
x dimension	1.0000	1.0000	1.0000	1.0000	0.4660	0.2308	0.0631
y dimension	1.0000	1.0000	1.0000	1.0000	0.4484	0.2084	0.0451
z dimension	1.0000	1.0000	1.0000	1.0000	0.4985	0.2531	0.0737
Error Correction (# of corrected) values)	133	251	303	365	Failed	Failed	Failed
FRR	0.3333	0.3333	0.3333	0.3333	1.0000	1.0000	1.0000
FAR	0.0381	0.0381	0.0381	0.0381	0.0000	0.0000	0.0000

Table 5.15: 3D Model *Dinopet*- Impact of Gaussian Noise on Voice Biometric Watermark of Length 1275 that Accommodates a Voiceprint of Size 75 (GMM order 3) that is split into 5 parts with each part forming a codeword of size 255

Proportion of Vertices Affected by Noise	10%	20%	30%	40%	45%	50%	100%
Correlation Value							
x dimension	1.0000	1.0000	1.0000	1.0000	0.6274	0.4750	0.1251
y dimension	1.0000	1.0000	1.0000	1.0000	0.6364	0.4586	0.0334
z dimension	1.0000	1.0000	1.0000	1.0000	0.4761	0.3343	0.1134
Error Correction (# of corrected) values)	124	244	373	498	423, Part 4 Failed	231, Part 2,4, 5 Failed	Failed
FRR	0.0000	0.0000	0.0000	0.0000	0.0000	0.3333	1.0000
FAR	0.1905	0.1905	0.1905	0.1905	0.1905	0.1905	0.0000

Table 5.16: 3D Model *MaxPlanck*- Impact of Gaussian Noise on Voice Biometric Watermark of Length 510 that Accommodates a Voiceprint of Size 150 (GMM order 6)

Proportion of Vertices Affected by Noise	10%	20%	25%	30%	35%	40%	100%
Correlation Value							
x dimension	1.0000	1.0000	1.0000	1.0000	1.0000	0.2970	0.1406
y dimension	1.0000	1.0000	1.0000	1.0000	1.0000	0.2593	0.1066
z dimension	1.0000	1.0000	1.0000	1.0000	1.0000	0.2620	0.1175
Error Correction (# of corrected) values)	46	105	127	146	169	Failed	Failed
FRR	0.0000	0.0000	0.0000	0.0000	0.0000	1.0000	1.0000
FAR	0.0571	0.0571	0.0571	0.0571	0.0571	0.0000	0.0000

Since *Camel* has the same embedding capacity as *Horse* (765 values), instead of splitting up the voice print into sections and generating codewords for each section to utilize the high embedding capacity of the model, a variation of the algorithm was experimented with the hope of improved performance. The codeword was embedded into the 3D model 3 times and resulted in degraded performance mainly due to the fact that lower level of error correction was being employed for each codeword as

Table 5.17: 3D Model *MaxPlanck*- Impact of Gaussian Noise on Voice Biometric Watermark of Length 510 that Accommodates a Voiceprint of Size 75 (GMM order 3) that is split into 2 parts with each part forming a codeword of size 255

Proportion of Vertices Affected by Noise	10%	20%	30%	40%	45%	50%	100%
Correlation Value							
x dimension	1.0000	1.0000	1.0000	1.0000	0.3063	0.2334	0.1102
y dimension	1.0000	1.0000	1.0000	1.0000	0.4448	0.1388	0.1448
z dimension	1.0000	1.0000	1.0000	1.0000	1.0000	0.2630	0.1644
Error Correction (# of corrected) values)	51	94	136	187	211	Failed	Failed
FRR	0.3333	0.3333	0.3333	0.3333	0.3333	1.0000	1.0000
FAR	0.1048	0.1048	0.1048	0.1048	0.1048	0.0000	0.0000

compared to the original strategy. Tables 5.18 and 5.19 demonstrate the system performance using the variation and the original strategy.

Table 5.18: 3D Model *Camel*- Impact of Gaussian Noise on Voice Biometric Watermark of Length 765 that Accommodates Voiceprint of Size 255 (GMM order 3) repeated three times

Proportion of Vertices Affected by Noise	10%	20%	30%	35%	40%	50%	100%
Correlation Value							
x dimension	1.0000	1.0000	1.0000	1.0000	0.4753	0.4939	0.2652
y dimension	1.0000	1.0000	1.0000	1.0000	0.4803	0.4440	0.3073
z dimension	1.0000	1.0000	1.0000	1.0000	0.3751	0.3573	0.0527
Error Correction (# of corrected) values)	21	42	69	85	Failed	Failed	Failed
FRR	0.0000	0.0000	0.0000	0.0000	1.0000	1.0000	1.0000
FAR	0.3429	0.3429	0.3429	0.3429	0.0000	0.0000	0.0000

Armadillo was also subject to experiments similar to that of *Camel*. Tables 5.20 and 5.21 illustrate the results.

Table 5.19: 3D Model *Camel*- Impact of Gaussian Noise on Voice Biometric Watermark of Length 765 that Accommodates Voiceprint of Size 75 (GMM order 3) split 3 times

Proportion of Vertices Affected by Noise	10%	20%	30%	40%	45%	50%	100%
Correlation Value							
x dimension	1.0000	1.0000	1.0000	1.0000	1.0000	0.3609	0.2362
y dimension	1.0000	1.0000	1.0000	1.0000	1.0000	0.4242	0.2235
z dimension	1.0000	1.0000	1.0000	1.0000	1.0000	0.2488	0.1367
Error Correction (# of corrected) values)	82	157	224	293	331	Failed	Failed
FRR	0.0000	0.0000	0.0000	0.0000	0.0000	1.0000	1.0000
FAR	0.3524	0.3524	0.3524	0.3524	0.3524	0.0000	0.0000

Table 5.20: 3D Model *Armadillo*- Impact of Gaussian Noise on Voice Biometric Watermark of Length 6630 that Accommodates a Voiceprint of Size 255 (GMM order 3) repeated 26 times

Proportion of Vertices Affected by Noise	10%	20%	30%	35%	40%	45%	100%
Correlation Value							
x dimension	1.0000	1.0000	1.0000	1.0000	0.4487	0.5430	0.2776
y dimension	1.0000	1.0000	1.0000	1.0000	0.4935	0.4937	0.2927
z dimension	1.0000	1.0000	1.0000	1.0000	0.5557	0.4829	0.4025
Error Correction (# of corrected) values)	19	56	77	86	88	Failed	Failed
FRR	0.0000	0.0000	0.0000	0.0000	0.0000	1.0000	1.0000
FAR	0.2000	0.2000	0.2000	0.2000	0.2000	0.0000	0.0000

Overall it was observed that as the payload capacity of the model increased, higher level of redundancy in the form of error correcting bytes could be achieved thereby increasing the noise tolerance level of the system. Figure 5.16 shows plots of the FRR and FAR for all the 3D models at various noise levels. From the plots, it can be concluded that the system is tolerant to 20%-45% noise levels for 3D models ranging from size 17KB to 1700KB.

Table 5.21: 3D Model *Armadillo*- Impact of Gaussian Noise on Voice Biometric Watermark of Length 6375 that Accommodates a Voiceprint of Size 75 (GMM order 3) split 25 times

Proportion of Vertices Affected by Noise	10%	20%	30%	40%	45%	50%	100%
Correlation Value							
x dimension	1.0000	1.0000	1.0000	1.0000	0.9691	0.3025	0.1110
y dimension	1.0000	1.0000	1.0000	1.0000	0.9997	0.0668	0.0175
z dimension	1.0000	1.0000	1.0000	1.0000	0.9949	0.0883	0.1554
Error Correction (# of corrected) values)	615	1264	1929	2577	2768, Part 1 Failed	1351, 14 Parts Failed	Failed
FRR	0.0000	0.0000	0.0000	0.0000	0.0000	1.0000	1.0000
FAR	0.2190	0.2190	0.2190	0.2190	0.2381	0.0000	0.0000

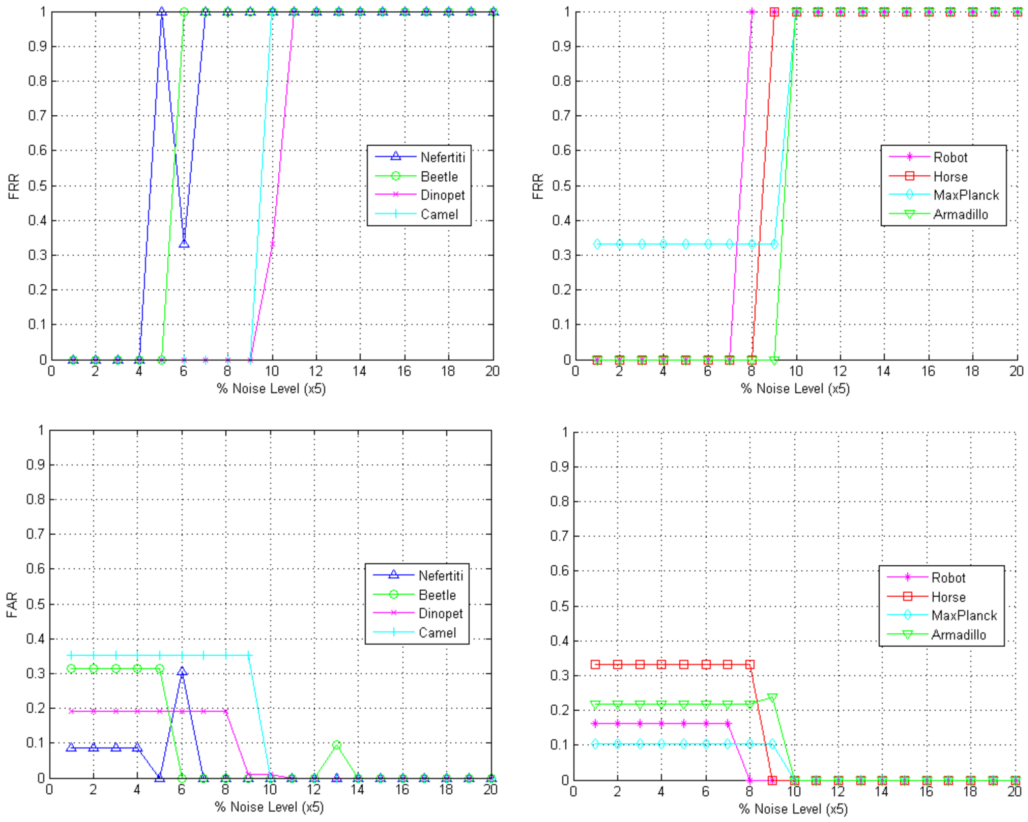

Figure 5.16: System performance when the watermarked 3D model is subject to noise attacks

Impact of Cropping Attack

The cropping attack is simulated in *MATLAB* by determining the minimum and maximum values of vertices in the x,y, and z dimension and using a threshold value that lies between this min-max range. All vertices that have a value above this threshold are cropped such that the new vertex value equals the threshold. Cropping along an axis resets the qualified vertices values to the threshold thereby truncating the 3D model in that dimension. The value of the threshold decides the level of cropping as it impacts the count of vertices that lie above this value. The proportion of vertices affected by cropping is ratio of the count of vertices adjusted by the threshold value and the total number of vertices in the 3D model. The watermark is inserted into 3 dimensions and therefore cropping along one or two dimension does not impact the user verification process as the watermark can be recovered from the third dimension. Table 5.22-5.24 show the impact of cropping along any one axis on the FAR and FRR. Tables 5.25-5.32 list the effect of various cropping levels in all three dimensions on the test subject's verification decision by the system.

Table 5.22: 3D Model *Nefertiti*- Impact of Cropping along X-Axis on Voice Biometric Watermark of Length 127 (m = 7) that Accommodates a Voice print of Size 75 (GMM order 3)

Proportion of Vertices Affected by Cropping	10%	25%	40%	60%	75%	90%	100%
Corrected Errors *x* dimension *y* dimension *z* dimension	7	20	Failed	Failed 0	Failed 0	Failed 0	Failed 0
FRR	0.0000	0.0000	0.0000	0.0000	0.0000	0.0000	0.0000
FAR	0.0857	0.0857	0.0857	0.0857	0.0857	0.0857	0.0857

Cropping attack on *Camel* highlights the fact that if the cropping occurs in regions where the watermark is inserted then the system tolerance to such attacks drops regardless of the 3D model and payload size. Cropping beyond 28% truncates those regions that accomodatethe watermark so the error correction routines fail to

Table 5.23: 3D Model *Nefertiti*- Impact of Cropping along Y-Axis on Voice Biometric Watermark of Length 127 (m = 7) that Accommodates a Voice print of Size 75 (GMM order 3)

Proportion of Vertices Affected by Cropping	10%	25%	40%	60%	75%	90%	100%
Corrected Errors							
x dimension							
y dimension	15	Failed	Failed	Failed	Failed	Failed	Failed
z dimension		0	0	0	0	0	0
FRR	0.0000	0.0000	0.0000	0.0000	0.0000	0.0000	0.0000
FAR	0.0857	0.0857	0.0857	0.0857	0.0857	0.0857	0.0857

Table 5.24: 3D Model *Nefertiti*- Impact of Cropping along Z-Axis on Voice Biometric Watermark of Length 127 (m = 7) that Accommodates a Voice print of Size 75 (GMM order 3)

Proportion of Vertices Affected by Cropping	10%	25%	40%	60%	75%	90%	100%
Corrected Errors							
x dimension		0	0	0	0	0	0
y dimension							
z dimension	8	Failed	Failed	Failed	Failed	Failed	Failed
FRR	0.0000	0.0000	0.0000	0.0000	0.0000	0.0000	0.0000
FAR	0.0857	0.0857	0.0857	0.0857	0.0857	0.0857	0.0857

Table 5.25: 3D Model *Nefertiti*- Impact of Cropping along X,Y and Z-Axes on Voice Biometric Watermark of Length 127 (m = 7) that Accommodates a Voice print of Size 75 (GMM order 3)

Proportion of Vertices Affected by Cropping	5-11%	17-26%	22-26%	35-37%	44-51%
Corrected Errors					
x dimension	7	15	20	Failed	Failed
y dimension	15	Failed	Failed	Failed	Failed
z dimension	8	Failed	Failed	Failed	Failed
FRR	0.0000	0.0000	0.0000	1.0000	1.0000
FAR	0.0857	0.0857	0.0857	0.0000	0.0000

recover the watermark and decline the performance of the system.

Table 5.26: 3D Model *Robot*- Impact of Cropping along X,Y and Z-Axes on Voice Biometric Watermark of Length 255 (m = 8) that Accommodates a Voice print of Size 75 (GMM order 3)

Proportion of Vertices Affected by Cropping	10-17%	23-27%	54-62%	72-82%	92-100%
Corrected Errors					
x dimension	10	54	Failed	Failed	Failed
y dimension	34	78	Failed	Failed	Failed
z dimension	40	54	Failed	Failed	Failed
FRR	0.0000	0.0000	1.0000	1.0000	1.0000
FAR	0.1619	0.1619	0.0000	0.0000	0.0000

Table 5.27: 3D Model *Beetle*- Impact of Cropping along X,Y and Z-Axes on Voice Biometric Watermark of Length 230 that Accommodates a Voiceprint of Size 75 (GMM order 3)

Proportion of Vertices Affected by Cropping	17-21%	21-26%	32-36%	43-47%	56-59%
Corrected Errors					
x dimension	79	79	Failed	Failed	Failed
y dimension	49	49	78	Failed	Failed
z dimension	85	Failed	Failed	Failed	Failed
FRR	0.0000	0.0000	0.0000	1.0000	1.0000
FAR	0.3143	0.3143	0.3143	0.0000	0.0000

Table 5.28: 3D Model *Horse*- Impact of Cropping along X,Y and Z-Axes on Voice Biometric Watermark of Length 765 (m =8), Voiceprint size is 75 (GMM order 3, voiceprint is split into 3 equal parts with each part having a codeword of size 255, the 3 codewords concatenate to form the watermark)

Proportion of Vertices Affected by Cropping	9-16%	24-28%	39-44%	44-48%	57-62%
Corrected Errors					
x dimension	70	158	282	Failed	Failed
y dimension	98	293	206	Failed	Failed
z dimension	130	168	Failed	Failed	Failed
FRR	0.0000	0.0000	0.0000	1.0000	1.0000
FAR	0.3333	0.3333	0.3333	0.0000	0.0000

Table 5.29: 3D Model *Dinopet*- Impact of Cropping along X,Y and Z-Axes on Voice Biometric Watermark of Length 1275 that Accommodates a Voiceprint of Size 75 (GMM order 3) that is split into 5 parts with each part forming a codeword of size 255

Proportion of Vertices Affected by Cropping	5-19%	27-31%	37-49%	49-57%	64-77%
Corrected Errors					
x dimension	174	484	Failed	Failed	Failed
y dimension	25	317	409	Failed	Failed
z dimension	167	233	291	Failed	Failed
FRR	0.0000	0.0000	0.0000	1.0000	1.0000
FAR	0.1905	0.1905	0.1905	0.0000	0.0000

Table 5.30: 3D Model *MaxPlanck*- Impact of Cropping along X,Y and Z-Axes on Voice Biometric Watermark of Length 510 that Accommodates a Voiceprint of Size 75 (GMM order 3) that is split into 2 parts with each part forming a codeword of size 255

Proportion of Vertices Affected by Cropping	6-11%	22-26%	31-40%	47-51%	57-64%
Corrected Errors					
x dimension	79	115	140	Failed	Failed
y dimension	65	84	Failed	Failed	Failed
z dimension	18	67	134	Failed	Failed
FRR	0.3333	0.0000	0.0000	1.0000	1.0000
FAR	0.1048	0.1048	0.1048	0.0000	0.0000

Table 5.31: 3D Model *Camel*- Impact of Cropping along X,Y and Z-Axes on Voice Biometric Watermark of Length 765 that Accommodates Voiceprint of Size 75 (GMM order 3) split 3 times

Proportion of Vertices Affected by Cropping	9-10%	17-28%	32-35%	35-41%	44-51%
Corrected Errors					
x dimension	112	205	Failed	Failed	Failed
y dimension	0	Failed	Failed	Failed	Failed
z dimension	46	178	Failed	Failed	Failed
FRR	0.0000	0.0000	1.0000	1.0000	1.0000
FAR	0.3524	0.3524	0.0000	0.0000	0.0000

Table 5.32: 3D Model *Armadillo*- Impact of Cropping along X,Y and Z-Axes on Voice Biometric Watermark of Length 6375 that Accommodates a Voiceprint of Size 75 (GMM order 3) split 25 times

Proportion of Vertices Affected by Cropping	4-8%	8-17%	17-27%	35-49%	51-63%
Corrected Errors					
x dimension	338	688	879	1312	Failed
y dimension	633	633	942	1500	Failed
z dimension	238	777	1020	1245	Failed
FRR	0.0000	0.0000	0.0000	0.0000	1.0000
FAR	0.2190	0.2190	0.2190	0.2190	0.0000

Overall it was observed that as the payload capacity of the model increased, higher level of redundancy in the form of error correcting bytes could be achieved thereby increasing the cropping tolerance level of the system. Figures 5.17 and 5.18 shows plots of the FRR and FAR for all the 3D models at various cropping levels. From the plots, it can be concluded that the system is tolerant to 20%-44% cropping levels for 3D models ranging from size 17KB to 1700KB.

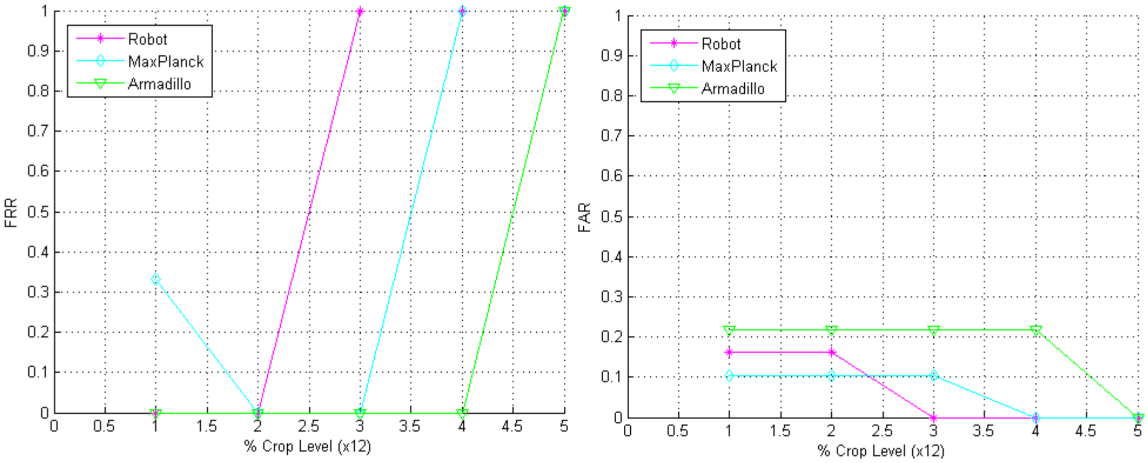

Figure 5.17: System performance when the watermarked 3D model is subject to cropping attacks

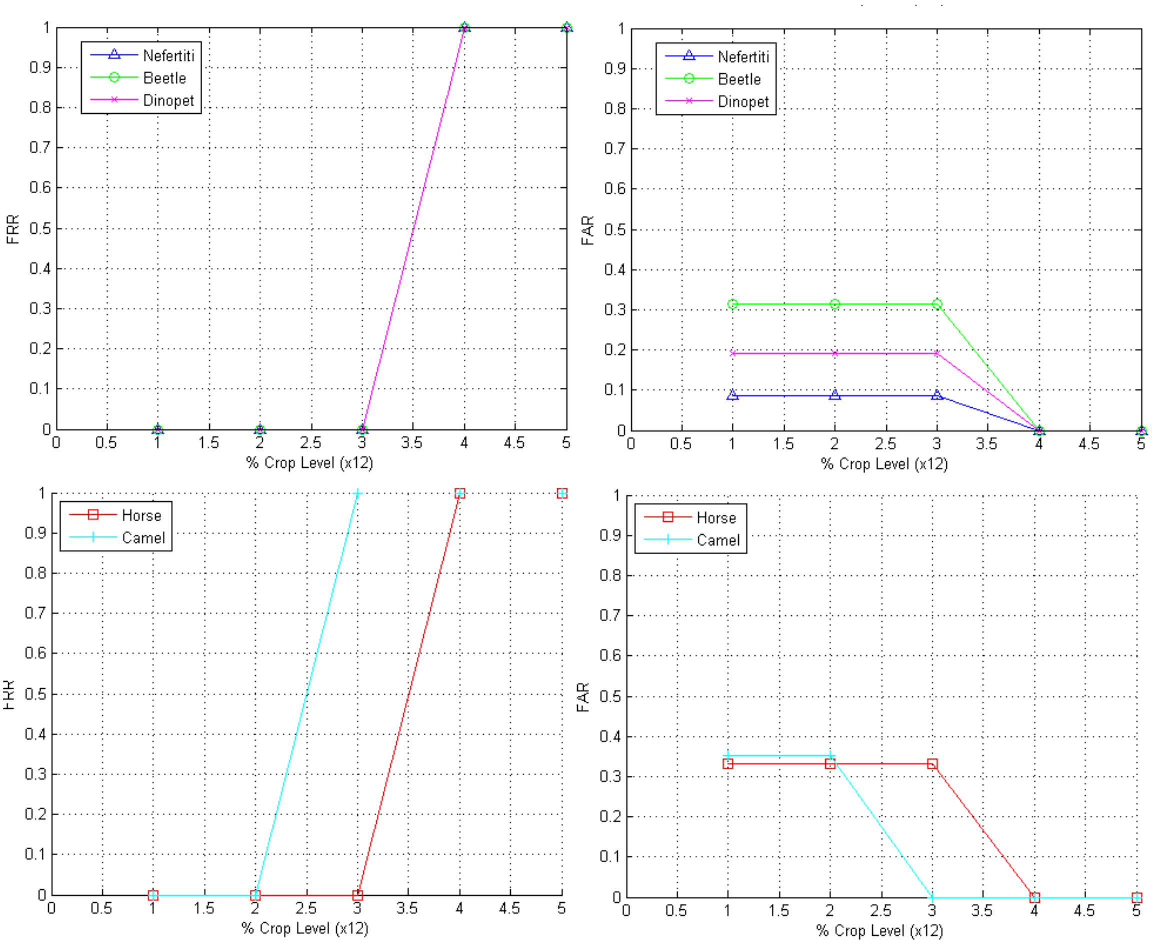

Figure 5.18: System performance when the watermarked 3D model is subject to cropping attacks

Impact of Smoothing Attack

The smoothing attack is simulated using the Taubin smoothing filter from *Meshlab* [86]. The parameters for Taubin smoothing $(\lambda : 0{-}1, \mu : negativevaluelessthan-)$ were experimented for variable steps to determine the system tolerance. Values of λ in the order of 10^{-3}-10^{-4} were used for experiments since the system rejected users for higher values. Smaller models had a tolerance for λ in the oder of 10^{-4}, while larger models could handle higher values as indicated by the tabulated results. The value of μ was set at $frac10$. Tables 5.33-5.40 outline the effect of the smoothing operations on the system's FRR and FAR.

Table 5.33: 3D Model *Nefertiti*- Impact of Smoothing on Voice Biometric Watermark of Length 127 (m = 7) that Accommodates a Voice print of Size 75 (GMM order 3)

Smoothing $\lambda = 0.0005$	1 step	2 steps	3 steps	5 steps	8 steps
Correlation Value					
x dimension	1.0000	1.0000	0.9994	0.9987	0.9968
y dimension	1.0000	1.0000	0.9994	0.9985	0.9965
z dimension	1.0000	0.9995	0.9992	0.9980	0.9957
Error Correction (# of corrections)	6	14	Failed	Failed	Failed
FRR	0.0000	0.0000	0.0000	0.0000	1.0000
FAR	0.0857	0.0857	0.1143	0.0762	0.0000

Table 5.34: 3D Model *Robot*- Impact of Smoothing on Voice Biometric Watermark of Length 255 (m = 8) that Accommodates a Voice print of Size 75 (GMM order 3)

Smoothing $\lambda = 0.0005$	10 steps	15 steps	20 steps	30 steps	40 steps	50 steps
Correlation Value						
x dimension	0.9996	0.9993	0.9986	0.9971	0.9948	0.9919
y dimension	0.9996	0.9993	0.9987	0.9971	0.9949	0.9916
z dimension	0.9997	0.9993	0.9988	0.9973	0.9952	0.9923
Error Correction (# of corrections)	Failed	Failed	Failed	Failed	Failed	Failed
FRR	0.0000	0.0000	0.0000	0.6667	0.0000	1.0000
FAR	0.2381	0.2571	0.2667	0.5238	0.3429	0.1619

Table 5.35: 3D Model *Beetle*- Impact of Smoothing on Voice Biometric Watermark of Length 230 that Accommodates a Voice print of Size 75 (GMM order 3)

Smoothing $\lambda = 0.001$	60steps	90 steps	150 steps	120 steps	200 steps
Correlation Value					
x dimension	0.9985	0.9968	0.9908	0.9943	0.9834
y dimension	0.9983	0.9962	0.9897	0.9931	0.9815
z dimension	0.9980	0.9956	0.9877	0.9921	0.9778
Error Correction (# of corrections)	Failed	Failed	Failed	Failed	Failed
FRR	0.0000	0.0000	0.0000	0.0000	1.0000
FAR	0.2381	0.1238	0.0571	0.1048	0.000

Due to a small value of λ *Beetle* could withstand a higher number of smoothing steps. Therefore, we increase the value of λ for the remaining models to test the system tolerance at difference levels of Taubin smoothing.

Table 5.36: 3D Model *Horse*- Impact of Smoothing on Voice Biometric Watermark of Length 765, Voiceprint size is 75 (GMM order 3), voiceprint is split into 3 equal parts with each part having a codeword of size 255, the 3 codewords concatenate to form the watermark)

Smoothing $\lambda = 0.0025$	2 step	3 steps	5 steps	8 steps	10 steps
Correlation Value					
x dimension	0.9979	0.9952	0.9870	0.9787	0.9496
y dimension	0.9986	0.9968	0.9914	0.9863	0.9680
z dimension	0.9980	0.9956	0.9878	0.9797	0.9509
Error Correction (# of corrections)	Failed	Failed	Failed	Failed	Failed
FRR	0.0000	0.6667	0.6667	1.0000	1.0000
FAR	0.0095	0.0095	0.2341	0.1714	0.0000

Table 5.37: 3D Model *Dinopet*- Impact of Smoothing on Voice Biometric Watermark of Length 1275 that Accommodates a Voiceprint of Size 75 (GMM order 3) that is split into 5 parts with each part forming a codeword of size 255

Smoothing $\lambda = 0.005$	3 step	5 steps	8 steps	10 steps	12 steps
Correlation Value					
x dimension	0.9992	0.9978	0.9945	0.9915	0.9876
y dimension	0.9988	0.9965	0.9910	0.9859	0.9795
z dimension	0.9992	0.9978	0.9943	0.9913	0.9871
Error Correction (# of corrections)	Failed	Failed	Failed	Failed	Failed
FRR	0.0000	0.0000	1.0000	1.0000	1.0000
FAR	0.1905	0.1048	0.0190	0.0000	0.0000

Table 5.38: 3D Model *MaxPlanck*- Impact of Smoothing on Voice Biometric Watermark of Length 510 that Accommodates a Voiceprint of Size 75 (GMM order 3) that is split into 2 parts with each part forming a codeword of size 255

Smoothing $\lambda = 0.002$	1 step	2 steps	3 steps	5 steps	8 steps
Correlation Value					
x dimension	0.9975	0.9995	0.9604	0.8987	0.7599
y dimension	0.9983	0.9995	0.9227	0.7958	0.7596
z dimension	0.9951	0.9995	0.9487	0.7981	0.8145
Error Correction (# of corrections)	Failed	Failed	Failed	Failed	Failed
FRR	0.0000	0.0000	1.0000	1.0000	1.0000
FAR	0.0347	0.0551	0.0000	0.0000	0.0000

Table 5.39: 3D Model *Camel*- Impact of Smoothing on Voice Biometric Watermark of Length 765 that Accommodates Voiceprint of Size 75 (GMM order 3) split 3 times

Smoothing $\lambda = 0.005$	5 step	10 steps	20 steps	35 steps	50 steps
Correlation Value					
x dimension	0.9993	0.9993	0.9970	0.9910	0.9809
y dimension	0.9992	0.9992	0.9970	0.9900	0.9785
z dimension	0.9993	0.9993	0.9973	0.9913	0.9819
Error Correction (# of corrections)	Failed	Failed	Failed	Failed	Failed
FRR	0.0000	0.0000	0.0000	0.0000	1.0000
FAR	0.3619	0.3619	0.2571	0.1333	0.0000

Table 5.40: 3D Model *Armadillo*- Impact of Smoothing on Voice Biometric Watermark of Length 6375 that Accommodates a Voiceprint of Size 75 (GMM order 3) split 25 times

Smoothing $\lambda = 0.005$	10 step	30 steps	50 steps	60 steps	80 steps
Correlation Value					
x dimension	0.9912	0.9831	0.9694	0.9287	0.9068
y dimension	0.9974	0.9745	0.9532	0.9485	0.9065
z dimension	0.9987	0.9990	0.9371	0.9583	0.9057
Error Correction (# of corrections)	Failed	Failed	Failed	Failed	Failed
FRR	0.0000	0.0000	0.0000	0.0000	1.0000
FAR	0.2318	0.0672	0.1457	0.5761	0.0000

5.3.1 Interpretation of Results

From the above experiments, the following conclusions can be drawn:

- The False Reject Rate of the system can be lowered by increasing the threshold value. In addition to that, the higher the variability in the voice samples provided during enrollment and the higher the number of voice samples provided by the user during enrollment the lower is the rate at which the system falsely rejects a legitimate user.

- The False Accept Rate of the system can be improved by increasing the order of the GMM, which in turn increases the size of the voice print thereby requiring a 3D model to have an embedding capacity high enough to accommodate the voice print with error correction encoding. The FAR can also be improved by extracting 16 instead of 12 features (MFCC coefficients) from each frame of the voice signal.

- The robustness of the system to attacks can be increased by increasing the level of redundancy offered by the error correction routines for the voice print.

Chapter 6

Summary and Discussion

6.1 Conclusions

This dissertation presents a novel approach to address the problem of piracy by employing a biometric watermarking scheme and proposes a client-server based DRM framework that - i) offers content access to a legitimate user, ii) offers device portability, iii) offers restriction-free usage to consumers, iv) eliminates the traditional use of licenses to govern the usage of the content, v) offers interoperability, and vi) deters piracy to protect artists and artwork sellers from incurring losses. The proposed system relies on the assumption that the user is willing to offer his voice samples to the graphics distribution agency (which is considered as a reliable authority). Since consumers are not accustomed to giving away their voice biometrics for desktop applications, user acceptance may seem to pose a barrier to adoption of the proposed system. However, according to a market analysis report released by Opus Research [120], one of the leading voice biometrics solutions provider, the global spending on speaker verification solutions was over $124 million in the year 2009. A majority of this spending came from high volume call centers at financial institutions, insurance companies, healthcare firms, and telecommunication companies for customer verification to prevent identity theft. Automatic speaker verification (ASV) systems are also penetrating into the government sector (for verification of employee identity), residential communities (to allow senior citizens access to apartments), online universities (to verify identity of test taker), credit card firms (for transaction authorization using voice), and iPhone applications (to secure contacts list by using voice to authenticate owner's identity). As ASV systems penetrate further and further into the market and begin to impact consumers, adoption of the proposed system will not be far from reality. Figure 6.1 compares the features of our system with existing 3D multimedia DRM systems. The work presented in this dissertation is a novel application as it integrates a speaker verification system with a 3D watermarking system. Such integration has not been done for any kind of digital medium., therefore providing a performance comparison is not feasible at this point.

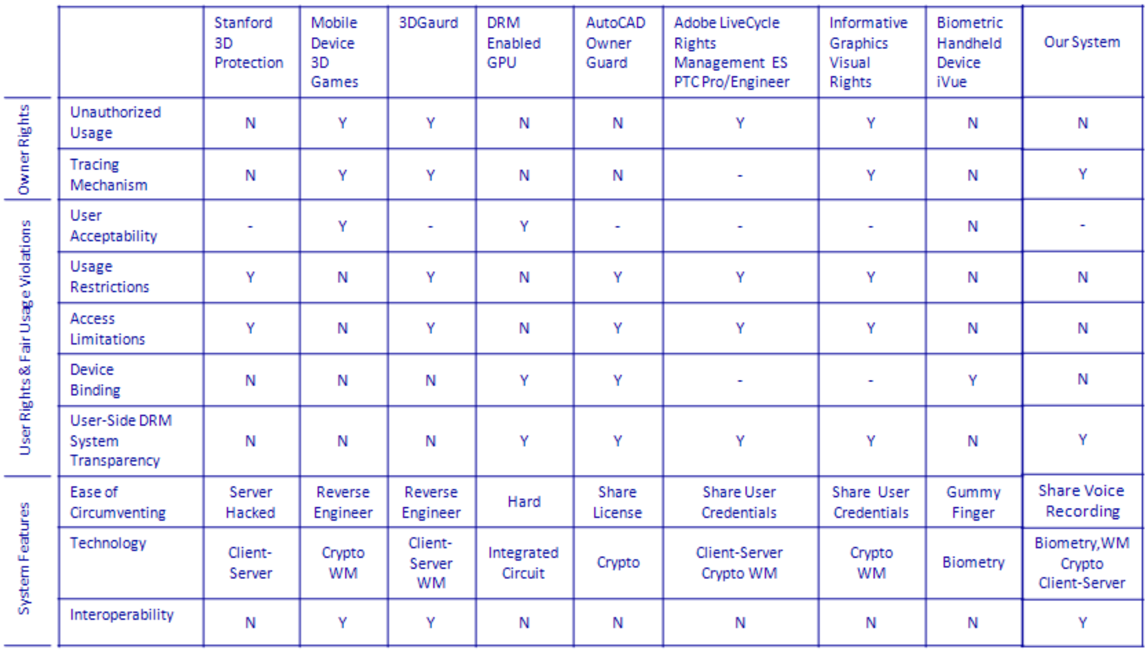

		Stanford 3D Protection	Mobile Device 3D Games	3DGaurd	DRM Enabled GPU	AutoCAD Owner Guard	Adobe LiveCycle Rights Management ES PTC Pro/Engineer	Informative Graphics Visual Rights	Biometric Handheld Device iVue	Our System
Owner Rights	Unauthorized Usage	N	Y	Y	N	N	Y	Y	N	N
	Tracing Mechanism	N	Y	Y	N	N	-	Y	N	Y
User Rights & Fair Usage Violations	User Acceptability	-	Y	-	Y	-	-	-	N	-
	Usage Restrictions	Y	N	Y	N	Y	Y	Y	N	N
	Access Limitations	Y	N	Y	N	Y	Y	Y	N	N
	Device Binding	N	N	N	Y	Y	-	-	Y	N
	User-Side DRM System Transparency	N	N	N	Y	Y	Y	Y	N	Y
System Features	Ease of Circumventing	Server Hacked	Reverse Engineer	Reverse Engineer	Hard	Share License	Share User Credentials	Share User Credentials	Gummy Finger	Share Voice Recording
	Technology	Client-Server	Crypto WM	Client-Server WM	Integrated Circuit	Crypto	Client-Server Crypto WM	Crypto WM	Biometry	Biometry,WM Crypto Client-Server
	Interoperability	N	Y	Y	N	N	N	N	N	Y

Figure 6.1: Feature Based Comparison of Existing 3D DRM Solutions with The Proposed System

The proposed DRM system can be adapted to support different digital content types such as documents, images, audio, and video. The proposed technique is superior to a biometric authentication system [106] that could utilize a unique ID watermark for tracing, because biometric-based sign-on procedure authenticates a user to gain access to the system, subsequently enabling an authorized user to copy the content out of the system and illegally redistribute it. In such cases, the unique ID watermark serves as a means to identify the user responsible for piracy. However, if such a system were to employ a custom file format, illegitimate users could not gain access to the system to consume the content without having access to the biometrics of the authorized user, so piracy would still be deterred but legitimate users would be restricted to that particular system and would not enjoy the feature of interoperability. To the contrary, even though the proposed approach utilizes a custom file format encrypted by a key, it supports interoperability because the custom format only serves as a container for the watermarked graphics in order to enforce access control. The watermarked graphics can be in any format. The custom format can be interpreted by any 3D graphics software that has the DRM client installed. In case of piracy, the biometric watermark travels with the graphics file and secures the graphics from illegitimate access. The pirated graphics file is accessible to the illegitimate user only if the authorized user who has leaked the graphics content, supplements the contents with his biometric data. If the key is compromised and the contents of the custom file format are decrypted, the access control mechanism is defeated and the biometric watermark serves as a tracer. While the biometric watermark and the unique ID both serve as tracers that assist in identifying the individual responsible for piracy, a biometric watermark serves as a stronger deterrent to piracy than a unique ID. This is because biometrics are a personal trait which not only give away the identity of the user (such as face, fingerprint images) but can also be potentially misused by illegitimate users. On the other hand, there are no such privacy issues associated with a unique ID-based watermark, since the scope of a unique ID is just limited to the context of the application. By making use of biometric data as a watermark, the proposed approach benefits in two ways - authentication and tracing, wherein lies the novelty of the approach.

This dissertation has also introduced a novel 3D model watermarking method and evaluated the use of voice biometrics as watermarks for 3D models. The primary focus of this work has been to test the verification accuracy of the biometric watermarking scheme in scenarios when the watermarked 3D model is subject to signal processing operations that potentially corrupt the embedded watermark. The experimental evaluation has examined and tuned several parameters for MFCC extraction and Gaussian mixture models to generate a watermark of appropriate length such that the payload size can be accommodated by the host 3D model without causing any perceptible distortions. The proposed method is resistant against affine transformations and mesh quantization since the watermark is embedded in the fourth decimal place of the floating point representation of the 3D mesh. The algorithm is immune to 20%-49% levels of noise and cropping attacks depending on the size of the 3D model. The algorithm has given good results for large size 3D models over 140 KB by verifying a user even after the watermarked model has been subject to higher levels of noise and cropping attacks.

Analogous to speaker verification systems, our system also trades off verification accuracy for user convenience by acquiring shorter durations of enrollment voice samples. The FRR and FAR can be improved by increasing the duration of the training voice sample, adjusting the threshold value, increasing the order of the Gaussian mixture model, and extracting higher number of cepstral coefficients as features. However, in application scenarios that demand high security of graphics content such as the government officials transferring confidential information, the issue of acquiring longer duration voice samples is eliminated as the high profile nature of the application requires the sender/receiver to co-operate for generating robust voice prints.

6.2 Contributions

The main objective of this research is to assess the viability of using voice biometrics as watermarks to verify user legitimacy. The main contribution of this dissertation lies in integrating a biometric system with a 3D watermarking system and measuring the performance of the aggregate system for feasibility in commercial or government applications.

This dissertation has also proposed a biometric DRM solution to address the key issues with current 3D graphics DRM implementations from two perspectives: artwork owners rights and users rights. Our approach suggests a different view to the problem by employing a biometric watermarking scheme and presents a DRM framework that offers device portability, fair usage to consumers and deters piracy to protect sellers form incurring losses. The presented work has analyzed the need and provided the architecture and design for a software-based DRM system that employs biometric watermarking for legitimate user access control of 3D graphics. While existing DRM solutions for audiovisual content cannot be applicable to 3D graphic content due to the extendibility and edit-ability requirements for graphic files (as opposed to just play-back requirement for music and movie content), the vice versa is not true. The proposed solution can be adopted for audio and video content as well. However, images and documents require system adaptations as these content types also demand editability in most cases.

In addition, a novel 3D mesh model watermarking algorithm has been implemented which is based on curvature estimation of local geometry. The algorithm has shown improved embedding capacity (1.98KB-99.6KB entirely dependent on the size and geometry of the model, with watermarking capacity ranging from 6% to 42% of the model size) as compared to other curvature based algorithms. In addition, our watermarking algorithm is also independent of the contents of the watermark to be embedded, unlike most of the related work that relies on the binary value of the watermark to alter the host signal. This feature makes our algorithm flexible to accept any content as watermark such as face or fingerprint templates, logos, images, text etc. Moreover, our previous work [94] and our further research work on variations of the proposed scheme [91, 92], different strategies [97] with improved embedding capacity and enhancements of the algorithm [96, 98, 99] that cater to different watermarking applications (owner identification and tamper proofing) have also been published.

6.3 Limitations

The system has not delivered good results for 3D models with size in the order of tens of kilobytes, thereby demanding higher embedding capacity algorithms for watermarking. The extendibility and edit-ability requirements for graphic files are not yet addressed by the system. Issues arising out of 3D graphics editability require 3D model segmentation based watermarking algorithms such that the watermark is embedded in all segments of the model so that it can be propagated into extended or edited versions of the original model. The system does not deal with analog attacks to address reconstruction of 3D graphics from 2D renderings obtained through screen capture of the graphics.

Limitations of the application include delaying the enrollment and verification process if artist suffers from a cough or cold, since that alters the features extracted from the voice sample. One of the major loopholes is that the system can be defeated by play backs of recorded voice of a genuine user speaking the predetermined text (0-10 digits). This loophole can be overcome by incorporating a text-prompted verification technique that does not rely on a predetermined phrase to be spoken by the user and safeguard the system from spoofing attacks that use pre-recorded voice samples of the pre-defined utterance from a genuine user.

The need for network access in order to decrypt the graphics content is an additional drawback of the proposed DRM system. A desirable feature would be the ability to authenticate and access user in offline situations. However, like any other DRM solution, some features are traded-off for others while designing the proposed solution. An offline system requires the keys to be stored locally on the consumer's PC, which if discovered by the consumer/adversary decrypts the packaged graphics and defeats the DRM system's access control mechanism. A client-server based architecture is not only more secure in this aspect but also safeguards users from compromised biometrics by deactivating old keys.

Practical realization of a biometric DRM system is far from reality unless a biometric infrastructure is in place and consumers are more tuned to giving away biometrics for all sorts of transactions/applications. When user's are mandated to give biometrics for transactions and access, then such systems will succeed. Therefore, we believe that this work is one step ahead of time from creating an impact on the commercial market. However, the proposed solution is appropriate for use in high security defense related scenarios that require strict access control of high profile graphics, since thus far biometrics have been very successfully deployed in government applications where individuals do not have a choice but to offer their biometrics.

6.4 Future Work

DRM systems limit access to only those consumers who have purchased a license to use the content. No DRM system to date has been able to provide 100% security. The attackers only have to succeed once to hack the system and distribute the illegal copies on a large scale. Against such circumstances, it is not surprising that many DRM systems have not succeeded. However, ongoing research attempts to counter attacks and come up with improved techniques for dealing with piracy. The proposed biometric based watermarking scheme in this dissertation paves the way for a DRM system for 3D multimedia serving the purpose of preventing naive attackers from bypassing such a DRM system, making it difficult and costly for skilled attackers to compromise such a DRM system, and minimizes the scope of breaks. Tie ups with popular 3D graphics creation software firms (similar to Digimarc's partnering with Adobe for protecting Photoshop images [47]) could be one way to address piracy issues with 3D graphics files. However, considerable amount of effort is required to build a secure and practical anti-piracy system that balances the needs of content owners and consumers. Further research is not limited to, but includes more work or decision making in the following areas:

1. An in-depth study of speech recognition systems to incorporate the feature of prompting for a random spoken phrase to address spoofing attacks resulting from using voice recordings of a legitimate user.

2. Dealing with analog attacks to address 3D graphics piracy arising from 2D renderings obtained through screen capture of the graphics.

3. In the event that the proprietary format is hacked, it is necessary to integrate anti-collusion codes into the watermark to deter collusion attacks. Collusion

attacks are applicable when adversaries obtain several watermarked copies of a particular media content and fuse all copies to remove traces of the watermark.

4. System renewability in case of error conditions is an important issue to be addressed. System renewability arises in case of false rejection of legitimate user due to intrinsic failure arising out of intra-user voiceprint variations, sensor failure or incorrect interaction by the user with the system while acquiring the biometric trait or adverse environmental conditions such as noise. Ongoing research is directed at reducing the probability of intrinsic failure, by developing invariant representation schemes and robust and efficient matching algorithms and use of multiple biometrics. However, some challenging questions remain on who assumes the liability if the user's access has been revoked in error. Should the system be allowed to recover after security has been compromised?

5. The embedded watermark should survive graphic file format conversions if the DRM system is designed to be interoperable such that any 3D graphics creation application can avail the same biometric enabled DRM plug-in.

6. Monitoring of illegal use to prohibit piracy by use of a tracking component that has agents to search illegal graphics files in networking, and a logging component that logs and sends certain messages to the tracking component

7. The system currently supports only personal use of files and must be extended to feature organizational buyers by allowing multiple owners for the same content, resellers for large organizations, and provisions for transfer of ownership.

Future work also entails research work on high embedding capacity algorithm to improve the performance of the overall system for 3D models with size in the order of tens of kilobytes. In addition, algorithmic enhancements are required to make the watermarked model robust against a wider variety of attacks such as vertex reordering (by storing the indexes of vertices in a hash table), mesh simplification (a common operation on 3D model used to transmit a low resolutions of the model), and local manipulations (by using 3D object segmentation and embedding the watermark in different segments). Accuracy of the system can be improved through the use of multi-modal biometrics, such as fusion of face and voice, so that the FRR/FAR of one biometric can be compensated by the use of a different biometric trait. Future direction for this application would also involve protecting various other forms of digital multimedia such as audio, video and animations in addition to providing support for other popular 3D graphic file formats other than the *.off* format such as *.max, .3ds. .blend, .lwo, .md2, .md3,* and *.x* .

Bibliography

[1] A.Jain, A. Ross, and U. Uludag. Biometric template security: Challenges and solutions. In *Proceedings of European Signal Processing Conference (EU-SIPCO)*, pages 469–472, September 2005.

[2] P. Alface. *Perception and Re-Synchronization Issues for the Watermarking of 3D Shapes*. PhD thesis, Universite catholique de Louvain(UCL), Belgium, 2006.

[3] P. Alface and B.Macq. Blind watermarking of 3D meshes using robust feature points detection. In *Proceedings of IEEE International Conference on Image Processing (ICIP)*, volume 1, pages 693–696, September 2005.

[4] Sharath Pankanti Anil K. Jain, Ruud Bolle. *Biometrics: personal identification in networked society*. 1999. Volume 479 of The Kluwer international series in engineering and computer science.

[5] Armjisoft. Autocad drawings security, drm, copy protection and distribution management solution. http://www.armjisoft.com/?page=autocadownerguard. Last Accessed August 11, 2009.

[6] B. Atal and L. Rabiner. A pattern recognition approach to voiced-unvoiced-silence classification with applications to speech recognition. *IEEE Transactions on Acoustics, Speech and Signal Processing*, 24(3):201–212, June 1976.

[7] Oliver Benedens. Watermarking of 3D polygon based models with robustness against mesh simplification. In *Proceedings of SPIE Security and Watermarking of Multimedia Contents*, volume 3657, pages 329–340, 1999.

[8] Ruud Bolle, Jonathan Connell, Sharath Pankanti, Nalini Ratha, and Andrew Senior. *Guide to Biometrics*. Springer, 2004.

[9] Koen Buyens, Sam Michiels, and Wouter Joosen. A software architecture to facilitate the creation of DRM systems. In *Proceedings of 4th IEEE Consumer Communications and Networking Conference*, pages 955–959, Jan. 2007.

[10] Joseph Campbell. Speaker recognition: A tutorial. In *Proceedings of the IEEE*, volume 85, page 14371462, September 1997.

[11] W. M. Campbell, J. P. Campbell, D. A. Reynolds, E. Singer, and P. A. Torres-carrasquillo. Support vector machines for speaker and language recognition. *Computer Speech and Language*, 20:210–229, 2006.

[12] P. Cignoni, C. Rocchini, and R. Scopigno. Metro: Measuring error on simplified surfaces. *Computer Graphics Forum*, 17(2):167–174, 1998.

[13] Civolution. Content identification technologies. http://www.civolution.com/. Last Accessed Aug 17, 2009.

[14] David Cohen-Steiner and Jean-Marie Morvan. Restricted delaunay triangulations and normal cycle. In *SCG '03: Proceedings of the nineteenth annual symposium on Computational geometry*, pages 312–321, New York, NY, USA, 2003. ACM.

[15] Nuance Communications. Speech technology. http://www.speechtechmag.com /Articles/Editorial/Q-&-A/Larry-Heck2c-Vice-President-of-R26D2c-Nuance-Communications-35442.aspx. Last Accessed April 4, 2009.

[16] MSI Copy Control. Digital audio watermarking. http://www. msicopycontrol.com/. Last Accessed Aug 17, 2009.

[17] Parametric Technology Corporation. Pro/engineer integrated 3d cad/cam/cae software. http://www.ptc.com/products/proengineer/. Last Accessed August 11, 2009.

[18] Ingemar Cox, Matthew Miller, Jeffrey Bloom, Jessica Fridrich, and Ton Kalker. *Digital Watermarking and Steganography*. Morgan Kaufmann Publishers, 2008.

[19] James Martin Daniel Jurafsky. *Speech and Language Processing: An Introduction to Natural Language Processing, Computational Linguistics, and Speech Recognition*. Prentice Hall Series in Artificial Intelligence, 2008.

[20] Anil K. Jain Davide Maltoni. *Handbook of fingerprint recognition*. Springer, 2003.

[21] S. Davis and P. Mermelstein. Comparison of parametric representations for monosyllabic word recognition in continuously spoken sentences. *IEEE Transactions on Acoustics, Speech and Signal Processing*, 28(4):357–366, Aug 1980.

[22] A Dempster, N. Laird, , and D. Rubin. Maximum likelihood from incomplete data via the EM algorithm. *Journal of the Royal Statistical Society*, 39(1):138, 1977.

[23] University College Dublin. VALID database. http://ee.ucd.ie/validdb /datasets.html. Last Accessed October 11, 2009.

[24] Gunnar Fant. *Acoustic theory of speech production*. Royal Institute of Technology, 1958.

[25] Gunnar Fant. *Acoustic theory of speech production, with calculations based on X-ray studies of Russian articulations*. Walter de Gruyter, 1970.

[26] Hannes Federrath. Scientific evaluation of DRM systems. In *Proceedings of Konferenz Digital Rights Management, Berlin*, pages 228–232, 2002.

[27] Gui Feng and Qiwei Lin. Iris feature based watermarking algorithm for personal identification. In *Proceedings of MIPPR Remote Sensing and GIS Data Processing and Applications*, volume 6790, page 45, 2007.

[28] Gerard Fernando, Tom Jacobs, and Vishy Swaminathan. Project dream:an architectural overview. http://www. openmediacommons.org/documentation.html, September 2005.

[29] J. Flanagan. *Speech Analysis Synthesis and Perception*. Springer-Verlag, 1972.

[30] P. Flynn and A. Jain. On reliable curvature estimation. In *Proceedings of IEEE Computer Society Conference on Computer Vision and Pattern Recognition*, pages 110–116, June 1989.

[31] F. Frattolillo and F. Landolfi. Designing a DRM system. In *Proceedings of Fourth International Conference on Information Assurance and Security*, pages 221–226, Sept. 2008.

[32] Sadaoki Furui. *Digital Speech Processing, Synthesis, and Recognition*. Marcel Dekker, 2000.

[33] Philips Global. Philips watermarking. www.ces.philips.com. Last Accessed Aug 17, 2009.

[34] J. Godfrey, D. Graff, and A. Martin. Public databases for speaker recognition and verification. In *In Proceedings of ESCA Workshop on Automatic Speaker Recognition Identification and Verification*, pages 39–42, April 1994.

[35] Fabien Gouyon, Francois Pachet, and Olivier Delerue. On the use of zero-crossing rate for an application of classification of percussive sounds. In *Proceedings of the COST G-6 Conference on Digital Audio Effects*, pages 147–152, 2000.

[36] Informative Graphics. Informative graphics visual rights. http://www. infograph.com/press/VisualRights_pr.htm. Last Accessed August 11, 2009.

[37] Susanne Guth. A sample drm system. In *Lecture Notes in Computer Science, Book Digital Rights Management*, volume 2770, pages 150–161. Springer-Verlag Berlin, Heidelberg, 2003.

[38] Dazhi Han, Xingqiang Yang, and Caiming Zhang. A novel robust 3D mesh watermarking ensuring the human visual system. In *Proceedings of Second International Workshop on Knowledge Discovery and Data Mining*, pages 705–709, Jan. 2009.

[39] J. Harrington and S. Cassidy. *Techniques in Speech Acoustics*. Springer, 1999.

[40] A. E. Hassanien. Hiding iris data for authentication of digital images using wavelet theory. In *Proceedings of Patten Recognition and Image Analysis*, volume 16, pages 637–643, 2006.

[41] A. Higgins, L. Bahler, and J. Porter. Speaker verification using randomized phrase prompting. In *Digital Signal Processing*, pages 89–106, 1991.

[42] Tuan Hoang, D. Tran, and D. Sharma. Bit priority-based biometric watermarking. In *Proceedings of Second International Conference on Communications and Electronics*, pages 191–195, June 2008.

[43] Tuan Hoang, Dat Tran, and D. Sharma. Remote multimodal biometric authentication using bit priority-based fragile watermarking. In *Proceedings of 19th International Conference on Pattern Recognition*, pages 1–4, Dec. 2008.

[44] Berthold Horn. Extended gaussian images. *Proceedings of the IEEE*, 72(2):1671–1686, 1984.

[45] Shang-Lin Hsieh, Hsuan-Chieh Huang, and I-Ju Tsai. A copyright protection scheme for gray-level images using human fingerprint. In *Proceedings of Third International Conference on Information Technology*, pages 482–489, April 2006.

[46] Rajibul I., Shohel S., and A. Samraj. Multimodality to improve security and privacy in fingerprint authentication system. In *Proceedings of International Conference on Intelligent and Advanced Systems*, pages 753–757, Nov. 2007.

[47] DigiMarc For Images. Digital watermarking embedder plug-in. https://www.digimarc.com/solutions/images/downloads.asp. Last Accessed Aug 17, 2009.

[48] Dolby Laboratories Inc. Dolby screen server (dss200). http://www.dolby.com. Last Accessed Aug 17, 2009.

[49] Side Effects Software Inc. Houdini 3D animation tools. http://www.adobe.com/products/livecycle/rightsmanagement/l. Last Accessed Aug 17, 2009.

[50] Adobe Systems Incorporated. Adobe livecycle rights management ES. http://www.adobe.com/products/livecycle/rightsmanagement/l. Last Accessed Aug 17, 2009.

[51] Ben Jabra and E. Zagrouba. A new approach of 3d watermarking based on image segmentation. In *Proceedings of IEEE Symposium on Computers and Communications*, pages 994–999, July 2008.

[52] A. Jain, P. Flynn, and A. Ross. *Handbook of Biometrics*. Springer-Verlag New York, Inc., 2007.

[53] A.K. Jain, S. Pankanti, S. Prabhakar, Lin Hong, and A. Ross. Biometrics: a grand challenge. In *Proceedings of the 17th International Conference on Pattern Recognition*, volume 2, pages 935–942, Aug. 2004.

[54] A.K. Jain and U. Uludag. Hiding biometric data. *IEEE Transactions on Pattern Analysis and Machine Intelligence,*, 25(11):1494–1498, Nov. 2003.

[55] A.K. Jain, U. Uludag, and Rein-Lien Hsu. Hiding a face in a fingerprint image. In *Proceedings of 16th International Conference on Pattern Recognition*, volume 3, pages 756–759 vol.3, 2002.

[56] Anil Jain and Umut Uludag. Hiding fingerprint minutiae in images. In *Proceedings of Third Workshop on Automatic Identification Advanced Technologies (AutoID), 2002*, pages 97–102, 2002.

[57] Anil K. Jain, Karthik Nandakumar, and Abhishek Nagar. Biometric template security. *EURASIP Journal of Advanced Signal Processing*, pages 1–17, 2008.

[58] L. Jamieson. Purdue electrical and computer engineering course ee649: Speech processing by computer. http://cobweb.ecn.purdue.edu/ ee649/. Last Accessed April 4, 2009.

[59] Pramod A. Jamkhedkar and Gregory L. Heileman. Digital rights management architectures. *Comput. Electr. Eng.*, 35(2):376–394, 2009.

[60] Mohamed Daoudi Jean-Luc Dugelay, Atilla Baskurt. *3D Object Processing: Compression, Indexing and Watermarking*. Wiley, 2008.

[61] Keith Johnson. *Acoustic and auditory phonetics*. Wiley-Blackwell, 2003.

[62] H. Jonker. Security of Digital Rights Managament Systems. Master's thesis, Technische Universiteit Eindhoven, Netherlands, 2004.

[63] H. Jonker and S. Mauw. Core security requirements of drm systems. In *Digital Rights Management - An Introduction, ICFAI University Press, Hyderabad, India*, pages 73–90, 2007.

[64] H. Jonker, S. Mauw, J. Verschuren, and A. Schoonen. Security aspects of DRM systems. In *Proceedings of 25th Symposium on Information Theory in The Benelux*, pages 169–176, 2004.

[65] S. Jung, D. Lee, S. Lee, and J. Paik. Biometric data-based robust watermarking scheme of video streams. In *Proceedings of 6th International Conference on Information, Communications and Signal Processing*, pages 1–5, Dec. 2007.

[66] Sooyeun Jung, Dongeun Lee, Seongwon Lee, and Joonki Paik. Robust watermarking for compressed video using fingerprints and its applications. *International Journal of Control, Automation and Systems*, 6:794–799, Dec. 2008.

[67] A. Kalivas, A. Tefas, and I. Pitas. Watermarking of 3d models using principal component analysis. In *Proceedings of IEEE International Conference on Acoustics, Speech, and Signal Processing*, volume 5, pages 676–679, April 2003.

[68] David Koller and Marc Levoy. Protecting 3D graphics content. *Commun. ACM*, 48(6):74–80, 2005.

[69] D. Kundur and D. Hatzinakos. Diversity and attack characterization for improved robust watermarking. *IEEE Transactions on Signal Processing,*, 49(10):2383–2396, Oct 2001.

[70] Ki-Ryong Kwon, Seong-Geun Kwon, Suk-Hawn Lee, Tae-Su Kim, and Kuhn-Il Lee. Watermarking for 3D polygonal meshes using normal vector distributions of each patch. In *Proceedings of International Conference on Image Processing*, volume 2, pages II–499–502 vol.3, Sept. 2003.

[71] Seong-Geun Kwon, Suk-Hwan Lee, Ki-Ryong Kwon, Eung-Joo Lee, Soo-Yol Ok, and Sung-Ho Bae. Mobile 3D game contents watermarking based on buyer-seller watermarking protocol. *IEICE - Trans. Inf. Syst.*, E91-D(7):2018–2026, 2008.

[72] Guillaume Lavoué. A roughness measure for 3d mesh visual masking. In *ACM Proceedings of the 4th symposium on Applied perception in graphics and visualization*, pages 57–60, 2007.

[73] Suk-Hwan Lee and Ki-Ryong Kwon. A watermarking for 3d mesh using the patch cegis. *Digit. Signal Process.*, 17(2):396–413, 2007.

[74] Rudolf Lidl and Harald Niederreiter. *Finite fields*, volume 20 of Encyclopedia of mathematics and its applications. Cambridge University Press, 1997.

[75] Qiong Liu, Reihaneh Safavi-Naini, and Nicholas Paul Sheppard. Digital rights management for content distribution. In *ACSW Frontiers '03: Proceedings of the Australasian information security workshop conference on ACSW frontiers 2003*, pages 49–58. Australian Computer Society, Inc., 2003.

[76] Quan Liu and Liu Yang. Watermarking of 3d polygonal meshes based on feature points. In *Proceedings of IEEE Conference on Industrial Electronics and Applications*, pages 1837–1841, May 2007.

[77] Wang Liu and Sheng Sun. Rotation, scaling and translation invariant blind digital watermarking for 3D mesh models. In *Proceedings of First International Conference on Innovative Computing, Information and Control*, volume 3, pages 463–466, 2006.

[78] Cheng-Yaw Low, A. Beng-Jin Teoh, and C. Tee. Support vector machines (svm)-based biometric watermarking for offline handwritten signature. In *Proceedings of 3rd IEEE Conference on Industrial Electronics and Applications*, pages 2095–2100, June 2008.

[79] Cheng-Yaw Low, Andrew Beng-Jin Teoh, and Connie Tee. Fusion of lsb and dwt biometric watermarking for offline handwritten signature. In *Proceedings of Congress on Image and Signal Processing*, volume 5, pages 702–708, May 2008.

[80] C.Y. Low, A.B.J. Teoh, and C. Tee. A preliminary study on biometric watermarking for offline handwritten signature. In *Proceedings of IEEE International Conference on Telecommunications and Malaysia International Conference on Communications*, pages 691–696, May 2007.

[81] Alpha Tec Ltd. Watermarking software. http://www.alphatecltd.com. Last Accessed Aug 17, 2009.

[82] VeriTouch Ltd. ivue media player. http://www.linuxdevices.com. Last Accessed April 4, 2009.

[83] A. Mansfield and J. Wayman. Best practices in testing and reporting performance of biometric devices. Technical report, Report CMSC 14/02, Nat'l Physics Laboratory, August 2002.

[84] J. Markowitz. Securing self-service telephone applications. http://www.jmarkowitz.com/images/white_paper.pdf. White Paper, Last Accessed April 4, 2009.

[85] N. Memon and Ping Wah Wong. A buyer-seller watermarking protocol. *IEEE Transactions on Image Processing*, 10(4):643–649, Apr 2001.

[86] MeshLab. 3D triangular mesh editing software. http://meshlab.sourceforge.net/. Last Accessed Aug 17, 2009.

[87] Mark Meyer, Mathieu Desbrun, Peter Schröder, and Alan H. Barr. Discrete differential-geometry operators for triangulated 2-manifolds. In *Proceedings of Visualization and Mathematics*, pages 52–58, 2002.

[88] Laurent Michaud, Mathieu Massot, and Alain Puissochet. Digital rights management(drm) - drm and virtual content distribution. Technical report, IDATE Digiworld, 2005.

[89] Sam Michiels, Kristof Verslype, Wouter Joosen, and Bart De Decker. Towards a software architecture for DRM. In *DRM '05: Proceedings of the 5th ACM workshop on Digital rights management*, pages 65–74, New York, NY, USA, 2005. ACM.

[90] M. Motwani, N. Beke, A. Bhoite, P. Apte, and F. Harris Jr. Adaptive fuzzy watermarking for 3D models. In *Proceedings of International Conference on Computational Intelligence and Multimedia Applications*, volume 4, pages 49–53, 2007.

[91] M. Motwani, B. Sridharan, R. Motwani, and F. Harris Jr. Copyright protection of 3D models using hausdorff distance. In *Proceedings of IEEE International Advance Computing Conference*, February 2010.

[92] M. Motwani, B. Sridharan, R. Motwani, and F. Harris Jr. Tamper proofing 3D models. In *Proceedings of IEEE International Conference on Signal Acquisition and Processing*, February 2010.

[93] R. Motwani, S. Dascalu, and F. Harris Jr. A voice biometric watermark for 3D models. In *Proceedings of IEEE International Conference on Computer Engineering and Technology*, April 2010.

[94] R. Motwani and F. Harris Jr. Robust 3D watermarking using vertex smoothness measure. In *Proceedings of the International Conference on Image Processing, Computer Vision, and Pattern Recognition*, July 2009.

[95] R. Motwani, F. Harris Jr, and K. Bekris. A proposed digital rights management system for 3D graphics using biometric watermarks. In *Proceedings of IEEE CCNC Digital Rights Management Workshop*, January 2010.

[96] R. Motwani, F. Harris Jr., and S. Dascalu. An eigen-normal approach for 3D mesh watermarking using support vector machines. *IACSIT International Journal of Computer Theory and Engineering*, 2010.

[97] R. Motwani, M. Motwani, and F. Harris Jr. Using radial basis function networks for watermark determination in 3D models. In *Proceedings of IEEE Indicon*, December 2009.

[98] R. Motwani, M. Motwani, and F. Harris Jr. An intelligent learning approach for information hiding in 3D multimedia. In *Proceedings of IEEE International Conference on Future Networks*, January 2010.

[99] R. Motwani, M. Motwani, F. Harris Jr., B. Bryant, and A. Agarwal. Watermark embedder optimization for 3D mesh objects using classication based approach. In *Proceedings of IEEE International Conference on Signal Acquisition and Processing*, February 2010.

[100] Clyde Musgrave. Biometric watermarks. In *United States Patent and Trademark Organization (USPTO),Patent number: 6208746*, Mar 2001.

[101] L. Myer. An exploration of voice biometrics. Technical report, SANS GSEC Practical, Maryland, 2004.

[102] J.M. Naik. Speaker verification: a tutorial. *IEEE Communications Magazine*, 28(1):42–48, Jan 1990.

[103] Anoop Namboodiri and Anil Jain. Multimedia document authentication using on-line signatures as watermarks. In *Security, Steganography, and Watermarking of Multimedia Contents VI*, volume 5306, pages 653–662, 2004.

[104] A. Noore, R. Singh, M. Vatsa, and M. Houck. Enhancing security of fingerprints through contextual biometric watermarking. In *Proceedings of Forensic Science International*, volume 169, pages 188–194, 2007.

[105] MIT OCW. Anatomy and physiology of speech production. http://ocw.mit.edu/NR/rdonlyres/Health-Sciences-and-Technology/HST-722JFall-2005/E9F65E7E-D732-41EE-AB29-5D1FD0096EE6/0/6_mot_con_sp_per.pdf. Last Accessed April 4, 2009.

[106] J. Ortega-Garcia, J. Bigun, D. Reynolds, and J. Gonzalez-Rodriguez. Authentication gets personal with biometrics. *IEEE Signal Processing Magazine*, 21(2):50–62, Mar 2004.

[107] PerSay Position Paper. The speaker biometrics and voicexml 3.0 workshop. http://www.w3.org/2008/08/siv/Papers/PerSay/PerSay_position_paper.pdf. Last Accessed April 4, 2009.

[108] Kang-Jun Park, Jeong and Lee. A study on iris feature watermarking on face data. In *Proceedings of the 8th international conference on Adaptive and Natural Computing Algorithms, Part II*, pages 415–423. Springer-Verlag, 2007.

[109] T. Parsons. *Voice and Speech Processing*. McGraw-Hill, 1987.

[110] Gordon Pelton. *Voice Processing*. McGraw-Hill, 1993.

[111] W. Peterson and E. Weldon. *Error-Correcting Codes*, volume 2nd edition. MIT Press, Cambridge, Mass., 1997.

[112] C. Qin and Miguel A. A comparison of acoustic features for articulatory inversion. In *Proceedings of Interspeech*, pages 2469–2472, 2007.

[113] Liu Quan and Liu Hong. An intelligent digital right management system based on multi-agent. In *Proceedings of International Conference on Computer Science and Software Engineering*, volume 1, pages 505–507, Dec. 2008.

[114] L. Rabiner and B. Juang. *Fundamentals of Speech Recognition.* Prentice Hall, 1995.

[115] L. Rabiner and R. Schafer. *Digital Processing of Speech Signals.* Prentice Hall, 1978.

[116] Dhamija Rachna. A framework for evaluating digital rights management proposals. In *Proceedings of 1st International Mobile IPR Workshop*, 2003.

[117] N. Rao, P. Thrimurthy, and R. Babu. A novel scheme for digital rights management of images using biometrics. *International Journal of Computer Science and Network Security*, 9:157–167, Mar 2009.

[118] Irving S. Reed and Gustave Solomon. Polynomial codes over certain finite fields. *Journal of the Society for Industrial and Applied Mathematics*, 2:300–304, 1960.

[119] Marek Rejman-Greene. Security considerations in the use of biometric devices. Technical report, 1998.

[120] Opus Research. Voice biometrics. http://www.voicebiocon.com/. Last Accessed April 4, 2009.

[121] D. Reynolds and R. Rose. Robust text-independent speaker identification using gaussian mixture speaker models. *IEEE Transactions on Speech and Audio Processing*, 3(1):72–83, Jan 1995.

[122] D.A. Reynolds. Experimental evaluation of features for robust speaker identification. *IEEE Transactions on Speech and Audio Processing*, 2(4):639–643, Oct 1994.

[123] Philip Rose. *Forensic speaker identification.* CRC Press, 2002.

[124] A.E. Rosenberg. Automatic speaker verification: A review. *Proceedings of the IEEE*, 64(4):475–487, April 1976.

[125] Walter Rudin. *Principles of Mathematical Analysis.* Third Edition, McGraw-Hill, 1976.

[126] G. Saha, S. Chakraborty, and S. Senapati. New silence removal and endpoint detection algorithm for speech and speaker recognition applications. In *Proceedings of the NCC*, pages 56–61, 2005.

[127] M. Sambur. Selection of acoustic features for speaker identification. *IEEE Transactions on Acoustics, Speech and Signal Processing*, 23(2):176–182, Apr 1975.

[128] T. Satonaka. Biometric watermark authentication with multiple verification rule. In *Proceedings of IEEE Workshop on Neural Networks for Signal Processing*, pages 597–606, 2002.

[129] Takami Satonaka. Biometric watermarking based on face recognition. In *Security and Watermarking of Multimedia Contents IV*, volume 4675, pages 641–651, 2002.

[130] T. Schurer. An experimental comparison of different feature extraction and classification methods for telephone speech. In *Proceedings of Second IEEE Workshop on Interactive Voice Technology for Telecommunications Applications*, pages 93–96, Sep 1994.

[131] C. E. Shannon. A mathematical theory of communication. *SIGMOBILE Mob. Comput. Commun. Rev.*, 5(1):3–55, 2001.

[132] W. Shi, H. Lee, R. Yoo, and A. Boldyreva. A digital rights enabled graphics processing system. In *Proceedings of the 21st ACM SIGGRAPH/EUROGRAPHICS Symposium on Graphics Hardware*, pages 17–26, 2006.

[133] Jun Shu, Yue Qi, Su Cai, and XuKun Shen. A novel blind robust digital watermarking on 3d meshes. In *Proceedings of Second Workshop on Digital Media and its Application in Museum & Heritages*, pages 25–31, Dec. 2007.

[134] Yuseung Sohn, G. Wallmann, and M. Fernandes. User transparent 3D watermarking system based on security policy. In *Proceedings of International Conference on Cyberworlds*, pages 89–92, Oct. 2007.

[135] K. Stevens. *Acoustic Phonetics*. MIT Press, Cambridge, MA, 1998.

[136] Thomson STS. Nexguard. http://nexguard.thomson.net. Last Accessed April 4, 2009.

[137] D. Sun, Q. Li, T. Liu, B. He, and Z. Qiu. A secure multimodal biometric verification scheme. In *Proceedings of IWBRS05*, page 233, 2005.

[138] Ann Syrdal, Raymond Bennett, and Steven Greenspan. *Applied Speech Technology*. CRC Press, 1995.

[139] GCS Research Geographic Communication Systems. Geospatial digital watermarking for advanced imagery services. http://www.gcs-research.com. Last Accessed Aug 17, 2009.

[140] Signum Technologies. Advanced digital watermarking solutions. http://www.signumtech.com/. Last Accessed Aug 17, 2009.

[141] Teletrax. Broadcast monitoring and verification service. http://www. teletrax.tv/. Last Accessed Aug 17, 2009.

[142] Hai Tian, Tom Trojak, and Charles Jones. Data communications over aircraft power lines. Technical report, EDWARDS AIR FORCE BASE, 2005.

[143] George Varbanov and Peter Blagoev. An improving model watermarking with iris biometric code. In *CompSysTech '07: Proceedings of the 2007 international conference on Computer systems and technologies*, pages 1–6. ACM, 2007.

[144] M. Vatsa, R.Singh, and A. Noore. Feature based rdwt watermarking for multimodal biometric system. *Image Vision Comput.*, 27(3):293–304, 2009.

[145] Mayank Vatsa, Richa Singh, and Afzel Noore. Improving biometric recognition accuracy and robustness using DWT and SVM watermarking. *IEICE Electronics Express*, 2(12):362–367, 2005.

[146] Verance. Evolution in sound technology. http://www.verance.com. Last Accessed Aug 17, 2009.

[147] Verimatrix. Video watermarking solutions. http://www.verimatrix.com. Last Accessed Aug 17, 2009.

[148] C. Vielhauer and R. Steinmetz. Approaches to biometric watermarks for owner authentication. In *Security and Watermarking of Multimedia Contents III*, volume 4314, pages 209–219, 2001.

[149] De-Song Wang, Jian-Ping Li, and Yue-Hao Yan. A novel authentication scheme of the DRM system based on multimodal biometric verification and watermarking technique. In *Proceedings of International Conference on Apperceiving Computing and Intelligence Analysis*, pages 212–215, Dec. 2008.

[150] Kai Wang, Guillaume Lavou, Florence Denis, and Atilla Baskurt. Three-dimensional meshes watermarking: Review and attack-centric investigation. In *International Workshop on Information Hiding*, Lecture Notes in Computer Science, pages 50–64. Springer-Verlag, June 2007.

[151] Qinghan Xiao. Security issues in biometric authentication. In *Proceedings of Sixth Annual IEEE SMC Information Assurance Workshop*, pages 8–13, June 2005.

[152] Zhu Xuan, Chen Yining, Liu Jia, and Liu Runsheng. Feature selection in mandarin large vocabulary continuous speech recognition. In *Proceedings of 6th International Conference on Signal Processing*, volume 1, pages 508–511, Aug. 2002.